An Adapted Convolutional Neural Network for Automatic Measurement of Pancreatic Fat and pancreatic Volume in Clinical Multi-protocol Magnetic Resonance Images: a retrospective study with multi-ethnic external validation of various fat deposition

Zhiyong (John) Yang

School of Biomedical Science

Faculty of Health and Environmental Sciences

Auckland University of Technology

2022

A thesis submitted to Auckland University of Technology in fulfilment of the requirement for the degree of Doctor of Philosophy (PhD)

Abstract

Anthropometric indices, such as body mass index (BMI), waist circumference (WC), and waist to height ratio (WHtR) have limitations in accurately predict the pathophysiology of diabetes mellitus, cardiovascular diseases, and metabolic syndrome due to ethnic differences in fat distribution. Recent studies showed that the visceral adipose tissue (VAT) deposition and fat content of internal organs, most notably intra-hepatic and intra-pancreatic fat, has emerged as a more important parameter. Measurement of fat fraction is now regarded as a challenge in clinical settings. Magnetic Resonance Imaging (MRI) based quantification of fat fraction requires highly accurate data reconstruction for the assessment of hepatic and pancreatic fat accumulation in medical diagnostics and biomedical research. So, automated pancreas segmentation and accurate fat content determination from medical images are important for clinical and research applications, including type 2 diabetes risk prediction.

In this study, we tried to assess the coordination between the traditional anthropometric indices and the various fat depositions within different ethnicities in New Zealand. We further established the signal model of oil and water emulsion used for phantom study with a field strength of 3.0 T. Finally, we modified a novel convolutional neural network (CNN) for pancreatic volume and fat fraction segmentation in magnetic resonance imaging (MRI) scans.

We used 104 previous participants with different ethnic backgrounds, including New Zealand European, Māori (the indigenous people of New Zealand), Pacific Islanders (PI), and Asian. Their weight, height, and waist circumference (WC) were measured, and subcutaneous, visceral, intra-hepatic, and intra-pancreatic fat depositions were obtained using magnetic resonance imaging (MRI). The results showed VAT depositions, but not subcutaneous adipose tissue (SAT) depositions, varied significantly at all levels among the three groups. BMI was best associated with L23SAT in NZ Europeans (30%) and L45VAT in Māori/PI (24.3%). Overall, WC and WHtR were correlated well with L45SAT (18.8% and 12.2% respectively). Intra-pancreatic fat deposition had positive Pearson relation with NZ European's BMI and Māori/PI's WC, but no regression correlation with anthropometric indices. Conventional anthropometric indices do not correspond to the same fat depositions across different ethnic groups. To accomplish the phantom study for machine learning, we used fat fraction quantification from phantom as a standard gradient to compare hepatic fat fraction and intrapancreatic fat fraction quantification with both algorithm of magnetic resonance

spectroscopy (MRS) and Iterative Decomposition with Echo Asymmetry and Least-squares estimation (IDEAL) in MRI. We also compared MRS and IDEAL pancreatic fat fraction quantification with expert manual pancreatic fat measurement. We noticed a strong correlation between true fat volume fraction and the fat fractions from both IDEAL (R^2=0.99) and MRS (R^2=0.99). Linear correlation and Pearson's correlation were applied to both the phantom and in vivo measurements. The results of in vivo measurement demonstrated a good correlation between MRI measurements of hepatic fat fractions, but varied for the pancreatic fat fraction. We also observed that the manual operation performed better than IDEAL and MRS pancreatic fat fractions reading, which helped with the further establishment of auto pancreatic fat measurement by machine learning. In this retrospective, prognostic study, we conducted pancreatic boundary identification and fat fraction segmentation. Images were modified to allow CNN with improved super pixel pre-processing. The formal training and testing of the artificial intelligence was established on more than 3,000 abdominal MR images. Validation was then conducted on 200 images from 10 additional patients who were each scanned twice. Our algorithm achieved a dice similarity coefficient (DSC) of 91.2%. This is the first algorithm for automated pancreas volume and intra-pancreatic fat determination with > 90% DSC, which has the potential to be widely used for rapid and accurate pancreatic fat quantification in research and clinical settings when using abdominal MRI.

Table of Contents

CHAPTER 1. BACKGROUND AND LITERATURE REVIEW 1

1.1 INTRODUCTION 1
1.2 OBESITY AND METABOLIC DISEASES 2
1.2.1 Introduction 2
1.2.2 Mechanism of obesity and metabolic diseases 3
1.2.3 Obesity and type 2 diabetes 3
1.3 PREVALENCE OF OBESITY TYPE 2 DIABETES 6
1.3.1 Diabetes global prevalence 6
..... 6
1.3.2 Diabetes national prevalence 7
1.4 FAT DEPOSITION IN DIFFERENT ETHNIC GROUPS 7
1.4.1 Definition of adipose tissues 7
1.4.2 Various types of fat in determining the risk of obesity 12
1.4.3 Diabetes risk in different Ethnicities 13
1.5 CLINICAL DIAGNOSIS FOR OBESITY TYPE 2 DIABETES 14
1.5.1 Anthropometric measurement 14
1.5.2 Prognostic biomarkers of T2DM 15
1.5.3 Intra-organ adipose tissue and T2DM 19
1.6 DIABETES TREATMENT 24
1.6.1 Diet and Exercise 24
1.6.2 Pharmacotherapy 25
1.6.3 Bariatric surgery 26
1.7 METHODS FOR PANCREATIC FAT CONTENT MEASUREMENTS AND ITS CORRELATION TO DISEASES 29
1.7.1 Segmentation of pancreas 31
1.8 FURTHER UNDERSTANDING OF CNN 37
1.8.1 Convolution layers 37
1.8.2 Activation functions 37
1.8.3 Pooling 38
1.8.4 Fully connected (FC) layer 38
1.8.5 Data pre-processing and augmentation 38
1.8.6 CNN architectures and frameworks 38
1.9 DESCRIPTION OF THIS RESEARCH 40
1.9.1 Aim of this research 40
1.9.2 Ethical Approval and Ethical Consideration 40

CHAPTER 2. EVALUATION OF ETHNIC VARIATIONS IN VISCERAL, SUBCUTANEOUS, INTRA-PANCREATIC, AND INTRA-HEPATIC FAT DEPOSITIONS BY MAGNETIC RESONANCE IMAGING AMONG NEW ZEALANDERS 42

2.1 INTRODUCTION 42
2.2 MATERIALS AND METHODS 43
2.2.1 Sample collection 43
2.2.2 Methods 43
2.3 RESULTS 48
2.3.1 Baseline characteristics for fat deposition variations in different ethnicities 48
2.3.2 Differences between the ethnic groups 49
2.3.3 Correlations between anthropometric indices and MRI-derived fat depositions across the ethnicities 50
2.3.4 Usefulness of measuring fat depositions at different levels 51
2.3.5 Ethnicity-specific predictive equations 53

CHAPTER 3. AN ADIPOSE TISSUE PHANTOM TO DETERMINE THE THEORETICAL ACCURACY FOR BOTH ARTIFICIAL AND AUTOMATIC MEASUREMENT OF FAT DEPOSITION IN MRI 55

3.1 INTRODUCTION 55

3.2 METHOD 57
3.2.1 IDEAL fat-water MRI *57*
3.2.2 MRS *58*
3.2.3 Phantom validation *58*
3.2.4 Clinical participants for validation *58*
3.2.5 Data and Statistical Analysis *60*
3.3 RESULTS 60
3.3.1 Summary of phantom experiment *60*
3.3.2 Illustrate HFF results of IDEAL and MRS from patients *61*

CHAPTER 4. AN IN CLINICAL MULTI-PROTOCOL MAGNETIC RESONANCE IMAGES: A RETROSPECTIVE STUDY WITH MULTI-ETHNIC EXTERNAL VALIDATION 65

4.1 INTRODUCTION 65
4.2 MATERIALS AND METHOD 69
4.2.1 Sample Size and details *69*
4.2.2 Image pre-processing and development of the automated pancreatic segmentation model *69*
4.2.3 The Design of Convolutional Neural Networks. *72*
4.2.4 Strategy of determining pancreas volume and pancreatic fat deposition *73*
4.2.5 Training and validating the novel CNN *74*
4.3 RESULTS 75
4.3.1 Testing the improved CNN *75*
4.3.2 Performance Evaluation of the improved CNN *77*
4.3.3 Clinical validation of the novel CNN *83*

CHAPTER 5 DISCUSSION 85

5.1 THE USEFULNESS OF DIFFERENT FAT TISSUES AMONG VARIOUS ETHNICITIES 85
5.2 THE FEASIBILITY OF APPLYING CNN FOR PANCREATIC PARAMETERS DETERMINATION 87
5.3 THE PROSPECT OF THE NEW CNN 89

CHAPTER 6 CONCLUSION, LIMITATIONS AND FUTURE RECOMMENDATIONS 92

6.1 CONCLUSION 92
6.2 LIMITATIONS 94
6.3 FUTURE STUDY RECOMMENDATION 96

REFERENCES 98

APPENDICES 119

List of Figures

Figure 1-1 Major complications associated with T2DM 5
Figure 2-2 Pearson correlation between various fat and athropometric index 50
Figure 3-1 Phantom results from oil-water emulsion experiment 61
Figure 3-2 Hepatic fat fraction (HFF) results from IDEAL and MRS 62
Figure 3-3 Pancreatic fat fraction (PFF) results from IDEAL and MRS 63
Figure 3-4 Correlation of the manually and machine derived PFF. 64
Figure 4-1 The overall workflow of the pancreatic volume and fat tissues segmentation 68
Figure 4-2 The overview of modified CNN process for pancreas volume and fat deposition 73
Figure 4-3 Super pixel cantered MR Image VS offset 73
Figure 4-4 Method of pancreatic volume and fat deposition 74
Figure 5-5 Comparison between improved LSC and SLIC0 by various evaluation index 75
Figure 5-6 The correlation of r values and I values.. 76
Figure 4-7 Result of super pixel segmentation and generation of schematic images by improved LSC 77
Figure 4-8 Optimum super pixel number for ideal DSC%. Correlation of the average performance and different super 77
Figure 4-9 Comparison of the Performance of modified CNN at different epoch with and without pre-processing of super pixel segmentation. 78
Figure 4-10 Performance summary comparing the super pixel segmentation methods of pancreas centred and non-centred 79
Figure 4-11 Correlation between Erosion algorithm kernel values adjusting and Dice Score 79
Figure 4-12 Fat fraction gradient from CNN based on phantom 80
Figure 4-13 Novel CNN performance on recognition of pancreas 81
Figure 4-14 3D rebuilt result of pancreas of one patient 82
Figure 4-15 Validation of the integrity of trained CNN. 84

List of Tables

Table 1-1 Clinical features to diagnose T2DM....4
Table 1-2 The activation functions details....37
Table 1-3 Various existing CNN frameworks (Sarvamangala and Kulkarni 2021)....39
Table 2-1 Characteristics of study participants....48
Table 2-2 Results of student's t-test for equality of means between the groups....49
Table 2-3 Regression Result for Ethnicity-Specific Associations Between BMI and fat depositions....51
Table 2-4 Regression Result for Ethnicity-Specific Associations Between WC and fat depositions....52
Table 2-5 Regression Result for Ethnicity-Specific Associations Between WHtR and fat depositions....53
Table 2-6 Ethnicity-Specific Equations to Estimate VAT depositions for NZ European....54
Table 2-7 Ethnicity-Specific Equations to Estimate VAT depositions for Māori/PI....54
Table 4-1 Comparison of different pancreatic....82
Table 4-2 Summary of details of 10 participants in validation....82

Attestation of Authorship

I hereby declare that this submission is my own work and that, to the best of my knowledge and belief, it contains no material previously published or written by another person (except where explicitly define in the acknowledgements), no material which to a substantial extent has been submitted for the award of any other degree or diploma of a university or other institution of higher learning.

Signature：

Acknowledgements

My doctoral journey was a voyage of discovery through the maze of academia. Numerous people have been involved and provided guidance and input, without whom this thesis would not have reached its end. I foremost wish to acknowledge and thank my kind supervisor, Professor Jun Lu who accepted me as his student. He provided me huge support, guidance, and encouragement to prepare this thesis. I would also like to express my regards to my co-supervisor, Professor Rinki Murphy from the University of Auckland. They achieved me in the best way with their precious suggestions and comprehensive knowledge.

My sincere thanks also to Associated Professor Lindsay Plank, nurse Elaine Yi, and MRI technologist Ms. Rachel Heron for your help and suggestions for the patient recruitment in my project. Without you, I couldn't have finished my thesis easily.

My special thanks to my lovely and tolerant wife, Qi Li, for encouraging and supporting me every step of the way. My wife gave me huge encouragement and very constructive suggestions for my Ph.D thesis.

My final thanks to my parents who gave me encouragement and all participants who support my study.

Chapter 1. Background and literature review

This chapter aims to give the readers an introduction about the project I conducted during my PhD period. The first section provides background information to familiarize the readers with the role of pancreatic size and fat deposition in the clinical prediabetes diagnosis and the cutting-edge methods of its quantification and segmentation. The second section gives a description of the application of artificial intelligence (AI) in clinical diagnosis worldwide. Lastly, it contextualizes the research question, its aims, and its healthcare significance within NZ and around the world.

1.1 Introduction

The World Health Organization (WHO) conducted a project called the global burden of disease (GBD) to evaluate health loss from hundreds of diseases, injuries, and risk factors, in order to improve health systems and eliminate disparities. (Mattiuzzi and Lippi 2020) The GBD results from 1990 to 2019 showed that the major diseases of concern have shifted from being communicable diseases to non-communicable diseases, such as diabetes, cancer, chronic respiratory, and cardiovascular disease.(Roth et al. 2020) Notably, non-communicable diseases are highly correlated to obesity, which is increasing dramatically among populations worldwide and New Zealand in recent decades. WHO defines being overweight and obesity as abnormal or excessive fat accumulation in the human body that influences their health. Currently, in clinical inspection, the most effective cut-off value used to identify obesity is the Body Mass Index (BMI), which is derived from a ratio between weight in kilograms and the square of the height in meters (kg/m^2). For adults, WHO defines obesity as having a BMI greater than or equal to 25 and 30. Obesity prevalence worldwide has tripled from 1975 to 2019. 1.9 billion adults, 340 million children and adolescents aged 5-19 y, and 39 million children under the age of 5 were overweight. Of these over 650 million were obese. Obesity statistics from Ministry of Health of New Zealand (Manatu Hauora, 2020) shows the situation is no better here; around 1 in 3 adults and 1 in 10 children aged 2-14 are obese, with Māori and Pacific Islanders having even higher rates. These rates are extremely disproportionate in New Zealand schoolchildren, with obesity prevalence rates of Māori (5.1%) and Pacific Islanders (10.9%) being more than 6 to 13 times higher than those of Europeans (0.8%), respectively.(Goulding et al. 2007) The New Zealand Ministry of Health (NZMH) has released a report regarding the dramatically increasing prevalence of obesity type 2 diabetes (OT2D) in

Māori and Pacific Islanders, and has claimed that Māori and Pacific Islanders have higher obesity and T2DM incidences than the national averages in recent years.

1.2 Obesity and metabolic diseases

1.2.1 Introduction

Obesity is a medical condition in which excess body fat has accumulated to the extent that it may have a negative effect on health. Body mass index (BMI) and waist circumference (WC) are now regarded as two efficient measurements for obesity. People are generally considered obese when their BMI is over 30 kg/m^2, with the range 25–30 kg/m^2 defined as being overweight .(WHO) Notably, if WC were to be less than 85 cm, nearly half of the metabolic related risks could be prevented.(Zhou 2002) Obesity increases the possibility of many metabolic diseases, particularly type 2 diabetes, cardiovascular diseases, certain types of cancer, depression and osteoarthritis, and it is reported more common in women than men. (Luppino et al. 2010) Authorities view obesity as one of the most serious public health problems of the 21st century.(DiBaise and Foxx-Orenstein 2013) The American Medical Association has classified obesity as a disease and 600 million adults (12%) and 100 million children have been were identified as being obese at the end of 2015.(Collaborators 2017) Obesity is also a leading preventable cause of death worldwide, with rates increasing in both adults and children. (WHO) It is predicted that the number will reach 366 million by 2030, mainly because of the rapid rise of obesity driving T2DM. New Zealand is no exception, with prevalence rates of obesity and extreme obesity being 21% and 2.6%, respectively, with Māori and Pacific Islanders having even higher rates.(Ministry of Health 2004) Furthermore, the extreme obesity prevalence rates in New Zealand schoolchildren of Māori (5.1%) and Pacific Islanders (10.9%) are more than 6 and 13 times higher than those of Europeans (0.8%), respectively.(Goulding et al. 2007) The New Zealand Ministry of Health has released a report regarding the dramatically increasing prevalence of obesity type 2 diabetes (T2D) in Māori and Pacific Islanders and claimed that Māori and Pacific Islanders have higher obesity and T2DM incidences than national averages in recent years (NZMH). Although T2DM risk in Māori and Pacific Islanders has been established, other ethnicities in New Zealand such as Asians, including Chinese, Indians and Koreans, are not well studied. The increasing obesity-related death rate is a call to find effective diagnostic methods for the prevalence of obesity-related diseases like T2D.

1.2.2 Mechanism of obesity and metabolic diseases

Implication of obesity can extend across multiple organ systems and diseases. Multiple of the most common metabolic diseases are closely correlated with obesity, such as certain types of cancer, pulmonary disease, and the development of insulin resistance and type 2 diabetes. Over the past decade, the search for a potential unifying mechanism behind the pathogenesis of obesity-associated diseases has come across one potential mechanism of excess nutrition causing derangement in cellular and molecular mediators of immunity and inflammation. This is known as "meta-inflammation".(Ouchi et al. 2011) Inflammation is a coordinated response to harmful stimuli, with the goal of returning the system back to a normal baseline. Pathogenic antigens trigger the inflammatory responses systematically and increase circulating inflammatory cytokines, acute phase proteins (such as C-reactive protein), the recruitment of leukocytes to inflamed tissues and activation of tissue leukocytes, and the generation of reparative tissue responses. However, meta-inflammation is unique compared with other inflammatory paradigms in many aspects. The chronic nature of obesity activates a tonic low-grade activation of the innate immune system that affects steady-state measures of metabolic homeostasis over time.(Kosteli et al. 2010, de Vries et al. 2014) Moreover, the multi-organ involvement of obesity-induced inflammation is unique and presents a challenge to researchers attempting to tease out disease mechanisms in complex metabolic systems. It is now clear that inflammation plays a key linking role between obesity and metabolic disease. Studies have demonstrated a robust pattern between the association of inflammatory genes overexpression in adipose tissue and obesity and metabolic disease. This also increases the overexpression of macrophage genes, which stimulates the circulating cytokines and decreases protective factors such as adiponectin.(Chen et al. 2008) Hence the communication between inflammatory and metabolic cells decreases.

1.2.3 Obesity and type 2 diabetes

1.2.3.1 Definition of type 2 diabetes

T2DM, or simply diabetes, is mainly defined by the high level of blood glucose which results from the inability of the human body to produce a sufficient amount of insulin. Based on the records of the American Diabetes Association (ADA), T2DM, which was previously termed as "non-insulin-dependent diabetes" or "adult-onset diabetes" , covers about 90-95% of all types of diabetes (ADA,2015). Currently, T2DM is mostly diagnosed based on HbA1c,

measuring fasting plasma glucose (FPG) or 2 hours postprandial glucose (2hPP) after a 75g glucose during on glucose tolerance test (OGTT). (Table 1.1)

Table 1-1 Clinical features to diagnose T2DM

HbA1 ≥ 6.5% using an accepted method based on NGSP and certified by DCCT	OR	FPG ≥ 7.0 mmol/L after 8 hours fasting
2hpp ≥ 11.1 mmol/L after ingesting 75 g glucose in water during 2 hour-time (OGTT)	OR	Random plasma glucose ≥ 11.1mmol/L for those patients with traditional symptoms of hyperglycaemia

Adapted from ADA (A.D. Association, 2015)

Homeostasis of glucose in the human body has a very important role in the pathophysiological presentation of T2DM. The balance between liver glucose and peripheral glucose uptake is responsible for energetic material dispersion and makes the regulation of feedback to the hypothalamus effective. Insulin is a key regulator in the process of glucose homeostasis. Insulin is an anabolic hormone, which can cause the storage of fat, amino acids, and carbohydrates in cells. The overaccumulation of glucose in the liver, skeletal muscle, and adipose tissues will gradually develop the occurrence of diabetes. The most common mechanism is the dysfunction of pancreatic beta cells, along with insulin deficiency resulting in IR. The inability to secrete insulin results in several abnormalities that influence the normal nutrient metabolism.(ELDerawi 2017) There are two ways for insulin deficiency to arise: first, the given tissue is deficient in its response to insulin; and, second, there is an inadequate secretion of insulin to the given tissue. Glucagon has an opposite function of insulin, working to keep glucose in the body's circulation through secretion from pancreatic alpha cells when the blood glucose is low. It stimulates glycogenesis and gluconeogenesis. Glucose production via the liver is increased through gluconeogenesis to reduce glucose uptake in skeletal muscle fat tissues. Diabetes is a major sequela of obesity and the link between T2DM and obesity is undeniable.(Cornelissen, Haslam and Balmer 2007) Among the obese individuals with fatty liver disease, the accumulation of fat near the pancreas (inner pancreatic fat) causes impaired insulin secretion. It has been shown that 30% of obese people have fatty liver disease. Since insulin is an anabolic hormone, more triglycerides (TGs) and fatty acids are stored in cases of hyperinsulinemia.

1.2.3.2 Complications of Diabetes

T2DM has many serious complications. People who are diagnosed with diabetes are at serious risk of developing several life-threatening and disabling diseases compared to healthy individuals. The long-term effect of T2DM on various organs leads to damage, dysfunction, and failure of almost all vital parts of the body including nephropathy, kidney failure neuropathy, foot ulcers, Charcot joints, and gastrointestinal, genitourinary, and cardiovascular diseases (ADA,2013). These complications can be classified into two groups: microvascular and macrovascular. (**Figure 1-1**) One of the significant restrictions of the aetiology of diabetes is identifying microvascular or macrovascular complications of the disease. At this stage, the details of these mechanisms of diabetes are still unknown. T2DM is often diagnosed in the presence of its complications, which includes a constant feeling of thirstiness, polyuria, blurry vision, weight loss, and insatiable appetite, which when combined with the hyperglycaemia and hypertension, may lead to coma and death regarding nonketotic hyperosmolar syndrome (NKHS).(Kitabchi et al. 2009) Unfortunately, controlling glycaemia is not easy to achieve in all diabetic individuals, even with good glycaemic control, the damaging of vascular cells still occurs due to intermittent hyperglycaemia. Furthermore, intensive use of insulin can lead to microvascular complications. Although traditional glycaemic management is still the best choice for diabetic treatment, it is urgent to develop novel therapies that effectively target the cause of diabetic complications and provide a sustainable effect for long-term control.

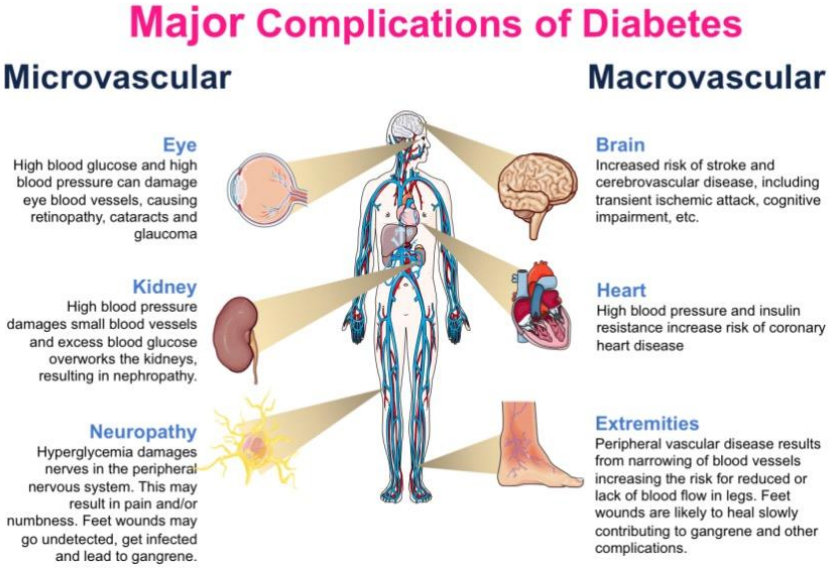

Figure 1-1 Major complications associated with T2DM (Adapted from Servier Medical Art)

1.3 Prevalence of Obesity Type 2 Diabetes

1.3.1 Diabetes global prevalence

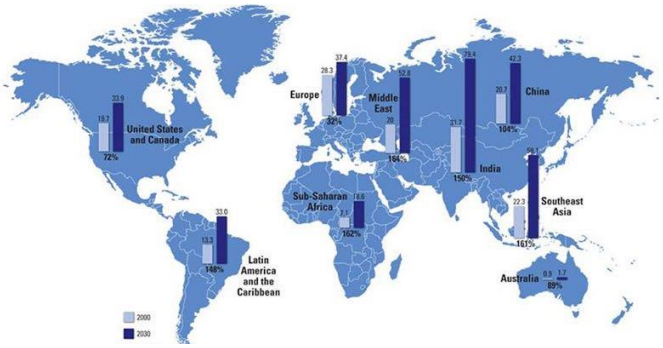

Figure 0-2 Global Prevalence of Diabetes

According to WHO, there were 171 million people with diabetes in the world. Diabetes has become the 6th leading cause of death globally with 1.5 million every year. (Mathers, Boerma and Ma Fat 2009) It is predicted that the number of people with diabetes will reach to 366 million by the end of 2030, majority of these cases are caused by the rapid rise of obesity rate (WHO, 1-2).

According to the data from each district health board (DHB) in New Zealand, the situation that the people with OT2D is also harsh, with approximate 5.4% of resident population were diagnosed by the end of 2013, and the number will predictably keep increasing. This also takes heavy load of financial issue to the government.

There are four common types of diabetes: type1, type2, gestational diabetes and "additional types". About 90-95% of all types of diabetes are T2DM, which is present in both adults and adolescents.(Fazeli Farsani et al. 2013) Data from WHO showed that diabetes is the fifth leading cause of death all around the world in 2005. More than 4000 people are diagnosed with diabetes and more than 650 people die from diabetes each day. It has been shown that the rate of diabetes-related deaths has risen by 45% since 1987. According to the latest IDF report, more than 415 million people currently live with T2DM, and it has been predicted this number will reach 642 million by the end of 2040 (IDF, 2015). A lot of people suffering from diabetes are in their working ages (40-59 years old). Diabetes is an economical and global burden, for instance, in the US diabetes-related expenses costs the government more than 132 billion dollars each year (www.diabetes.org). It has been predicted that the prevalence of diabetes will be increased to more than 330 million people by 2030 (WHO). However, by changing lifestyle or using effective medicine this prediction could be decreased significantly. It is therefore imperative to find affordable and user-friendly interventions or prognosis methods which can reduce the high expenditures predicted to arise with this theorised increase in diabetes prevalence.

1.3.2 Diabetes national prevalence

The exact prevalence of diabetes in New Zealand is unknown because of the identifying limitations and the suspected amount of many undiagnosed cases. Even under these circumstances, the prevalence of diabetes is increasing dramatically in New Zealand, according to the data from Ministry of Health New Zealand in 2015. The prevalence of prediabetes was up to 25.5% in NZ. Significantly, the prevalence of diabetes was higher in males (8.3%) than in females (5.8%).(Coppell et al. 2013) The prevalence of undiagnosed diabetes is higher among Pacific people, and this also varies among other ethnicities. The current population in NZ is confronted with an alarmingly high risk of diabetes. It is still challenging to provide a suitable management program to the New Zealand population, especially among the people aged 35-44, even though available information on diabetes treatment is established. The prevalence of diabetes has significant correlation with different ethnicities among New Zealanders. It has been shown that New Zealand Europeans have the lowest prevalence of diabetes (0.8%), while Pacific Islanders have the highest with 10.9%, and Māori have a prevalence of 5.1%.(Goulding et al. 2007) According to the Ministry of Health of New Zealand, 869 people have died of diabetes and the disease has been recognized as a "silent killer" in NZ society. Diabetes remission is an area of research which warrants further attention.

1.4 Fat Deposition in different Ethnic groups

1.4.1 Definition of adipose tissues

Body fat， Adipose tissues, or just fat is type of a loose connecting tissue most consist of adipocytes. (Birbrair et al. 2013) Other than adipocytes, adipose tissue also includes the stromal vascular fraction of cells containing fibroblasts, vascular endothelial cells, preadipocytes, and a variety of immune cells like adipose tissue macrophages. Adipose tissue is generated from pre-adipocytes, with a main role of storing energy in formation of lipids, while also types of adipose tissues are serving to cushion and insulate the body for its temperature. Despite from being hormonally inert, adipose tissue has been regarded as a main endocrine organ in most recent years, because it produces and secret hormones such as oestrogen, resistin, leptin, and many cytokines (such as TNF-α).(Kershaw and Flier 2004)

In obesity symptoms, adipose tissue is also play a role of implicating in the chronic release of pro-inflammatory markers known as adipokines, which are regarded as responsible for the

development of metabolic relevant syndromes, a constellation of diseases including T2D, CVD and atherosclerosis. (Mancuso 2016) In the other aspect, there are mainly two groups of adipose tissues and they are white adipose tissue (WAT), which responsible for storing energy, and brown adipose tissue (BAT), which produces body heat. The formation of adipose tissue is controlled in part by the adipose gene and regulated by epigenomic pathways which repones highly to environment. In recent years, the adipose tissues have been divided into various types to fit into different research areas. (Mancuso 2016)

1.4.1.1 Visceral fat

Visceral fat or abdominal fat (is also known as intra-abdominal fat or organ fat) is located inside the abdominal cavity, packed between the organs (such as the stomach, liver, intestines, kidneys, etc.). Chemical investigation of visceral fat have shown that it is composed of several adipose depots, including mesenteric, epididymal white adipose tissue (EWAT), and perirenal depots. An excess of visceral fat is known as central obesity, or "belly fat", in which the abdomen protrudes fat excessively. Fat in the lower body is subcutaneous and is not consistently spaced tissue, whereas fat in the abdomen is mostly visceral and semi-fluid.(Borkan et al. 1982) In clinical study, visceral fat is often expressed in terms of its area in cm^2 (VFA, visceral fat area). (Nagai et al. 2010)

Excess visceral fat is also linked to type 2 diabetes, insulin resistance, inflammatory diseases, and other obesity-related diseases.(Mokdad et al. 2003) Some research did show that the accumulation of neck fat (or cervical adipose tissue) is associated with mortality.(Maresky et al. 2015) Several studies have suggested that visceral fat can be predicted from simple anthropometric measures, and more accurately predicts mortality than body mass index or waist circumference.(Brown, Harhay and Harhay 2017) Visceral fat accumulation varies between the sexes. Men are more likely to have fat stored in the abdomen due to sex hormone differences. Female sex hormone causes fat to be stored in the buttocks, thighs, and hips.(Savard 2007) Oestrogen production by the ovaries declines when women reach menopause, and fat begins to be stored in the abdomen instead of the waist, buttocks, hips and thighs. (Brookheart, Michel and Schaffer 2009)

1.4.1.2 Subcutaneous fat

Subcutaneous fat (SAT) is located underneath the human skin. Most of the non-visceral fat is tend to be found at the hypodermis which is a region just below the skin. (Martin and Schwab 2013) Some SAT is known as intramuscular fat, which is interspersed in skeletal muscles. Unlike VAT, the SAT is not associated to most of the classic obesity-related diseases such as heart disease, cancer, and stroke, and some evidence even advised that it might be protective to some parts of human. (Porter et al. 2009) Due to the genetic impact, the typically female SAT pattern on body would be distributing around the hips, thighs, and buttocks, and therefore influenced less on their health compared to VAT.(Fitness)

Similar to all other fat intra-organs, SAT is a quite active member of the whole endocrine system, it can secrets a bunch of hormones like leptin and resistin.(Cummings) The association between the subcutaneous adipose layer and total body fat in a person is often modelled as adipose fat regression equations. Among those equations, the most popular one was derived by Durnin and Wormersley, whose experiment included rigorous tests on many types of skinfolds. They created two formulae to calculate the body density of both men and women based on their experiments. These equations did show an inverse proportional relationship between skinfolds and body density—as the sum of skinfolds increases, the body density decreases. (Brodie, Vicki Moscrip MSC and Hutcheon 1998) Factors such as sex, age, population size or other variables may take into consideration when make the equations invalid and unusable. Apart from this work, in 2012, Durnin and Wormersley's equations can only estimate a person's true level of fatness. New formulae are still being established.

1.4.1.3 Epicardial Fat

Epicardial adipose tissue (EAT) is a particular form of VAT deposited around the heart. It is found to be an very active organ which can generate a lot of bioactive molecules, and which might include significantly affection on the cardiac function metabolically. (Mazurek et al. 2003) Components with labelling was conducted a comparison in terms of both EAT. The result suggests a depot specific influence on storing fatty acids on adipocyte function and metabolism. (Pezeshkian et al. 2009)

1.4.1.4 Marrow fat

Marrow fat, also known as marrow adipose tissue (MAT), is the poorest type of fat tissue that can be understood. It is a type of fat tissue that resides in bones and is interspersed with hematopoietic cells and same as bony elements. The marrow fat adipocyte are derived from mesenchymal stem cells (MSC) that enrich the amount of nearly all types of cells including fat and bone cell. There exist significant distinguishes between MAT and other types of fat depots in terms of increasing calorie restriction or anorexia feature. (Styner et al. 2017) Exercise regulates MAT, decreasing MAT quantity and diminishing the size of marrow adipocytes. (Styner et al. 2014) Doing exercise can regulate the marrow fat and this means it bears some physiologic similarities to other WAT. Moreover, increased MAT in obesity further suggests a similarity to white fat depots. (Styner et al. 2017)

1.4.1.5 Ectopic fat

Ectopic fat is the storage of triglycerides in tissues other than adipose tissue. They are supposed to contain only small amounts of fat, such as the liver, skeletal muscle, heart, and pancreas.(Birbrair et al. 2013) This can interfere with cellular functions and hence organ function and is associated with insulin resistance in type-2 diabetes.(Snel et al. 2012) It is stored in relatively high amounts around the organs of the abdominal cavity, but is not to be confused with visceral fat.

The specific cause for the accumulation of ectopic fat is unknown. The cause is likely a combination of genetic, environmental, and behavioural factors that are involved in excess energy intake and decreased physical activity. Substantial weight loss can reduce ectopic fat stores in all organs and this is associated with an improvement of the function of that organ. (Snel et al. 2012)

In the latter case, non-invasive weight loss interventions like diet or exercise can decrease ectopic fat (particularly in heart and liver) in overweight or obese children and adults. (Hens et al. 2017)·(Hens et al. 2016)

1.4.1.6 Free fatty acids

Free fatty acids (FFAs) are digested from lipoproteins by lipoprotein lipase (LPL) and enter the adipocyte, where they are reassembled into triglycerides by esterifying them onto glycerol. There is about 87% lipids contained in human fat tissue.(Thomas 1962) There is always a constant flux of FFAs going in and out of adipose tissue. The total direction of this flow is controlled by the hormones, insulin and leptin. When insulin is elevated, there is a net inward flux of FFA, and only when insulin is low can FFA leave adipose tissue. Insulin secretion is stimulated by high blood sugar, which results from consuming carbohydrates.(Amitani et al. 2013)

Fat cells have a very important physiological role in maintaining triglyceride and free fatty acid levels, as well as determining insulin resistance. Abdominal fat has a different metabolic profile—being more prone to induce insulin resistance. This explains to a large degree why central obesity is a marker of impaired glucose tolerance and is an independent risk factor for cardiovascular disease (even in the absence of diabetes mellitus and hypertension).(Dhaliwal and Welborn 2009) Studies of female monkeys at Wake Forest University (2009) discovered that individuals suffering from higher stress have higher levels of visceral fat in their bodies. This suggests a possible cause-and-effect link between the two, wherein stress promotes the accumulation of visceral fat, which in turn causes hormonal and metabolic changes that contribute to heart disease and other health problems.(Park 2009)

Recent advances in biotechnology have allowed for the harvesting of adult stem cells from adipose tissue, allowing stimulation of tissue regrowth using a patient's own cells. In addition, adipose-derived stem cells from both human and animals reportedly can be efficiently reprogrammed into induced pluripotent stem cells without the need for feeder cells.(Sugii et al. 2010) The use of a patient's own cells reduces the chance of tissue rejection and avoids ethical issues associated with the use of human embryonic stem cells.(Atzmon et al. 2002) A growing body of evidence also suggests that different fat depots (i.e., abdominal, omental, pericardial) yield adipose-derived stem cells with different characteristics.(Baglioni et al. 2012) These depot-dependent features include proliferation rate, immunophenotype, differentiation potential, gene expression, as well as sensitivity to hypoxic culture conditions.(Russo et al. 2014) Oxygen levels seem to play an important role on the metabolism and in general the function of adipose-derived stem cells.

Adipose tissue is a major peripheral source of aromatase in both males and females, contributing to the production of estradiol. Adipose derived hormones include:

- Adiponectin
- Resistin
- Plasminogen activator inhibitor-1 (PAI-1)
- TNFα
- IL-6
- Leptin
- Estradiol (E2)

Adipose tissues also secrete a type of cytokine (cell-to-cell signalling proteins) called adipokines (adipose cytokines), which play a role in obesity-associated complications. Perivascular adipose tissue releases adipokines such as adiponectin that affect the contractile function of the vessels that they surround.(Birbrair et al. 2013)

1.4.2 Various types of fat in determining the risk of obesity

The risk of obesity varies among genders and ethnicities. Fat content located under the belly or around the organs are known as subcutaneous adipose tissue (SAT) and visceral adipose tissue (VAT), respectively (Fig 1-3). (Thomas et al. 2013) At comparable levels of total adiposity (measurement either from BMI or MRI), women have more SAT in both the gluteofemoral and abdominal area, and relatively lower VAT than men of the same ethnicity. Interestingly, the VAT content difference between the two genders is minimized in elder groups. Meanwhile, women from Asian countries such as China or South Asian have higher VAT content than Caucasians. (Karastergiou et al. 2012) Researchers revealed that deep subcutaneous adipose tissue (DSAT), superficial subcutaneous tissue (SSAT) and body fat mass (BFM) were higher in South Asians than in European men, (Puhl and Heuer 2010) and Asians are found to have higher proportions of VAT accumulation but lower SAT than Caucasian populations. (Deurenberg, Deurenberg-Yap and Guricci 2002) Women with Asian ancestry even have greater adiposity than those from a Mixed or "White ethnicity". (Morimoto et al. 2012) The report on the relationship between body composition and various ethnic groups was reported briefly by Stone et al. (2008) who conducted research on European students, finding that students with South Asian ancestry had higher body fat percentages than their

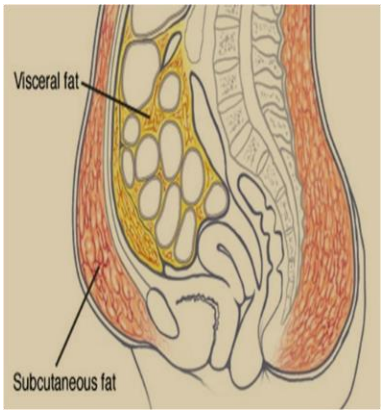

Figure 0-3 Dispersion of adipose

European counterparts. Asians are reported to have at least a two times higher prevalence of diabetes in comparison to Caucasians of the same age group. (Maskarinec et al. 2009) The study conducted by Wang identified that there were differences in both body fat distribution and the risk of obesity related diseases between Chinese and Caucasian males in China. The same author also found that Chinese males had more body fat and central fat accumulation than Caucasians. Kagawa et al. (2009) stated that when examining the anthropometric markers and fat composition in Caucasian and indigenous Australian children, there is a need for more ethnic-specific screening criteria for assessing obesity status. Sundborn et al. (2007) conducted a study on the prevalence of novel and known MDs as well as the status of glucose tolerance in the New Zealand population, finding that the prevalence of diabetes was higher in some ethnic groups; in comparison to their European counterparts, Pacific Islanders and Māori had 4.2 times and 2.8 times greater prevalence. These findings demonstrate that fat content deposition is highly correlated with ethnicity and gender. This may be affected by differences in body frame and prove that BMI and BF% is ethnic-specific and must be accounted for in the identification of diabetes. In New Zealand, studies have previously found that Māori and Pacific Islanders have higher incidences of obesity and T2DM than the national averages (NZMH), which strongly suggests that the prevalence of OT2D is biased towards specific ethnic groups. Thus, in order to construct a "gold-standard" for OT2D prognosis, ethnicity has to be considered as a crucial factor.

1.4.3 Diabetes risk in different Ethnicities

Various studies have shown that diabetes is correlated with ethnicity. People of native American, Polynesian or Micronesian, Asian-Indian Hispanic, or African-American descent are at higher risk of diabetes compared with people who have European ancestry.(King, Rewers and Group 1993) In NZ, the prevalence of diabetes is highest among Pacific people and lowest among Europeans. The highest and largest proportion of new or known diagnosed diabetics belongs to Pacific men and women aged between 45-64 years. For the prevalence of IGT, Pacific Islanders and Māori in working ages, less than 45 years, have the highest rate. Pacific people constitute almost 8% of the entire NZ population. Māori people also have a disproportionately high rate of diabetes in NZ [15]. Ethnicities have an impact on the complications of T2DM. For example, Māori people tend to suffer from renal complications and die of renal diseases at significantly higher rates than those of European descent. (Joshy et al. 2009) Accordingly, the highest risk populations should be considered as a priority to try any successful treatment for diabetes.

1.5 Clinical Diagnosis for Obesity Type 2 Diabetes

It is strongly believed that an unhealthy lifestyle is directly linked to becoming overweight and obese, which is the leading cause of type 2 diabetes. (Puhl and Heuer 2010) Nowadays, the easiest and most effective clinical prediction of the risk of obesity type 2 diabetes developing is based on anthropometric measurements, including body mass index (BMI), waist circumference (WC), and Body Fat Percentage (BF%). These indices have an established correlation with intra-abdominal obesity in subjects, and are regarded as directive indices for assessing type 2 diabetes prevalence. (Yalçın et al. 2021) In general, the BMI of 24kg/m^2 is regarded as the boundary between being a healthy weight, and being overweight. It is thought that keeping the WC value less than 85cm could help keep half of the metabolic relevant diseases from occurring. Other clinical studies claimed that central body fat distribution, and waist-to-hip ratio (WHR) can also be regarded as risk assessment for diabetes, especially T2D. (Zheng et al. 2011, Kim et al. 2012)

Pre-diabetes is also known as impaired glucose tolerance (IGT). This occurs when glucose in the bloodstream is higher than normal, but not high enough to be called diabetes (Diabetes US). Early-stage insulin resistance is an important cause of failure of glucose transportation from the bloodstream to muscle, the liver, and fat cells where it is used for energy. However, most of the early stage of pre-diabetes can be diagnosed and treated with proper interventions. Thus, finding efficient measurements which can diagnose T2DM is crucial. Rarely have studies been systematically reviewed to summarize the prognosis of diabetes. We reviewed the potential factors that can be used as prognosis of diabetes and are summarized as follows.

1.5.1 Anthropometric measurement

Currently, anthropometric measurements such as body mass index (BMI) and waist circumference (WC) are used as effective indices in diagnosing intra-abdominal obesity in subjects, and are regarded as a direct indicator for assessing type 2 diabetes prevalence. In general, the BMI of 24kg/m^2 is regarded as the boundary between being normal weight and overweight, and notably, if WC values could be lower than 85cm, half of relevant metabolic diseases could be prevented. Other researchers claimed that total body fat (TBF), percentage of body weight (%BW), central body fat distribution, and waist-to-hip ratio (WHR) can be regarded as risk assessment for diabetes, especially T2D. (Zheng et al. 2011, Kim et al. 2012) One study performed their research on Chinese, African American, and Caucasian

subjects and found that BMI had a strong link with high incidence of lipid abnormalities[157]. This link was observed in low density lipoprotein cholesterol (LDL-C) and triglyceride (TG) levels, with minor effects. Truesdale, Stevens and Cai (2011) also indicated that BMI had more impact on lowering levels of high-density lipoprotein cholesterol (HDL-C) in Caucasians than in Chinese or Africans. Huxley et al. (2005) provided useful evidence that showed a link between anthropometric measurements of adiposity and the risk factors for CVD in the same ethnicity both within and across the Asia-Pacific region. The author also suggested using ethnic-specific cut-offs as a tool for management of obesity for each ethnic group.

1.5.2 Prognostic biomarkers of T2DM

When the diabetes symptoms develop, the patient suffers from hyperglycaemia as their bodies are not able to respond to or produce adequate insulin. Despite the tremendous effort put into prolonging the lives of patients with T2DM, it remains the 5th leading death cause globally. It has been estimated that the number of pre-diabetic cases will increase to more than 470 million by the end of 2030. It is undoubtedly a miserable trend. Thus, finding an effective and user-friendly diabetes prognostic system is an urgent matter. Currently the most common treatment recommendation for T2DM remission is through changing one's lifestyle, however, this does not work in the long-term for most patients. There are a few typical biomarkers in the market which are useful for the diagnosis of pre-diabetes. Here is the summary of these biomarkers.

1.5.2.1 HbA_{1c}

HbA_{1c} is now formally endorsed in many countries as a diagnostic test for T2DM and a monitoring tool, although some debate continues regarding its applicability for diagnosis. (Organization 2011) The diagnosis of diabetes is primarily concerned with defining a disease state rather than establishing a reference interval for health. In particular, the evidence base is focused on predicting a clinical outcome, and is considered to be the pinnacle of the Stockholm Hierarchy when applied to reference intervals and clinical decision limits. The major outcomes of interest in diabetes are the long-term microvascular complications, for which a large body of data has been accumulated. The debate surrounding the role of HbA_{1c} as a diagnostic test addresses the relative merits and disadvantages of glucose versus HbA_{1c} and brings into focus many pre-analytical, analytical and other biological considerations, as well as other factors such as cost and accessibility.(Sikaris 2012)

Traditionally, blood glucose levels measured either in the fasting state, or following a standard glucose load, have formed the basis of the diagnosis of diabetes. For OGTT, more extensive

pre-test preparation is required, including a standardized diet for 3 days before the test and a satisfactory period of overnight fasting. The OGTT is a time-consuming process which takes at least 2 hours, and furthermore, a large number of people who cannot tolerate the load of glucose will have an invalid test result. Furthermore, the test needs to be repeated, and thus, few people complete the test. According to a South Australian study, only 27% of hospital patients who indicated a possibility of having diabetes followed through with a diagnostic OGTT. (Valentine et al. 2011) Compared with OGTT, HbA_{1c} is not affected by prandial status and has no diurnal rhythm, allowing measurement at any time of day.

HbA_{1c} gives an indication of chronic glycaemia rather than being a test of glycaemia at a single point in time. It is a relatively integrated indicator of glycaemia over the entire 120-day lifespan of the red blood cell, which logically reflects the level of blood glycaemia. 50% of the HbA_{1c} formed in the month prior to sampling and 25% in the month before that.(Tahara and Shima 1995) It is also a relatively convenient test which is crucial for clinical use; the test does not require the patient to fast and only uses a single blood sample. HbA_{1c} also shows limited pre-analytical variability with no change in the concentration in the collection tube compared to plasma glucose.

The recommendations for HbA_{1c} as a diagnostic test was put forward as early as the mid-1980s but there exist concerns regarding its availability and poor assay standardization prevented its uptake. The international expert committee recommended HbA_{1c} be introduced into diagnostic criteria from 2009.(Committee 2009) The cut-off value was introduced as ≥ 48mmol/mol (≥6.5%), which was also adopted by both the American Diabetes Association (ADA) and the WHO. Individuals with an HbA_{1c} of 39-46 mmol/mol (5.7-6.4%) are considered to be at increased risk for diabetes as well as cardiovascular disease, and are recommended to undertake effective treatment strategies such as weight loss and physical activity, in order to lower the risk. In New Zealand, HbA_{1c} as a diagnostic test was formally established by the New Zealand Society for the Study of Diabetes (NZSSD) from 3rd October 2011. This recommendation was following a two-year period of dual reporting of the United Kingdom, with the cut-off diagnostic value up to ≥ 50 mmol/mol (≥ 6.7%) on double tests in asymptomatic individuals. People with HbA_{1c} in the range of 41-49 mmol/mol are categorized as having ‘dysglycaemia’ or abnormal glucose tolerance, with the recommendation for re-testing in 6-12 months following the implementation of cardiovascular risk management.

However, there are some disadvantages when applying HbA_{1c} as a biomarker. Firstly, the testing result can be affected by haemolysis and other conditions with increased red cell turnover, or conditions with reduced red cell turnover, as with iron deficiency or other chronic disease states. Secondly, test results may vary between age and ethnic groups. Thirdly, it is an expensive test compared to OGTT, and thereby may not be affordable in many low-income communities.

1.5.2.2 Adipokines

Adipokines refer to a series of chemical compounds released from adipose tissue, which not only regulate lipid metabolism, but also function in a wide array of physiological and pathological processes involved in host defence, such as inflammation, apoptosis, autoimmunity, cell differentiation, and organogenesis. (Liang and dong Ye 2019) Examples of adipokines include tumour necrosis factor α (TNF-α), interleukin-6 (IL-6), leptin, plasminogen activator inhibitor 1 (PAI-1), angiotensinogen, resistin, monocyte chemoattractant protein-1 (MCP-1) and C-reactive protein (CRP). Recently, a low serum adiponectin level has been identified as a CVD risk factor.

Insulin resistance can be attributed to pancreatic β-cell failure and is regarded as one of the two key events that leads to the development of type 2 diabetes.(Leahy et al. 2010) In the early stages of the development of disease, insulin resistance is countered by an increase in pancreatic β-cell mass and function which can often delay the diagnosis for a duration of years.(Chang-Chen, Mullur and Bernal-Mizrachi 2008) The β-cell eventually succumbs to rising insulin resistance via various mechanisms (including glucotoxicity, lipotoxicity and endoplasmic reticulum stress) and hyperglycaemia ensues. (Jonas et al. 2009) The ability of maintaining both pancreatic β-cell mass and function is the key to preventing the onset of type 2 diabetes.

The correlation between the adipose tissue and pancreas was believed to be something of a one-way street for many years. It was widely accepted that insulin secretion from pancreatic islets in response to increased blood glucose caused uptake of glucose into adipocytes via insulin receptor binding and signalling, and thus led to the increased storage of triacylglycerol. Insulin resistance in adipose tissue was found to contribute to β-cell failure. (Weir et al. 2001) Our knowledge of adipose tissue has grown immensely, as we have learned over the past few

decades that adipose tissue is not simply inert excess fat which stores energy, but an active endocrine organ with a wide, biologically active secretum. (Deng and Scherer 2010)

Furthermore, the molecular list of adipokines increases every year, as both novel and existing molecules are seen to be secreted by adipose tissue or adipocytes. Most, but not all, adipokines are peptides/proteins with hormone-like properties (some of which are known cytokines), but in this context, non-esterified fatty acids (NEFAs; free fatty acids) can also be considered adipokines. Various studies have shown that the increased accumulation of adipose tissue depots in obesity can cause dysregulated adipokine secretion, representing a potential pathophysiological link between obesity, type 2 diabetes, and vascular disease. (Wellen and Hotamisligil 2005) Research into their correlations in terms of metabolic disorders is ongoing. It is becoming increasingly clear that adipokines form an important part of an 'adipo-insular axis' (Fig. 1-4), the dysregulation of which may contribute to β-cell failure and hence contribute to the development of type 2 diabetes. These characteristics make adipokines a potential biomarker for prognosis.

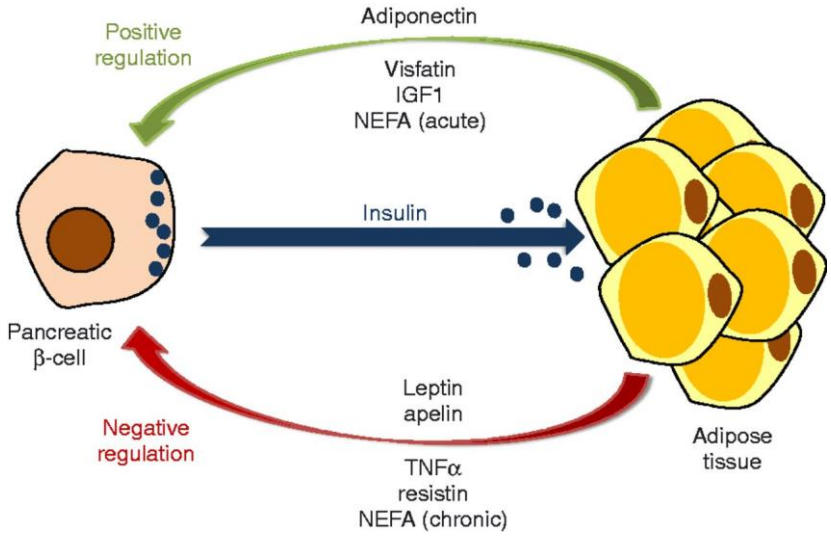

Figure 1-4 Diagrammatic representation of the interrelationship between adipose tissue and the pancreatic β-cell. *Citation: Journal of Endocrinology 216,1;10.1530/JOE-12-0278*

1.5.2.3 miRNA

Detection methods for molecular, single nucleotide polymorphisms, DNA methylation, microRNAs (miRNAs), mRNAs, proteomes, metabolomes, and exosomes have developed rapidly, while also demonstrating their potential as biomarkers for various cancers.(Grant and Golden 2019, Sun et al. 2018) miRNAs are found not only intracellularly but also extracellularly, including body tissue fluids, such as serum, saliva, and nasal secretions.

Extracellular miRNAs were discovered to be a stable substance in serum or plasma due to their presence as protein complexes. Abnormal expression of miRNAs is related to the occurrence and development of many diseases, such as T2DM. (Rome 2013, Banerjee et al. 2017, Sandiford et al. 2018, Yaribeygi et al. 2018) The miRNAs in the serum or plasma are stable and can be repeatedly detected, and therefore, they have the potential to be novel biomarkers for a variety of diseases. Many previous studies have shown that miRNAs are related to the occurrence and development of T2DM. miR-375 and miR-9 were found to be dramatically increased in the peripheral blood of patients with pre-diabetes and T2DM, and are positively related to blood glucose levels.(Al-Muhtaresh and Al-Kafaji 2018) The miR-192 and miR-194 were also demonstrated to be correlated with the development of T2DM. (Fornari et al. 2015) By Solexa sequencing, miR-126-3p, miR-28- 3p, and miR-486-5p were found to be present only in pre-diabetes.(Matsha et al. 2018) In addition, miR184, miR-182-5p, and miR-127-3p are involved in insulin biosynthesis and secretion, and miR-125, miR-29, miR-103/107, and miR-15a are involved in insulin resistance. Through a meta-analysis of reports from PubMed, ENBASE, and ISI Web of Science databases and three Chinese databases, miR-148b, miR-223, miR-130a, miR-19a, miR26b, and miR27b were found to be potential biomarkers for T2DM.(Liang et al. 2020)

1.5.3 Intra-organ adipose tissue and T2DM

It has been well established that fat contents, especially VAT, have a huge impact on T2D. (Camastra et al. 2017) Obese people have a primary defect in beta cells before the progression to impaired glucose tolerance. Research showed that beta cell mass in diabetes samples was 35 % lower than the control group, and when BMI and type of treatment were taken into account, this figure increased to 39 %. (Cali et al. 2009, Rahier et al. 2008) Although progression to type 2 diabetes occurs more frequently in obese humans compared to lean individuals, this association is highly dependent on genetic background. (Guilherme et al. 2008) It is generally accepted that two features are particularly critical for obesity to develop into type 2 diabetes. First, impaired responsiveness of skeletal muscle to insulin is a primary condition in obesity and a precondition for the onset of type 2 diabetes.(Sims et al. 1973) The association between obesity and skeletal muscle insulin resistance is probably a causal relationship, as studies in humans and animals indicate that weight loss and gain correlate with increasing and decreasing insulin sensitivity, respectively. (Freidenberg et al. 1988) Second, a defect required

for progression from insulin resistance to type 2 diabetes is the failure of β-cells to secrete the required levels of insulin that maintain normal fasting blood glucose levels. (Rhodes 2005)

1.5.3.1 *Relevant obesity metabolism pathways that can cause Type 2 Diabetes*

Plasma free fatty acids (*FFA*) play important physiological roles in skeletal muscle, as well as the heart, liver, and pancreas. High concentration of FFA is linked to insulin resistance in skeletal muscle by a decrease in GLUT-4 translocation. (Boden and Shulman 2002) In the liver, elevated FFA may lead to hyperglycaemia by antagonizing the effects of insulin on endogenous glucose production. However, it is still under discussion how FFA affects insulin secretion in pancreases. These facts show that FFA are close to being a vital therapeutic target in obesity and T2D. (Butler et al. 2003a) Thus, discovery of new targets that regulate fatty acids in adipocytes might ultimately lead to therapeutic modalities that can prevent insulin resistance and type 2 diabetes mellitus. Tissue inflammation is another binding phenomenon of insulin resistance. Fat cells actively release molecules called adipokines, such as Interleukin-6 (IL-6), Monocyte chemotactic protein-1 (MCP-1), and Tumour necrosis factor-alpha (TNF-α), which can have negative effects on the rest of the body in terms of insulin resistance and cancer. (Coppack 2001) This complex fat metabolism process also involves many organs in the human body which release various hormones and metabolic factors which can be influenced by the lesions that turn normal adipocytes into adipose tissues. For instance, *Adiponectin* (which is secreted by normal adipocytes) has anti-atherogenic and anti-inflammatory effects, is involved in regulating glucose levels and fatty acid breakdown, but is significantly reduced in obese patients. Studies show that lower levels of adiponectin are greatly linked to the risk of insulin resistance and disrupting the normal function of beta cells. (Arslanian et al. 2017) *Irisin*, which is secreted from muscle tissue, is a protein that is encoded by the FNDC5 gene. (Erickson 2013) Researchers found that there are two types of fat cell tissue in the human body: white and brown fat. When upregulating the dose of a protein called UCP1, which contributes to the browning of white fat, it was found that markers indicating the browning of white cells and fat cells were more metabolically active. (Jeremic, Chaturvedi and Tyagi 2017) Obesity patients with higher FNDC5/Irisin levels have a better metabolic profile, lower lipopolysaccharide levels and type 2 diabetes risk. (Bonfante et al. 2017) Fibroblast growth factor 21 (*FGF 21*) is a highly reserved protein in mammals that is encoded by the FGF21 gene. The protein is a member of the fibroblast growth factor (FGF) family and specifically a member of the endocrine subfamily, including FGF23 and FGF15/19, which act through a family of four FGF receptors.(Nishimura et al. 2000) FGF21 is produced mainly in the liver and promotes fatty

acid oxidation, improves insulin sensitivity and increases energy expenditure. (Owen, Mangelsdorf and Kliewer 2015) FGF21 is paradoxically increased in obesity, suggesting that obesity is a FGF21-resistant state. (Chui et al. 2010) Both FGF19 and FGF21 have been involved in the etiopathology of obesity and T2D, representing potential therapeutic targets for the treatment of these metabolic diseases. (Angelin, Larsson and Rudling 2012)

1.5.3.2 Pancreatic fat

Tabak performed a prospective occupational cohort study to characterize trajectories of diabetic markers such as glucose concentration, insulin sensitivity, Tabák et al. (2009) and insulin secretion, finding that these indicators changed as much as 3 to 6 years before patients were diagnosed with diabetes in the 13 years of follow-up. Horng-Yih investigated the correlation of fat content in the pancreas and non-alcoholic fatty liver disease (NAFLD) and found that a fatty pancreas was positively related to prediabetes and diabetes in Chinese male subjects. Horng-Yih et al. (2013) In female samples, no significant difference had been observed. Cali et al. (2009) revealed that obese people have a primary defect in beta cells before the progression to impaired glucose tolerance. Tushuizen found that pancreatic fat may play a role in beta cell dysfunction and further type 2 diabetes by using MRS and oral glucose tolerance test (OGTT) in susceptible people, Tushuizen et al. (2007) but this finding has been disputed by Saisho, Butler, and Butler (2008) because of inadequate sampling. Bagust developed a model to assess beta cell function that may be used for further strategies in preventing diabetic complications and therapy plans. Bagust and Beale (2003) The same author also suggested brief strategies for coping with the decline of beta cell function for the three questions proposed.

Macauley found that DM patients on Metformin therapy alone had nearly 33% less mean pancreatic volume than control subjects, and this volume was positively correlated with HOMA-beta in type 2 DM and control subjects. Macauley In contrast, DM patients had 23% more pancreatic triglyceride than the control group. Pancreatic fat fractions can be measured by using the CT technique as demonstrated by Lim, who conducted a multi-row computed tomography with a 64 detector-row scanner for measuring pancreatic fat content and volume. Lim They performed the measurements in T2D patients who had varied durations of the disease, and found that patients with T2D had smaller pancreatic volume, but higher fat contents. Kreel also used a CT scan approach to assess normal pancreas sizes in post-mortem samples and

normal patients in order to establish average sizes of the pancreas' head, neck, body, and tail. Kreel, Haertel and Katz (1977)

Pancreatic fat content plays an important role in the clinical consequences in youth aged 8-18 years old, but to a lesser degree than visceral and liver fat. (Cohen et al. 2014) The authors found the range of the hepatic fat fraction to be between 0 to 36 % in youths. Ventura assessed ethnic and gender variations in pancreatic fat fraction (PFF) and related this fraction to other fat depots, and markers. Lê et al. (2011) The authors found that PFF is higher in Hispanics than in African Americans and this figure increases substantially with age. They proposed that this fat content may have a close link to the increasing risk for type 2 diabetes and other metabolic disorders.

Pancreatic fat, along with hepatic fat, also contributes to obesity. This contribution was identified by Rossi who used in-phase and out-of-phase magnetic resonance imaging (MRI) sequencing for measuring the lipid content of both organs, and found that obese men had higher visceral adipose tissue and ectopic fat deposition than obese women. Rossi et al. (2011) MRI can be used as a tool for predicting fat content in both the liver and pancreas. Sijens established that the median fat content in the pancreas was 2.7% (interquartile range: 1.0% - 6.5%) which was correlated with the liver, BMI, and subcutaneous fat. Sijens et al. (2010) The authors also pointed out that renal fat content was not observed in obese people and this fat may not contribute to the pathogenesis of renal disease in obese patients.

Zyromski analysed pancreatic lipids by using metabolomics analysis and conventional chromatography, such as thin layer chromatography and gas chromatography, and found a positive correlation within the analysed methods. Zyromski et al. (2009) They also proposed that metabolomics analysis may be used in further research for the definition of other mechanisms in pancreatic disease. In an animal model, Pinnick demonstrated that high-fat diets had an impact on pancreatic fat by using morphometric and chromatographic techniques. Pinnick et al. (2008) They also studied pancreatic fat in post-mortem pancreatic samples and revealed that it had a positive correlation with type 2 diabetes. Maggio quantified pancreatic fat in lean and obese adolescents and found a positive correlation between this fat and the presence of metabolic syndrome and other markers. Maggio et al. (2012) This finding may be a clue as to why beta cell dysfunction occurs in young people before they are diagnosed with diabetes. Butler examined post-mortem samples and assessed beta cell mass in both lean non-

diabetic humans and in those with type 2 diabetes. Butler et al. (2003b) They found that beta cell mass decreased in type 2 diabetes via apoptosis processes and proposed that therapeutic approaches other than glycaemic control alone should be introduced to stop this process.

In recent years, with the rapid development of computed tomography (CT) and magnetic resonance imaging (MRI) techniques, the intra-fat content has also been employed as a diagnostic indicator of OT2D, providing a non-invasive way to gather results that are more accurate and reliable than the indexes of anthropometric measurements. Compared to BMI, the factor of VAT has greater correlation with heart disease and diabetes.(Wajchenberg 2000, Wisse 2004) However, the fat content from various adipose tissues carry different 'weight' in terms of OT2D diagnosis.

A study done in 2004 showed that patients who instantly lost 30 pounds of SAT through liposuction surgery had no health improvement if significant amounts of VAT remained. (Reynolds et al. 2006) Risk factors, such as blood pressure, cholesterol, and insulin sensitivity, are not improved with loss of SAT from liposuction operations.

Among the areas of VAT analysis for the purpose of OT2D diagnosis from different internal organs, increased attention has been given to the pancreatic fat in recent years. The pancreas plays a critical physiological role in maintaining glucose homeostasis and energy metabolism. Recent studies have reported the clinical relevance of pancreas volume (PV) to some metabolic disorders, find that PV shrank in the patients with type 1 diabetes (T1DM) and type 2 diabetes (T2DM), (Goda et al. 2001b, Burute et al. 2014, Williams et al. 2020) and pancreatic fat content increased in the individuals with T2DM (Garcia, Rech and Leitão 2017). Some studies reported the associations between metabolic disorders and either ectopic fat deposition in the pancreas(Singh et al. 2019, Singh et al. 2017a, Singh et al. 2017c, Singh et al. 2017b) or pancreas size, which is determined by pancreas diameter, area, and length.(Desouza et al. 2018a) Thus, quantification of these changes in the pancreas shows great promise with regards to diagnosis, treatment, and reduction of metabolic disorders. However, using such changes of pancreatic features as a diagnostic indicator for OT2D requires further research and validation. In our study, we intend to fill this gap.

1.6 Diabetes Treatment

The treatment of T2DM has to follow three methods. Firstly, risk reduction of microvascular complications, such as eye and kidney diseases, via glycaemic control and blood pressure management. Secondly, risk mitigation of macrovascular complications, such as CVDs and peripheral vascular disease, via controlling lipids, high blood pressure (or hypertension) management, and smoking cessation. Third, risk reduction of metabolic and neurological diseases through glycaemic control.(Inzucchi et al. 2012) Chronic illnesses such as diabetes and obesity require self-management skills along with medical treatment in order to be treated successfully. Stages of lifestyle changes associated with management of illness include pre-contemplation, contemplation, preparation, action, and maintenance. (Bazata et al. 2008) However, there are no strong solutions which can prevent individuals from developing metabolic diseases such as obesity and diabetes over extended periods of time. Even with numerous studies done across the years, the concept of the normalisation of blood glucose has not been universally accepted as a prevention of diabetes or its complications.(Rotella and Mannucci 2013) Even through an intensive glucose lowering management program, the risk of diabetes complications in a short period was shown to increase. It is of vital importance to find a solution which can control diabetes for a longer period of time.

1.6.1 Diet and Exercise

There is a direct correlation between diabetes and obesity. (Prevention 2018) Thus, weight loss can seemingly reduce the incidence of diabetes. The first step to reduce weight is to make and maintain a healthy lifestyle with habitual exercise. It has been found that a mean weight loss of 11 kg reduced blood glucose from 10.4 to 7 mmol/L. (Goulding et al. 2007) Exercise which increases muscle mass and reduces weight and adipose tissues can effectively reduce the destructive effects of diabetes. Visceral fat can be caused by excess cortisol levels. At least 10 MET-hours per week of aerobic exercise leads to visceral fat reduction in those without metabolic-related disorders. (Ohkawara et al. 2007) Resistance training and caloric restriction also reduce visceral fat, although their effect may not be accumulative. Both exercise and hypocaloric diets cause loss of visceral fat, but exercise has a larger effect on visceral fat versus total fat.(Verheggen et al. 2016) High-intensity exercise is one way to effectively reduce total abdominal fat.(Irving et al. 2008) An energy restricted diet combined with exercise will reduce total body fat and the ratio of visceral adipose tissue to subcutaneous adipose tissue, suggesting a preferential mobilization for visceral fat over subcutaneous fat.(Ross and Rissanen 1994)

Other than exercise, a very low-caloric diet (VLCD) is also a well-known intervention for the remission of T2DM, whose mechanism is quite similar to bariatric surgery. When using a VLCD, which reduces energy consumption to 1,100 kcal/d, people with T2DM were found to lose weight and have a superior effect to reduce FPG compared to individuals who do not change their lifestyle. (Tsai and Wadden 2006) Four to five kilograms of weight loss is significantly correlated with improving IR and hyperlipidaemia along with hypertension. Six kilograms of weight loss was reported to significantly increase insulin sensitivity, but a calorie restriction diet has no positive impact on pancreatic beta cells' capacity to release insulin.(Marchal et al. 2012)

However, long-term lifestyle changes such as more exercise and less food intake do not have a promising effect on the remission of diabetes and obesity.(Wilding 2014) Compared with exercise, weight loss by long-term energy restriction interventions such as VLCD caused some serious problems with malnutrition. (Rynders et al. 2019) People with diabetes need to take extra care in nutritional evaluation, and replace harmful eating with a realistic dietary plan. Exercise plays a vital role in maintaining blood glucose levels by increasing the sensitivity of insulin. (Horton 1988) However, it also causes serious consequences if it is not managed properly, such as hypoglycaemia. Exercise is time-consuming and by itself has only a modest influence on losing weight. Thus, most people with diabetes take medicine rather than commit to long-term exercise.

1.6.2 Pharmacotherapy

Pharmaceutical agents are now widely applied for the treatment of diabetes even though there is no guarantee of being cured.(Crandall et al. 2008) Some medications have been used to control body weight between 5 and 10 percent in a year while maintaining good glycaemic control.(Pratley et al. 2011) We still do not have a medicine which can act as a reliable long-term intervention for diabetes. Although many pharmacotherapies have been employed in the treatment of diabetes, the results are not as good as caloric restriction diets and bariatric surgery.(Holst et al. 2018) Combined with the application of any pharmaceutical agent, the side-effects are an issue that cannot be waived off, and weight loss alone is not always associated with an improvement in glucose metabolism.(Ross et al. 2000) Most people with diabetes are potentially on multiple medications, overweight, or obese, and when more pharmacological agents are taken, it can result in unexpected side effects and high monetary

costs.(Sadeghabadi et al. 2021) For instance, one study showed that 70% of diabetic patients who take medications are overweight or obese.(Scheen et al. 2006) If they are not treated appropriately, they are likely to gain more weight and increase waist circumference, blood pressure, and the risk of CVD. Thus, IR may be worse, and consequently, there is a rise of microvascular-related mortalities caused by T2DM. The function of pharmacotherapy in diabetes requires further investigation, and a procedure for the remission of diabetes should consider some important criteria, including being reliable, safe, user-friendly, and economical.

1.6.3 Bariatric surgery

Currently, bariatric surgery is one the most effective ways to treat obese diabetic patients, and four bariatric procedures are being used conventionally, namely: laparoscopic gastric bypass (LGBP), laparoscopic sleeve gastrectomy (LSG), laparoscopic adjustable gastric band (LAGB) and biliopancreatic diversion with/without duodenal switch (BPD-DS). Emerging data suggests that bariatric surgery provides a more sustained and effective treatment for obesity and T2D. (Buchwald et al. 2004, Sjöström et al. 2004)

It has been reported that significant metabolic improvements are seen in obese diabetic patients within days after surgery before any significant change in BMI has occurred, (Wickremesekera et al. 2005) which cannot solely be explained by mechanical restrictions of meal size and/or malabsorption of nutrients. Growing evidence shows that the beneficial metabolic effects of bariatric surgery are likely to be caused at least partially by other factors such as bile acids, blood lipids and cytokines change. (Gerhard et al. 2013) The mechanism of action of each type of surgery is still under investigation.

The most common bariatric surgery procedures are sleeve gastrectomy (LSG) and Roux-en-Y gastric bypass (LGBP). LGBP combines a restrictive and malabsorptive component leading to significant weight loss but is a technically complex operation with a steep learning curve. This procedure provides a mean excess weight loss of 61.6% following LRYGB and a T2D resolution rate of 83.8%. SG is a predominantly restrictive procedure that is gaining popularity due to its relatively lower technical complexity, with a mean excess weight loss of > 45% (range 6.3-74.6%) and T2D resolution rate ranging from 47 – 94% of patients at 1 year with a mean of 66.2% reported.(Yip, Plank and Murphy 2013) In comparison with GBP, SG is a relatively simple and less expensive surgery procedure. The influence of both types of surgery

on the possible key metabolic mediators mentioned above, including bile acids, cytokines, blood lipids and organ fat, is still under investigation. However, it is unknown whether liver and pancreatic fat is immediately reduced along with the observed metabolic improvement.

The prevalence of obesity has increased and become a global health issue. Relevant chronic diseases such as T2D, CVD, and cancer account for 84% of health care costs.(Moses et al. 2013) Nowadays, bariatric surgery is regarded as the best treatment for obesity and can dramatically reduce the morbidities of diabetes, CVDs, and cancer.(Buchwald and Oien 2013) By using bariatric surgery, large numbers of people have lost weight effectively. However, the mechanism causing the resolution of diabetes which arises from this surgery is yet to be fully understood.(Holst et al. 2018) There are several types of bariatric surgeries with or without a duodenal switch, including: gastric bypass or RYGB, SG, biliopancreatic diversion (BPD), and adjustable gastric band shown in **Figure 1-5.**

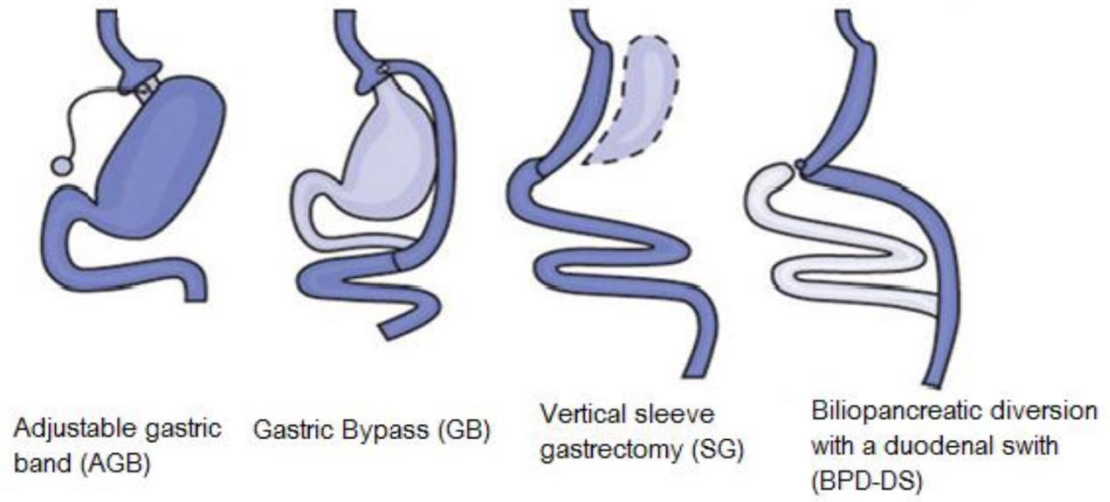

Figure 0-5 Four common different types of bariatric surgeries *(Vetter et al., 2012)*

Different types of bariatric surgeries have different influences on diabetes remission. Each type of bariatric surgery shares the common goal of initiating weight loss by restricting calorie intake, however, this surgery can cause complications such as intestinal malabsorption, enzyme and hormonal alterations, and structural differences in the digestive system. We can hypothesize that the remission of diabetes may be correlated with the weight loss.(Turnbaugh et al. 2009) All bariatric surgeries follow malabsorption, restriction or a mixture of both. It has been documented that bariatric surgery in the improvement of T2DM acts through modulation of Bas, gut microbiota, and the alteration of incretin hormones. In clinical settings, the most efficient types of bariatric surgeries for the remission of diabetes are RYGB and SG.(Mantziari et al. 2020)

1.6.3.1 Fat changes after bariatric surgery

Bariatric surgery is gaining acceptance as an effective treatment for obese patients. Weiss et al. (2009) revealed that visceral fat and subcutaneous fat were reduced by 35% and 32% after the surgery, respectively. Kashyap et al. (2013) assessed the effect of different types of bariatric surgeries on insulin sensitivity and pointed out that gastric bypass has a more beneficial effect in restoring beta-cell function than sleeve gastrectomy. Not only reducing fat contents, but bariatric surgeries also cause reductions in BMI and waist and hip circumference by the reduction of fat tissue. (Jastrzębska-Mierzyńska et al. 2015)

According to Toro-Ramos et al. (2015), body composition was continuously reduced for 1 year in a follow-up study conducted in female subjects. Gaborit et al. (2015c) used the MRS technique to determine the effect of bariatric surgery toward ectopic fat in the pancreas, finding that there was a positive effect of bariatric surgery in reducing fat content of T2DM patients. Furthermore, bariatric surgery also has an impact on epicardial fat volume (Gaborit et al.). (2012) However, the acute effect of bariatric surgery on fat contents remains unclear and requires further investigation.

1.6.3.2 Potential change factors after Bariatric surgery

Free fatty acid changes after bariatric surgery has been reported by Kashyap et al. (2010) who performed a study in RYGB patients, finding that this surgery provides a more rapid improvement in glucose regulation compared with GR. This improvement is accompanied by enhanced insulin sensitivity and beta-cell responsiveness to glucose. The reduction in free fatty acids (FFAs) after bariatric surgery had been observed with the number of roughly 40-50%, and the reduction of FFA levels in post-surgery samples supported the notion that there was a reversibility of insulin resistance after bariatric surgery. (Benedetti et al. 2000) The relationship between FFAs and insulin resistance was first described by Randle et al. (1963), in that oxidation of FFAs impacts glucose oxidation and leads to a reduction of glycolytic flux. The mechanism related to the reduction of insulin resistance after bariatric surgery needs further study, however, Mingrone et al. (1997) proposed that the reduction in plasma lipids, rather than weight loss, is the cause of the reversibility of insulin resistance. The experiment in which FFA had an effect on glucose and glycogen in moderately obese women was performed by Bevilacqua et al. (1987). The authors proposed that an acute increment in plasma FFA levels induces hepatic insulin resistance and observed that an increase in endogenous glucose production is sustained by hepatic gluconeogenesis. Roden et al. (1996) pointed out that free fatty acids induce insulin resistance in humans by the initial inhibition of glucose

transport/phosphorylation which is then followed by a 50% reduction in both the rate of muscle glycogen synthesis and glucose oxidation. The changes of other pro-inflammatory cytokines are rarely reported. A study found that while the sample size of its participants was low, significant increases in adiponectin levels 2 weeks after surgery were observed in the subcutaneous adipose tissue. Serum adiponectin in LRYGB patients showed an increasing trend, while MCP-1 showed a decreasing trend post-surgery. There was no difference in TNF-α among the groups. (Sams et al. 2016) Therefore, detecting the acute changes of FFAs and other pro-inflammatory cytokines should be further investigated in post-bariatric surgery studies.

1.7 Methods for pancreatic fat content measurements and its correlation to diseases

The development of modern imaging techniques, such as CT and MRI, makes it possible to investigate internal organ composition. Many researchers have investigated this process. Kim used CT scans and attenuation indices to assess pancreatic fat in a patient undergoing surgery, finding a positive correlation with glucose metabolism after adjustment for related variations. Saisho et al. (2007) assessed pancreas volume using CT scan imaging techniques in subjects whose age ranged from birth to late adulthood, finding that there was a substantial increase in volume up until 20 years of age. Volume remains constant for people between the ages of 20 to 60 years old and declines thereafter. The same author also found no difference between normal subjects and diabetic patients. Goda et al. (2001a) measured pancreatic volume by using helical computed tomography and explored the relationship with other indicators. The author found that this fat was strongly correlated with body surface area in both healthy and type 1 diabetes subjects. The same author also found that pancreatic volume was reduced in patients with type 1 diabetes.

On the other hand, MRI techniques allow non-invasive in vivo quantification of pancreatic fat and have higher sensitivity than CT. MRI allows not only the detection of the abnormalities of the pancreas' structure but also the quantification of the dimension and composition of the organ based on various imaging parameters. Although the price is comparatively high, MRI protocol is currently regarded as one of the most efficient methods for measuring areas of adipose tissues in humans.(Mitsiopoulos et al. 1998) MRS is an important MRI protocol and is generally regarded as the gold-standard non-invasive technique for *in vivo* fat and its

metabolic quantification in vast clinical trials. It is typically used for the measurement of liver fat, (Kim et al. 2008, Thomsen et al. 1994) tissue composition, (Machann et al. 2003) myocellular adipose tissue,(Ren et al. 2008) and brain metabolites. *Szczepaniak, et al.* established abdominal MRI protocols by using adult mini-pigs as a model in comparison with human subjects.(Szczepaniak et al. 2005) This method was highly reproducible and was consistent with other measurements such as CT scans and suggested that these methods can be useful for further studies. *Heni, M., et al.* studied fat content in the pancreas by using MRI and found a positive correlation with BMI, visceral adipose tissue and waist circumference.(Heni et al. 2010) The author found that this fat had a negative association with insulin secretion and has more influence than visceral fat to determine insulin function of the pancreas. *Lingvay, I., et al.* validated magnetic resonance spectroscopy and quantified fat contents in humans and rats and revealed that the median pancreatic triglyceride contents to water ratio were as follows: 0.46 % in normal group, 3.16 % in overweight or obese subjects except in the normoglycemic control group, 5.64% in impaired fasting glucose or impaired glucose tolerance group, and 5.54% in untreated T2D. Lingvay et al. (2009a) The author also pointed out that the method has good reproducibility and could be useful for ectopic pancreatic fat studies. *Patel, N.S., et al.* using a novel MRI technique to determine pancreatic fat, found that these fat contents have a positive correlation with hepatic steatosis but are inversely correlated with liver fibrosis.Patel et al. (2013b) *Niraj, S.P., et al.* extended the use of MRI measurements in analysing non-alcoholic fatty liver disease (NAFLD) patients to compare fat content in the pancreas with insulin resistance and liver fat. They found that NAFLD patients had a higher pancreatic fat content that correlated strongly with insulin resistance. Niraj et al. (2013) *Szczepaniak, et al.* also used proton magnetic resonance spectroscopy to measure hepatic and pancreatic fat levels in a Hispanic population. Szczepaniak et al. (2012a) They proposed that pancreatic fat levels should be used as a novel biomarker for pancreatic beta cell dysfunction. Over the past 20 years, huge improvements made on Dixon's reconstruction algorithms enabled an advanced 3-dimensional (3D) imaging technique called Iterative Decomposition with Echo Asymmetry and Least squares estimation (IDEAL) for MRI images.(Hardy, Hinks and Tkach 1995, Xiang 2006) IDEAL provides more reliable resonance offsets of separating fat and water images by optimizing their signal-to-noise ratio, which could have been difficult to calculate due to the impact of magnetic field nonuniformity. (Reeder et al. 2005) Some researchers tried using IDEAL (Iterative Decomposition with Echo Asymmetry and Least square estimation) for assessing hepatic and pancreatic fat and there was good agreement with Single-voxel (1H)

proton magnetic resonance spectroscopy from the interference of surrounding fat.Hu et al. (2010a)

Both IDEAL and MRS are based on the chemical-shift principles, where the resonant frequencies of protons in water and the primary methylene groups $(-CH_2-)_n$ of triglyceride fatty acid chains are separated at around 3.4 p.p.m. in the magnetic field. The water is characterized by a single spectral peak, whereas the fat tissue includes several continuous minor peaks, which represent methyl, olefinic, and carboxyl groups respectively. These peaks have slightly different chemical shifts with respect to water.(Brix et al. 1993) Compared with MRS, IDEAL, and particularly the multi-fat-peak T_2*-IDEAL, is a 3D imaging technique which presents spatial information and yields fat-to-water ratio by systematically evaluating the transverse relaxation and intravoxel dephasing effects in the acquired MRI signal. This enables a more accurate measure of the proton ratio between fat and water underlying tissues.(Yu et al. 2008)

Quantification of fat deposition inside relatively small organs such as the pancreas is still challenging as it is based on delineating tissues entirely within the pancreas. MRI has been reported to be unreliable at times when evaluating the fat value in small organs such as the pancreas. Values of greater than 20% in excess of histological estimation have been reported. (van der Zijl et al. 2011, Gaborit et al. 2015a) Quantification of the percentage of fat within the parenchyma of the pancreas is challenging as it depends upon delineating tissue entirely within the organ. A normal pancreas has an irregular border, but even more so in type 2 diabetes. As the irregularity of the pancreas has been reported to be directly proportional to its fat content distribution,(Al-Mrabeh et al. 2016) it is possible that any interlobular intrusion of visceral fat might be interpreted as intra-pancreatic fat and therefore cause an overestimate of the true value. Further, the volume of pancreas is decreased by 30% and 50% in recent onset T2D patients and those who have been troubled by the disease for greater than 10 years, respectively. This has made it more difficult to draw an accurate T2D diagnostic conclusion for patients based on their pancreatic fat content in comparison to the non-diabetic group because of the obscurity of small differences in true parenchymal fat content.(Macauley et al. 2015)

1.7.1 Segmentation of pancreas

The pancreas plays a critical physiological role in maintaining glucose homeostasis. Thus, precise characterization of the pancreas has the potential for improving diabetes risk stratification and treatment selection.

1.7.1.1 MRI techniques and Manual segmentation of pancreas

Although the price is comparatively high, Magnetic resonance imaging （MRI）protocol is currently regarded as one of the most efficient methods for measuring the areas of adipose tissues in humans. (Mitsiopoulos et al. 1998) Szczepaniak et al. (2013a) once established abdominal MRI protocols by using adult mini-pigs as a model, and compared them to human subjects. This method was highly reproducible and had a strong congruence with other measurements such as CT scans, and suggested that these methods can be useful for further studies. Other than MRI, some researchers have used CT scans and CT attenuation indices to assess pancreatic fat in surgical specimens, often finding a positive correlation with glucose metabolism after adjusted with related variations. Kim et al. (2014a) Pancreas volume was assessed by using the CT scan imaging technique in various samples with ages ranging from birth to late adulthood, and this study identified a substantial increase in volume until 20 years of age. Saisho et al. (2007) The volume remains constant for people between the ages of 20 to 60 years old and declines thereafter. The same author also found no difference between normal subjects and diabetes patients. Other researchers tried using other techniques, such as IDEAL (Iterative Decomposition with Echo Asymmetry and Least square estimation), for assessing hepatic and pancreatic fat, which produced results in line with Single-voxel (1H) proton magnetic resonance spectroscopy from the interference of surrounding fat.Hu et al. (2010a) Pancreatic volume was measured by using helical computed tomography in order to explore its relationship with other indicators. Goda et al. (2001a) The same author found that this fat was significantly correlated with body surface area in both healthy and type 1 diabetes subjects. The same author also found that pancreatic volume was reduced in patients with type 1 diabetes. Traditional intra-organ investigating techniques such as computed tomography (CT) has lower response sensitivity of fat tissue gradients in the pancreas. (Patel et al. 2013a, Kim et al. 2014b) Over the past two decades, progress made in magnetic resonance imaging (MRI) processing along with the development of reconstruction algorithms have dramatically improved MRI techniques, and enabled advanced fat fraction quantification function to what is now called proton density fat fraction mapping (PDFF). (Stine et al. 2021) PDFF, which is currently regarded as the most practical and meaningful MR-based biomarker of tissue fat fraction, (Reeder, Hu and Sirlin 2012) provides a reliable fat fraction result by exploiting the difference in resonance frequencies of protons in water and fat. (Mashhood et al. 2013)

Based on MRI techniques, many recent studies have reported associations between reduced pancreas volume (PV) (determined by pancreas diameter, area, and length) and type 1 diabetes (T1DM) and type 2 diabetes (T2DM), (Goda et al. 2001b, Burute et al. 2014, Desouza et al. 2018a, Macauley et al. 2015) while others have reported an increase in ectopic fat deposition in the pancreas in individuals with T2DM. (Garcia, Rech and Leitão 2017, Garcia et al. 2018, Singh et al. 2019, Singh et al. 2017a, Singh et al. 2017c, Singh et al. 2017b, Al-Mrabeh et al. 2016) Recently, mendelian randomization studies have documented a causal role for pancreatic fat (and volume) in type 2 diabetes. However, pancreas segmentation using MRI is challenging due to the high variability in its size, texture, and location among different individuals. The relative softness of the pancreas means it is easily squeezed by the surrounding organs, which reduces the demarcation of the boundaries of the pancreas and causes it to collide with other non-pancreatic soft tissues, such as the small intestine, blood vessels, and visceral adipose tissues of the abdomen. Consequently, measurements of pancreatic volume and fat deposition by MRI are highly variable (Szczepaniak et al. 2013b, Lingvay et al. 2009b) with poor validation. (Hu et al. 2010b, Pinnick et al. 2008) One manual pancreatic segmentation method (MRopsy) quantifies regions of interest within the pancreatic head, body, and tail, and excludes pixels with fat values of <1% and >20% which represent histological verified blood vessels, ducts or visceral fat. While MRI offers highly sensitive pancreatic fat estimations over other imaging methods, the delineation of pancreatic fat incorporates high inter- and intra-observer variability, and is very time consuming.

In order to make up for the issue of MRI scans on pancreatic fat, a manual pancreatic segmentation method has been developed and proven effective with true values of parenchymal fat content.(Steven et al. 2016a, Steven et al. 2016b) This method employed professional medical imaging software, Image J (National Institutes of Health, Bethesda, MD, USA), to quantify the pancreas. Researchers circle around the border of pancreas on the MRI and segmented it with a specific tool in Image J, and further increased the validity by excluding the pixels with fat values of < 1% and > 20%, which represented histological verified blood vessels, ducts, or visceral fat, respectively. In order to decrease the manual labour, the method has been updated to ‘biopsying’ the image to minimise inclusion of non-parenchymal tissues. The new MR image ‘biopsy’(MR-opsy) technique was only utilized in three spots located inside of specific regions of interest within the pancreatic head, body, and tail, away from pancreatic borders and main blood vessels, in order to effectively avoid contamination from non-pancreatic tissue. This method was compared to the original method by 6 experienced

independent observers who stated that this method was in-line with the traditional ones in terms of segmentation of low intrapancreatic fat and diverse in high intrapancreatic fat.(Al-Mrabeh et al. 2017) These methods provide an alternative, new, and prospective way to accurately segment the intrapancreatic fat tissues. However, these methods must involve freehand drawing around a region of interest by an experienced operator and is extremely time consuming.

To compensate for measurement boundary uncertainty, a manual pancreatic segmentation method called MR image 'biopsy' (MR-opsy), based on the pixel recognition from MRI, has been developed. (Steven et al. 2016a, Al-Mrabeh et al. 2016) This method quantifies specific regions of interest within the pancreatic head, body, and tail, away from pancreas' borders and main blood vessels in order to avoid contamination from non-pancreatic tissue in the regions of interest, and excludes pixels with fat values of < 1% and > 20%, which represent histologically verified blood vessels, ducts or visceral fat, respectively. The segmentation result of MR-opsy demonstrated higher inter-observer agreement.(Al-Mrabeh et al. 2017) However, this relies on freehand drawing within and around the pancreas region and is extremely time consuming.

1.7.1.2 Automatic segmentation of pancreas

Automated segmentation of the pancreas to calculate pancreas volume (PV) and generate 3D models has considerable potential as a research and clinical tool. A 2018 systematic literature review on PV (with the use of manual or semi-automated segmentation) found that type 2 DM and type 1 DM are associated with a progressively reduced PV, whereas being overweight and obesity are associated with a progressively increased PV. (DeSouza et al. 2018b) Both 3D reconstruction and PV calculation have been investigated in the context of pancreatic surgery, which is technically challenging and is associated with significant morbidity. (Petrov 2018) Small pre-operative PV (< 53.4 cm^3) can be regarded as an independent risk factor for the development of non-alcoholic fatty liver disease after pancreatic surgery. The automation of pancreas segmentation has the potential to enhance the translation of pancreas volumetry and 3D reconstruction into clinical practice through minimising the associated time burden and human costs. Automated segmentation of anatomical structures is already used in modern clinical practice in assisting diagnosis and surgical management of complex pathology. For example, software for automated segmentation of the liver has already been developed. (Ohshima 2014) A retrospective review investigating the effect of pre-operative 3D digital simulation training on perioperative outcomes for hepatectomies or segmentectomies reported

shorter operating times while maintaining a strong correlation between expected resection volumes to actual resection weights in the preoperative 3D simulation group. (Nakayama et al. 2017)

With the rapid development of Convolutional Neural Networks (CNNs) based on U-Net, it has advanced much of medical image analysis. Many classical CNNs have been established in regards to the segmentation of pancreas, such as full convolutional network (FCN) and conditional random fields (CRF) (Ronneberger, Fischer and Brox 2015, Long, Shelhamer and Darrell 2015, Krähenbühl and Koltun 2011, Roth et al. 2018, Zhou et al. 2017) has advanced much of medical imaging analysis by enabling computers to learn organ segmentation tasks from large MRI datasets obtained from the heart, liver, kidney and spleen. (Alom et al. 2018, Cai et al. 2016) However, automatic pancreas segmentation has rarely been investigated due to the high inter-observer variation of this retroperitoneal organ. Furthermore, additional information obtained from 3D MRI scans compared to 2D images, makes it more complicated to establish 3D models by using the classical Atlas model(Wolz et al. 2013) for context learning due to the limitation of current GPU memory. While there are flaws in each method, both 2D and 3D networks have been developed along with strategies to improve the accuracy of segmentation results, such as the coarse-to-fine framework, and recurrent and ensemble learning. (Li et al. 2019, Zeng and Zheng 2019, Yu et al. 2018, Zhu et al. 2018)

1.7.1.3 Convolutional Neural Network (CNN)

Imaging techniques are now commonly used to capture anomalies in the human body. Both the loss of human life can be prevented and the medical trauma experienced associated with injury or disease can be reduced through the timely diagnosis of such medical anomalies. This might include diabetic retinopathy, glaucoma, tumours, (Jiao et al. 2016) interstitial lung diseases, heart disease, and tuberculosis. (Li et al. 2014) Diagnosis and prognosis involves the understanding of the images of affected areas obtained in X-rays, CT, MRI, and so on. Image understanding involves the detection of anomalies, ascertaining their locations and boundaries, and detecting the organs' size and the severity of its condition. Experts do high quality work in terms of diagnosing and identifying the images; however, high consultation fees and the rough estimates of procedures limit the effectiveness of imaging. Moreover, the medical anomalies' shape, locations, and structures are greatly variable. This makes diagnosis difficult even for skilled physicians. Thus, experts usually feel a need for support tools to aid in making precise

readings of the medical images. This motivates the progression of intelligent image understanding systems. (Pereira et al. 2016)

Machine learning (ML) techniques have evolved quickly in recent years. Types of ML include: decision tree learning, clustering, support vector machines (SVMs), k-means nearest neighbor (K-NN), restricted Boltzmann machines (RBMs) and random forests (RFs). To make ML efficiently extract high quality and discriminant features of images, the prerequisite is always required. Different types of medical images have various significant features which are generally challenging to apply algorithms to for segmentation. A logical step to overcome this was to create intelligent machines that could learn features needed for image understanding in order to extract it on its own. This type of technology was successfully developed and is known as the convolutional neural network (CNN), which automatically learns the needed features and extracts it for medical image understanding. It became popular from 2012, due to AlexNet, (Krizhevsky, Sutskever and Hinton 2012) whose CNN model beat other competitors with a record accuracy and low error rate in the ImageNet challenge 2012. CNN is made of a couple of filters. The primary layer's function is to learn and extract key features for efficient medical imaging to convolute the pooling layers, and deconvolute the images. The major applications of the CNN are in image and signal processing, natural language processing, and data analytics. GoogleNet used CNN to detect cancer at an accuracy of 89% while human pathologists could achieve the accuracy of only 70%.(Al-Rfou et al. 2016)

Image understanding by animals is a very simple task, but there are a lot of hidden complexities during the process. Animals capture the images with their eyes and send the signal to the brain for further interpretation. CNN is a deep learning algorithm inspired by the visual cortex of the animal brain and aims to imitate the visual machinery of animals. CNNs represent a quantum leap in the field of image understanding, involving image classification, segmentation, localization, detection, and so on. The efficacy of CNNs in image understanding is the main reason for its abundant use. CNNs are made of layers of convolutions with learnable weights and biases akin to the neurons of animals. Convolutional layers, activation functions, pooling, and fully connected layers are the core building blocks of CNNs, as shown in **Fig 1-6**. (Sarvamangala and Kulkarni 2021)

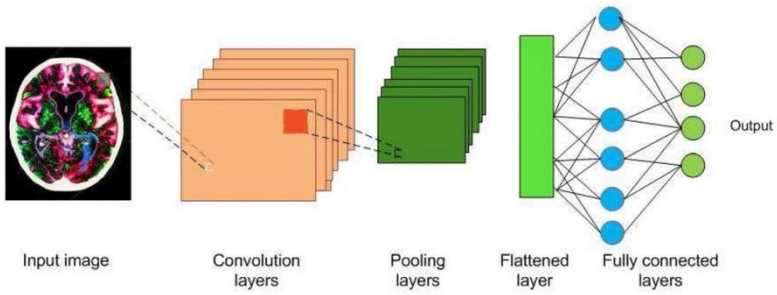

Figure 1-6 Building blocks of a CNN. Adapted from Sarvamangala. et al. 2021
(Sarvamangala and Kulkarni 2021)

1.8 Further understanding of CNN

1.8.1 Convolution layers

The visual cortex of the animal brain is made of neuronal cells which extract features of the images. The different features are extracted by each neuronal cell and understood by the central nervous system. The conv layer mimics neuronal cells and extracts image features, such as rim, colors, texture, and gradient orientation. Conv layers, or kernels, calculate size using n×m×d, where d is the depth of the images. The kernels are convolved across the width and height of input volume, and the dot produced is computed between the entries of the filter and the input. Intuitively, the CNN learns filters which are activated when they come across edge, colour, texture, and so on. The output of the conv layer is fed into an activation layer.

1.8.2 Activation functions

Because of the nonlinear properties of real-world data, activation functions are applied for nonlinear transformation of the collected data. They are used to make sure the representation in the input space is mapped to a different output space as per the requirements. The various activation functions are listed in **Table 1-2.**

Table 1-2 The activation functions details

Activation functions	Expressed formula	Note
Sigmoid	$f(x) = \frac{1}{1+e^{-x}}$	x is real-valued number range between 0 and 1. In particular, large negative and positive inputs are placed very close to 0 and unity, respectively.
Tan hyperbolic	$f(x) = \frac{1-e^{-2x}}{1+e^{-2x}}$	x is a real-valued number and squashes t between -1 to 1
Rectified linear unit (ReLU)	$f(x) = \max(0, x)$	x is a real-valued number and converts to 0 if x is negative. ReLU is the most often used nonlinear function for CNN.

1.8.3 Pooling

The pooling layer performs a nonlinear down sampling of convolved features. It reduces the dimension of the images so that it decreases the computational power requirement of data processing. The pooling layer reduces the spatial size via aggregating data on space or feature type, controls overfitting, and overcomes translation and rotational variance of images. Results of pooling are to turn images into a set of rectangular patches, each of which get replaced by a single value depending on the type of pooling selected. The different types are average and maximum pooling.

1.8.4 Fully connected (FC) layer

The fully connected (FC) layer is regarded as being similar to an artificial neural network, where each node has incoming connections from all inputs and all the connections have the weights linked with them. The output is the sum of all inputs multiplied by the weights. The FC layer is followed by the sigmoid activation function and performs the classifier job.

1.8.5 Data pre-processing and augmentation

Generally, the raw images obtained from the machine need to be pre-processed and augmented before sending to CNN. This is because the raw image data might be skewed, altered by bias distortion[228], or experience intensity inhomogeneity during the capture. Multiple data pre-processing methods exist, the preferred methods of which are mean subtraction and normalization. CNN needs to be trained on a larger dataset to achieve the best performance. Data augmentation increases the existing set of images by horizontal and vertical flips, transformations, scaling, random cropping, colour jittering and intensity variations. The pre-processed, augmented image data is then fed into CNN.

1.8.6 CNN architectures and frameworks

Many CNN architectures have been proposed by researchers depending on kind of task to be performed. A few award-winning architectures are listed in Table 3. CNN frameworks (toolkits) enable the efficient development and implementation of deep learning methods. Various frameworks used by researchers and developers are listed in **Table 1-3**.

Table 1-3 Various existing CNN frameworks (Sarvamangala and Kulkarni 2021)

Deep learning framework	Developed at	Implemented using	Pros	Cons
Cafe (Vedaldi et al. 2014)	Berkeley Vision and Learning Centre	C++	Cross platform, easy to deploy, fast, has good MATLAB and Python interface, models can be trained without writing code	Usability drops outside ConvNets, not very good with new architectures
Keras (Arnold 2017)	Francois Chollet, Google	Python	Easiest deep learning framework, clean API, huge active community, easily extensible, user-friendly, works with Theano and TensorFlow	Poor support for multi node training, cannot be used efficiently as an independent framework
TensorFlow (Abadi et al. 2016)	Google Brainteam	Python C++	Has modular architecture, supports multiple front ends and execution platforms, availability of tensor board for visualization	low, slower than Theano and Torch in terms of execution time, lacks many pre-trained models, not completely open source
Torch (Collobert, Kavukcuoglu and Farabet 2011)	New York University	Lua	Modular architecture, easy to setup, displays helpful error messages and has a large amount of tutorials	Difcult to integrate since it is implemented in Lua and its data science stack in R or Python
PyTorch (Paskze and Chintala 2017)	Facebook artificial intelligence group	Python, C++, CUDA	Fast, minimal framework overhead, understanding error messages and stack traces is easy and hence easy to debug, good for research and development	Depends on Matplotlib and Seaborn for visualization, lacks distributed training
Theano (Al-Rfou et al. 2016)		Python	Expressive Python syntax, large help on net, supports high level wrappers	Cross platform, needs secondary libraries for deploying, supports single GPU, error messages are not helpful
Neon	Nervana System	Python	Very fast due to fast matrix operations, the same code runs on GPU and CPU	Too many errors with scattered dependencies, less material on web, architecture not user friendly, not general-purpose
Deeplearning4j (Ranzato, Hinton and LeCun 2015)		Java	Performance equal to Cafe and better than TensorFlow or Torch, fast	Generally not preferred because Java is unpopular in ML circles
Cognitive Toolkit (CNTK) (Seide and Agarwal 2016)	Microsoft	C++	Fast, accurate scalable over GPUs, flexible, allows distributed training, supports C++, Java, Python and C#	Lacks visualizations, crashes with error, no Matlab or Python bindings

1.9 Description of this Research

1.9.1 Aim of this research

This overall target of this research intends to build up a novel convolutional neural network (CNN) for pancreas segmentation in terms of both size and fat fraction based on the latest manual MRI segmentation method. The current study mainly included three tasks: 1.) patient recruitment and data collection for the evaluation of ethnic variations in various fat tissues among New Zealanders, 2.) evaluate the similarity of the manual adipose tissues segmentation by phantom study, and 3.) establishment of novel CNN for pancreatic volume and fat content segmentation. In my thesis, I divided the methods into two parts for the continence for presentation.

To the specific objectives, it includes:

1. Compare SAT, VAT, and intra-hepatic and intra-pancreatic fat depositions in various ethnicities in New Zealand.
2. evaluate the ethnicity-specific associations between traditional anthropometric indices and MRI-derived fat content across the ethnicities.
3. compare the usefulness of measuring fat depositions at different lumbar spine levels;
4. Conducting phantom study to establish baseline of fat signal gradient from MRI for the novel CNN segmentation.
5. Establish and train new 2D CNN by upgrading relevant algorithms.

1.9.2 Ethical Approval and Ethical Consideration

Ethical Approval of this study was received from New Zealand regional ethics committee (NZ93405). This study was prospectively registered at ANZCTR (ACTRN12611000751976) and retrospectively registered at http://clinicaltrials.gov/(NCT01486680). The information sheet of this study was provided to the subjects to decide to join in this study (Appendix A). For all the confirmed subjects for the bariatric surgery, a written informed consent form was obtained (Appendix B).

This study was approved by the Health and Disability Committee and included healthy people aged 18 or above. Investigation of health and ethnic background was conducted to all patients before they went through MRI to make sure that they had no drug history and no malignancy,

diabetes, coeliac disease, cystic fibrosis, chronic pancreatitis, pregnancy or symptoms of upper abdominal pain and nausea. They also had no endocrine disorders and history of acute infectious or inflammatory conditions requiring medical evaluation or treatment in the three months prior to the study date. All participants included in the study provided informed consent. Participants were excluded if they had general contraindications for MRI (such as metallic foreign body or electronic device implantation).

Chapter 2. Evaluation of Ethnic Variations in Visceral, Subcutaneous, Intra-Pancreatic, and Intra-Hepatic Fat Depositions by Magnetic Resonance Imaging among New Zealanders

2.1 Introduction

Distribution of fat is increasingly recognized as a key factor predisposing to type 2 diabetes, metabolic syndrome, and cardiovascular disease(Singh et al. 2019). Fat around abdominal organs, termed 'visceral adipose tissue' (VAT), is associated more closely with metabolic disorders than subcutaneous adipose tissue (SAT) (Ibrahim 2010, Jensen et al. 2014). VAT is regarded as more active than SAT in terms of triggering the release of mediators of inflammation and contributing to insulin resistance and deranged lipid metabolism(Gillies et al. 2016, García Torres et al. 2017, Singh et al. 2017a, Després and Lemieux 2006). Estimation of abdominal fat content is often done with the use of anthropometric indices, such as body mass index (BMI), waist circumference (WC), and waist-to-height ratio (WHtR). These indices are widely used as screening tool for adult cardiometabolic risk and are widely applied in the public as a way to predict metabolic syndrome and mortality(Ashwell, Gunn and Gibson 2012). However, in recent years, the fat content of internal organs, most notably intra-hepatic and intra-pancreatic fat, has emerged as more important parameter in obesity, type 2 diabetes, and certain types of cancer(Cheng et al. 2010, Catanzaro et al. 2016, Coe et al. 2018, Sreedhar et al. 2019, Petrov 2018).

Modern cross-sectional imaging, such as computed tomography (CT) and magnetic resonance imaging (MRI), are regarded as the gold standard as they can accurately quantify the specific distribution of adipose tissue in the abdomen and internal organs(Abate et al. 1994). It is not considered practical to take large number of images from each individual because it is costly and a time-consuming process, so it is crucial to establish a practical alternative method to estimate the fat content and distribution. The usefulness of different lumbar spine fat contents was reported weight differently in terms of evaluating the metabolic disorders, some studies showed that the best single slice to evaluate VAT is at the two lowest vertebrae of the lumbar spine, L4-L5(Shuman et al. 1986, Seidell et al. 1987, O'Connor, Ryan and Foley 2015). Other studies suggested that L1-L2 or L2-L3 can be better predictors of metabolic syndrome than L4-L5(Irlbeck et al. 2010, Shen et al. 2007, Kuk et al. 2006). This discrepancy can be explained, at least in part, by the fact that these associations vary between different ethnicities(Lovejoy et

al. 1996, Misra, Wasir and Vikram 2005, Kadowaki et al. 2006). To date, there have been no published data on the best level to measure abdominal fat in Māori (the indigenous people of New Zealand) and Pacific Islanders (PI) adults compared with other major ethnic groups in New Zealand (i.e., NZ European and Asian). Further, there is a lack of data on ethnic variations in intra-pancreatic and intra-hepatic fat in New Zealand.

The aims of the study were to: (1) Compare SAT, VAT, intra-hepatic and intra-pancreatic fat depositions in various ethnicities in New Zealand; (2) Evaluate the ethnicity-specific associations between traditional anthropometric indices and MRI-derived fat content across the ethnicities. (3) Compare the usefulness of measuring fat depositions at different lumbar spine levels.

2.2 Materials and Methods

2.2.1 Sample collection

The participants were recruited and asked to sign the consent forms. They were then grouped into NZ Europeans, Asians, and Māori/PI. The recruitment is at single centre, Auckland central hospital.

2.2.2 Methods

2.2.2.1 Anthropometric measurements

In order to investigate the correlation between the traditional anthropometric measurement and fat deposition, the data of body composition such as weight, height, waist circumference was collected. The data of fat deposition was collected by MRI scan at the Center of Advanced MRI (University of Auckland).

BMI (kg/m^2) and WC (cm) were measured at the time of MRI acquisition. WC was measured circling over light clothing from navel on participants. BMI was measured via a digital weight scale with a stadiometer (Health o meter Professional®, 2013; ©Pelstar LLC, McCook, IL, USA). The height was measured by wall mount height meter first. The participants were asked to take off their shoes, stand with their back against the wall with their feet together. The back on their feet, buttocks, shoulders, and the back of their head is adjusted by the researcher. They were also asked to look straight ahead to make sure that their bodies were standing as straight

as possible. Their head level positions were located by the bar of height meter and noted. Then they were guided to stand on electronic weight measuring machine, the results were noted. The BMI was calculated by via the equation 1:

$$BMI = \frac{weight\ (kg)}{height^2 (m^2)}$$

Waist and hip circumference were measured by measuring tape. The patients were The measurements were conducted at least twice. If the difference between the adjacent results were not more than 2 cm, they were accepted and noted, or the third measurement was taken. The result reflected the average two closest measurements. To measure the WC, the tape was circling over light clothing from navel on participants. The participants were requested to stand erect with the belly relaxed. The tape was positioned in a horizontal position at the nearest part of the torso. For over obese subjects, the area between the ribs and iliac crest was considered to represent the WC values. To measure the Hip circumference, the patients were asked to lift their arms aside and keep feet together. The tape was circling around their hips horizontally with the skin naturally flapped. The waist to hip ratio (WHR) was calculated according to a guideline from WHO (Consultation, 2008).

2.2.2.2 Blood Samples

The new recruited patients were requested to donate their blood samples to this research. All participants were asked to fast at least 12 hours (usually overnight). Blood samples were collected both before and after their bariatric surgeries for the purpose of further biomarker testing experiment. Patients were guided to sit still for 10 minutes. An intravenous cannula was injected into the target vein to minimize the discomfort of repeated blood sampling, and 20 ml blood sample was drawn from subject. The collected plasma was centrifuged at 4500xg for 5 minutes at -4 ºC and plasma was aliquoted into a clean tube and stored in -80 ºC for further analysis. (The part results are not used in my project, will leave it for the future validation and molecular analysis use)

2.2.2.3 Dual-Energy X-ran Absorptiometry

All newly recruited patients were asked to conducted DXA scans at Body Composition Unit, Auckland City Hospital for further analysis. TBF, BMC, and BMD were measured by DXA (model iDXA, software V.15, GE-Lunar, Madison, Wisconsin, USA) according to the method described by *Peng et al* (Peng et al. 2007). The DXA machine was calibrated according to the manufacturer's protocol. After the data of patients' height and weight were collected, they were

facilitated to lie on the scanner bed in a supine position and machine measured from the head to toe. The measurement took approximately 20-30 minutes. (The part results are also not used in my project, will leave it for the future validation and molecular analysis use)

2.2.2.4 MRI acquisition

All participants underwent abdominal MRI at the Center of Advanced MRI (University of Auckland) with a field strength of 3.0 Tesla MAGNETOM Skyra scanner (Siemens, Erlangen, Germany). The axial T1-weighted volumetric interpolated breath-hold examination Dixon sequence was used in this study. The ratio of fat and water volume was used in analysis.

The HISTO (high-speed T_2-corrected multi-echo single voxel spectroscopy) protocol in the Siemens Skyra 3.0 software was used to determine the intra-hepatic fat. It ran with 5 TEs ranging from 12 to 72 ms and a voxel of size 3 x 3 x 3 cm^3, which was placed in the liver avoiding major vessels and ducts. Proton Density Fat Fraction (PDFF) was derived and corrected for fat and water transverse relaxation. The sequence was a 15 second breath-hold spectroscopy sequence for each patient. The HISTO automatic inline processing integrated the water and fat parts of the spectrum for individual echoes and performed a T_2 relaxation correction. The fat signal was expressed as a percentage. A spectrum of the shortest TE and a list of quantification values for the individual echoes were added for quality control of the signal fitting.

To acquire data on SAT, VAT and intra-pancreatic fat volume, all MRI images were imported into 3D-slicer software(Fedorov et al. 2012) to accurately locate and identify the first lumbar (L1) through to the fifth (L5) vertebral levels. Then the corresponding water (the boundary size measurement) and fat scans at L12, L23, L34, L45 and the pancreas were separately cut out using the ImageJ software (National Institutes of Health, USA). The VAT compartment was then segmented and separated from SAT (**Figure 2-1**). The intra-pancreatic fat content was separated after comparing the corresponding water and fat scans. Water scan images were scaled by the free hand tool of ImageJ to visualize the boundary of each image for SAT, VAT, and pancreas (**Figure 2-1**. a, a_1, c_1), according to which the fat scan images were separated into equivalent sections (**Figure 2-1**. b_1, b_3, d). The total sum of each slice boundary value was then multiplied by slice thickness to obtain total volume. Applying the threshold function in ImageJ on fat images, the light gray images were converted into binary images. The threshold was adjusted until the adipose tissue pixels were fully separated from the non-adipose tissue, such as blood vessels and the main pancreatic duct. The total pixels count of each slice image was measured (**Figure 2-1**. b_2, b_4, d_1) to yield the adipose tissue content of SAT, VAT, and pancreas. Total pixel counts in each slice were summed up and then the ratio of fat to water was derived in each slice. The two series of images were analysed and the ratio of the volume of fat content to water area was then calculated and defined as L12SAT, L23SAT, L34SAT, L45SAT, L12VAT, L23VAT, L34VAT, L45VAT, and PAT

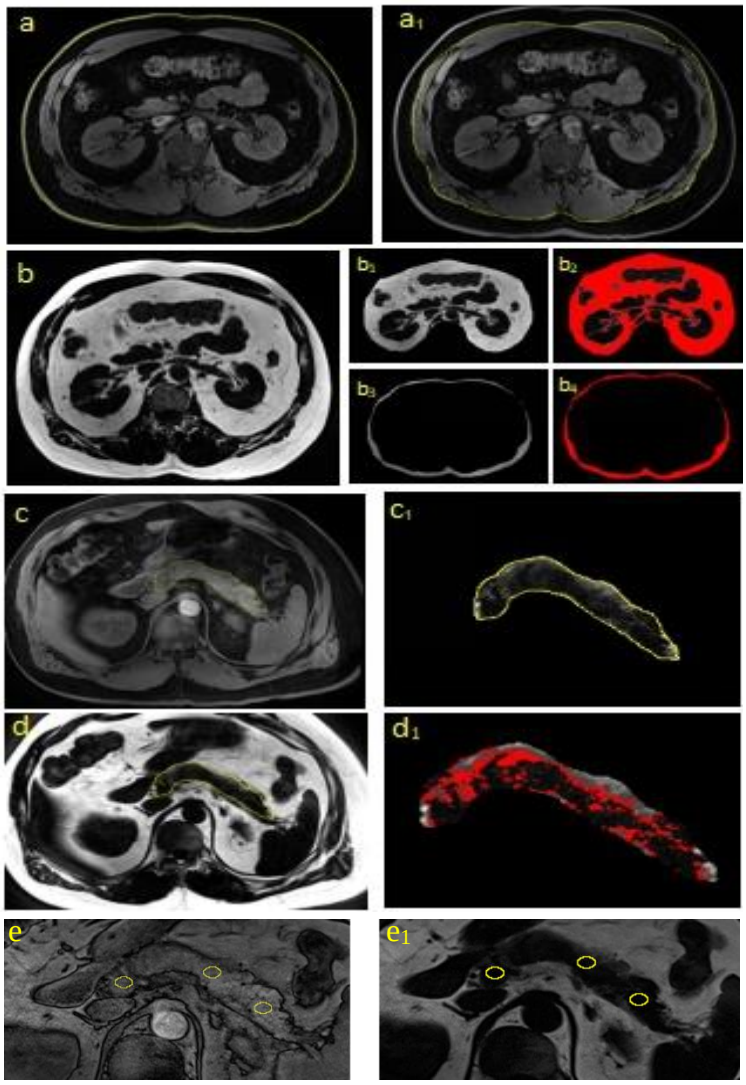

Figure 2-1 Water and fat content segmentation of SAT, VAT, and intra-pancreatic fat using the ImageJ software a, a1are the segmentation of subcutaneous and visceral water; b-b4 are the segmentation of subcutaneous and visceral fat; c, c1 are segmentation of pancreatic water; d-d1 are the segmentation of intra-pancreatic fat; e, e1 are MR-ospy segmentation on water and fat images respectively.

respectively. The intra-hepatic fat content was read directly from the result of MR Spectrum, and termed as LAT. For the traditional segmentation method, the Image J Polygon tool was applied to select a region of interest (ROI) in the parenchymal tissue of the pancreas as large as possible whilst being clear of the pancreas borders to avoid any possible contamination of surrounding visceral fat (**Figure 2-1 c_1, d_1**). For MR-opsy, we used Oval tool of image J to choose ROI (around 100mm^2 each) at pancreas head, body, and tail. The optimum size was decided by the pilot studies, which consider the irregularity in pancreas morphology and permit easy placement entirely within the pancreas (**Figure 2-1 e,e_1**). To those images with uneven distribution of parenchymal fat between different regions of pancreas, sampling regions were placed equally throughout the pancreatic regions for the purpose of avoiding bias. These operations were all blinded to glucose tolerance and any other clinical conditions. According to the previous research from *Pinnick et al,* any MRI fat signal below 1% cannot be discriminated and above 20% were considered as contamination of internal fat tissues (Pinnick et al. 2008), so we excluded these pixels by the operation shown in Appendix D:

2.2.2.5 Statistical analysis

STATA for Windows (Stata Corp., 2019) and SPSS 23.0 for Windows (IBM Corp., 2015). were used for all statistical analyses. One-way ANOVA was applied to all variables to assess differences in baseline characteristics between the three ethnic groups. Data were presented as mean ± standard error. The independent t-test was then used to investigate the difference in each variable between each pair of the ethnic groups.

First, to investigate the association between anthropometric indices and MRI-derived fat depositions in the entire cohort and each of the ethnic group, the Pearson's correlation was used. Both p and r values were presented to show the correlation between each variable.

Second, total and ethnicity-specific linear regression was performed in order to evaluate the usefulness of measuring fat contents at different lumbar spine levels, which represents the accurate regression relationship of the anthropometric measurements and each corresponding MRI scan. Age and sex variables were adjusted in analysis Each adipose tissue volume percentage (L12SAT, L12VAT, L23SAT, L23VAT, L34SAT, L34VAT, L45SAT, L45VAT, LAT and PAT) was treated as dependent variable and BMI, WC and WHtR as used as independent variable in unadjusted and adjusted modes. Data were presented as β coefficients, 95%CI and R^2 metric.

Third, ethnicity-specific equations were derived from multicollinearity model in terms of estimating various lumbar spine VAT and PAT deposition from variables which do not require the use of MRI. The model included all predictor variables, collinear variables (as shown by the highest variance inflation factor (VIF)) were removed one at a time until multicollinearity was minimized (VIF<5). Back elimination method was applied to establish the equations that removed predict variables which didn't significantly contribute to the model (P>0.05).

2.3 Results

2.3.1 Baseline characteristics for fat deposition variations in different ethnicities

At this stage, we totally used data from 104 participants. 53 were New Zealand Europeans, which occupy the percentage of 51%, 30 were Māori/Pacific Islanders (Māori/Pl), which take up 28.8%, and 21 were Asians, which take up 20.2%. Overall, there were 66 (63.5%) males and 39 (37.5%) were females in this study. The average age of all participants was 53.0±1.6 years. Other characteristics such as the BMI, WC, and fat deposition results of different layers of body are listed in **Table 2-1**.

Table 2-1 Characteristics of study participants

Characteristics	Total	NZ European	Māori/Pl	Asian	P value[1]
No. of participants	104	53	30	21	
Age (years)	53.0±1.6	56±2.4	57.7±2.0	39.1±2.6	0.0001***
Sex					0.092
Male	66	31	21	14	
Female	38	22	9	7	
Height (cm)	171.4±1.1	172.4±1.2	172.5±2.2	167.2±2.1	0.109
Weight (kg)	82.6±1.9	80.7±2.1	93.7±3.6	68.4±4.0	0.0002***
WC (cm)	100.0±0.7	96.6±0.6	109.0±1.2	95.7±0.5	0.0002***
BMI (kg/ m^2)	28.1±0.6	27.1±0.6	31.7±1.3	25.4±1.0	0.0001***
WHtR	58.6±0.6	56.2±0.5	63.6±1.2	57.4±0.7	0.0001***
L12SAT	22.2±1.0	20.3±1.3	26.3±2.3	21.1±1.8	0.035**
L12VAT	31.7±1.0	29.2±1.2	35.4±1.4	32.6±1.8	0.019***
L23SAT	26.7±1.1	25.1±1.5	29.3±2.4	27.0±2.2	0.280
L23VAT	32.4±1.0	29.2±1.5	36.8±1.7	34.0±1.9	0.004***
L34SAT	32.7±1.1	31.1±1.5	34.5±2.3	34.0±2.5	0.360
L34VAT	34.0±1.1	31.8±1.6	39.3±2.4	39.0±2.4	0.014***
L45SAT	37.9±1.2	36.6±1.6	39.3±2.4	39.1±2.4	0.549
L45VAT	32.4±1.0	30.4±1.4	36.0±1.6	32.6±2.2	0.039**
SATA	30.0±1.1	28.5±1.4	32.4±2.2	30.3±2.1	0.291
VATA	32.6±0.9	30.2±1.4	36.8±1.4	32.9±1.9	0.008***
LAT	9.9±1.0	8.2±1.0	11.0±1.9	13.5±3.5	0.125
PAT	8.2±0.4	7.5±0.5	9.4±0.6	8.0±0.9	0.062

[1] One-way ANOVA significant difference value is P, * p<0.1, **p<0.05, ***p<0.01, respectively. Data are presented as mean± standard error. WC, BMI, and WHtR are represent for waist circumference, body mass index, and weight to Height ratio respectively. L12-L45 are represented for vertebrae of the lumbar spine respectively. SAT and VAT stand for the percentage of subcutaneous and visceral fat, correspondingly. SATA, VATA are the mean values of all SAT and VAT volume. LAT and PAT stand for intra-hepatic and intra-pancreatic fat percentage, respectively. (Same in the following tables)

2.3.2 Differences between the ethnic groups

Table 2-1 shows that there were significant differences between the ethnic groups in terms of both anthropometric measurements and all visceral adipose tissue percentage. However, there was no significant difference in terms of intra-hepatic and intra-pancreatic fat percentage. The P values for different lumbar slices in evaluating visceral fat (i.e., L12VAT, L23VAT, L34VAT, L45VAT) were 0.019, 0.004, 0.014, 0.039, respectively. Among them the L23VAT was more significantly different (P<0.01) than other levels. When different lumbar slices in evaluating subcutaneous fat were considered, only L12SAT was significantly different between the groups.

Further, the independent student t-test was used to investigate the difference between each pair of groups (**Table 2-2**). There were differences when comparing NZ European and Māori/PI, Māori/PI and Asian groups in terms of all anthropometric indices, but there was no significant difference between NZ European and Asian other than WC. The P values for VAT and PAT reached the conventional level of statistical significance between NZ European and Māori/PI, but the significant difference only existed between NZ European and Asian in terms of LAT and between Māori/PI and Asian in terms of L34VAT.

Table 2-2 Results of student's t-test for equality of means between the groups

	NZ European vs Māori/Pl	NZ European vs Asian	Māori/Pl vs Asian
BMI	3.086***	1.471	3.0478***
WC	10.639***	2.208**	12.539***
WHtR	6.796***	0.785	5.096***
L12SAT	2.362***	0.353	1.757
L12VAT	2.874***	1.287	1.101
L23SAT	1.684	0.651	0.864
L23VAT	3.07***	1.767	1.028
L34SAT	0.199	1.043	0.278
L34VAT	1.478***	0.224	2.227**
L45SAT	1.184	0.818	0.256
L45VAT	2.431***	0.860	1.148
LAT	1.565	1.454*	0.541
PAT	2.256**	0.546	1.243

Student t-test significant difference value is P, *, **, ***indicates significance at the 90%,95%, and 99% level, respectively

2.3.3 Correlations between anthropometric indices and MRI-derived fat depositions across the ethnicities

The ethnicity-specific Pearson's Correlation Coefficient (PCC) was calculated and the r and the p values were reported in the **Fig. 2-2**. BMI, WC and WHtR were used as independent variables, and each fat percentage as dependent variable.

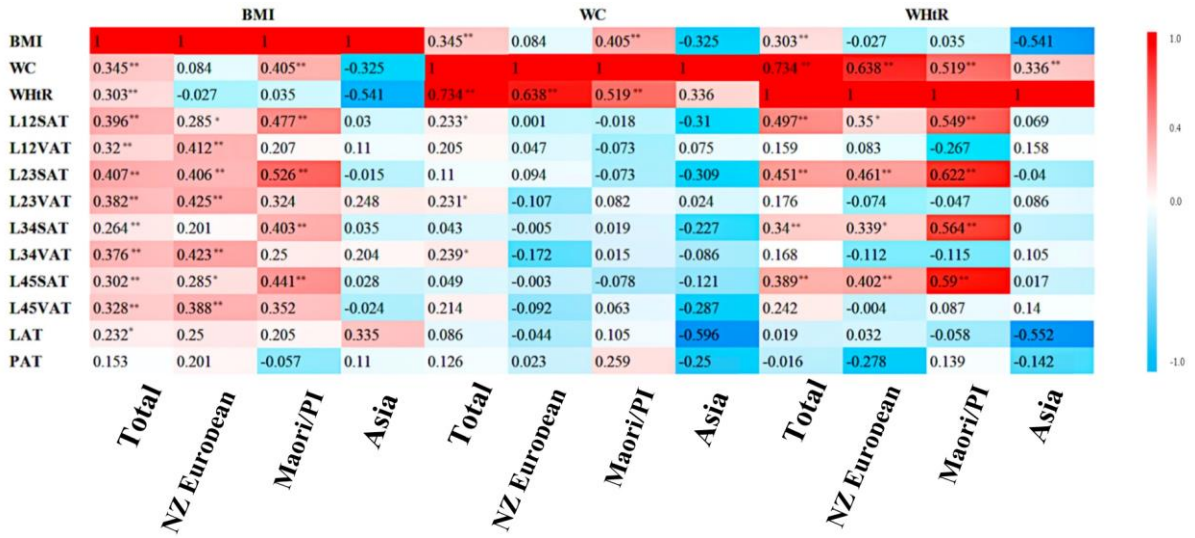

Figure 2-2 Pearson's r values are presented, significant difference value is P, *, ** indicates significance at the 95%, and 99% level, respectively

Overall, BMI was positively correlated with subcutaneous, visceral adipose tissues and intra-hepatic fat, but not intra-pancreatic fat. The largest r value was 0.407 (for L23SAT). The WHtR was more significantly correlated ($p<0.01$) with more dependent variables than WC. The WHtR was strongly correlated with each SAT whereas WC was weakly correlated with VAT. The largest r value of WC was 0.239 (for L34VAT) and the one of WHtR was 0.497 (for L12SAT).

In NZ Europeans, BMI was positively correlated with all the studied fat depositions. The largest r value was 0.425 (for L23VAT). The WHtR correlated with every SAT with the maximum r value of 0.461 (for L23SAT). WC had no significant correlation with any fat deposition.

In Māori/PI, BMI was more strongly correlated with SAT than VAT. The L23SAT correlated most with BMI (r value of 0.526). The WHtR in Māori/PI was strongly correlated with each

single SAT. The L23SAT showed the largest r value of 0.622. WC did not correlate with either SAT or VAT but correlated weakly with intra-pancreatic fat (r value of 0.259).

In Asian, there were weak correlations between traditional indices and fat depositions. BMI correlated with intra-hepatic fat (r value of 0.335) and L23VAT (r value of 0.248).

2.3.4 Usefulness of measuring fat depositions at different levels

2.3.4.1 Body Mass Index

In the overall cohort, BMI was associated with all slices of SAT and VAT, among which the L23SAT slice had the highest R^2 - up to 24%, with a β coefficient of 0.203 ($p<0.01$); and the L45VAT slice had the highest R^2 - up to 13.9%, with a β coefficient of 0.237 ($p<0.01$).

In NZ European, BMI was associated with the L23SAT with the highest R2 - up to 30%, with a β coefficient of 0.296 ($p<0.01$); the L45VAT slice had the highest R2 - up to 16.8%, with a β coefficient of 0.223 ($p<0.01$).

In Māori/PI, BMI, was significantly associated with VAT only. The best level was L45VAT, with R2 up to 24.3% and a β coefficient of 0.301 ($p<0.05$).

There were no significant associations between BMI and fat depositions in Asian (**Table 2-3**).

Table 2-3 Regression Result for Ethnicity-Specific Associations Between BMI and fat depositions

	L12SAT	*L23SAT*	*L34SAT*	*L45SAT*	*L12VAT*	*L23VAT*	*L34VAT*	*L45VAT*
Unadjusted								
Total	0.225***	0.209***	0.137***	0.147***	0.196***	0.218***	0.202***	0.200***
	(0.052)	(0.047)	(0.050)	(0.047)	(0.057)	(0.052)	(0.049)	(0.057)
NZ European	0.135***	0.164***	0.085	0.109***	0.176***	0.177***	0.163***	0.178***
	(0.064)	(0.052)	(0.058)	(0.051)	(0.055)	(0.053)	(0.049)	(0.059)
Māori/PI	0.283***	0.297***	0.240***	0.247***	0.185	0.215*	0.203	0.282*
	(0.098)	(0.090)	(0.102)	(0.095)	(0.174)	(0.144)	(0.153)	(0.153)
Asian	0.018	-0.007	0.015	0.012	0.062	0.135	0.091	-0.011
	(0.135)	(0.110)	(0.096)	(0.097)	(0.127)	(0.121)	(0.101)	(0.108)
Adjusted for age and sex								
Total	0.310***	0.203***	0.337***	0.229***	0.207***	0.237***	0.201***	0.237***
	(0.187)	(0.239)	(0.085)	(0.124)	(0.089)	(0.135)	(0.085)	(0.139)
NZ European	0.221***	0.296***	0.165**	0.226***	0.190***	0.204***	0.204***	0.223***
	(0.108)	(0.300)	(0.056)	(0.165)	(0.126)	(0.146)	(0.115)	(0.169)
Māori/PI	0.209	0.318	0.077	0.131	0.315*	0.271**	0.275*	0.301**
	(0.149)	(0.196)	(0.118)	(0.137)	(0.228)	(0.238)	(0.223)	(0.243)
Asian	0.073	0.038	0.062	0.063	0.064	0.174	0.105	0.004
	(-0.111)	(-0.119)	(-0.111)	(-0.112)	(-0.110)	(-0.031)	(-0.066)	(-0.123)
***, **, ***indicates significance at the 90%, 95%, and 99% level, respectively.**								
R-squared are reported in parentheses.								

2.3.4.2 Waist Circumference

In the overall cohort, WC had the strongest association with the L45SAT slice, with R^2 up to 12.2% and β coefficient of 0.263 ($p<0.01$). None of the associations was statistically significant in the three ethnic groups (**Table 2-4**).

Table 2-4 Regression Result for Ethnicity-Specific Associations Between WC and fat depositions

	L12SAT	*L23SAT*	*L34SAT*	*L45SAT*	*L12VAT*	*L23VAT*	*L34VAT*	*L45VAT*
Unadjusted								
Total	0.133***	0.040	0.033	0.029	0.120*	0.111*	0.149*	0.0100
	(0.065)	(0.060)	(0.061)	(0.057)	(0.070)	(0.065)	(0.061)	(0.070)
NZ	0.047	0.012	0.017	0.043	0.008	0.002	0.012	-0.065
European	(0.062)	(0.053)	(0.055)	(0.049)	(0.056)	(0.054)	(0.050)	(0.059)
Māori/PI	-0.050	-0.088	-0.059	-0.077	-0.052	-0.076	0.015	0.025
	(0.079)	(0.074)	(0.079)	(0.074)	(0.126)	(0.107)	(0.112)	(0.115)
Asian	0.008	-0.004	0.012	0.024	-0.012	-0.028	-0.005	0.016
	(0.056)	(0.046)	(0.040)	(0.040)	(0.053)	(0.052)	(0.043)	(0.045)
Adjusted for age and sex								
Total	0.196***	0.153***	0.115**	0.140***	0.083	0.073	0.096*	0.082
	(0.230)	(0.193)	(0.164)	(0.188)	(0.147)	(0.135)	(0.158)	(0.146)
NZ European	0.073	0.055	0.026	0.077	0.046	0.029	0.059	-0.025
	(0.231)	(0.225)	(0.213)	(0.240)	(0.223)	(0.215)	(0.228)	(0.213)
Māori/PI	0.117	0.198	0.120	0.149	-0.118	-0.093	-0.061	0.029
	(0.244)	(0.288)	(0.255)	(0.290)	(0.253)	(0.250)	(0.230)	(0.221)
Asian	0.034	-0.06	0.016	0.020	0.066	0.017	0.041	0.068
	(0.300)	(0.297)	(-0.111)	(0.296)	(0.319)	(0.297)	(0.310)	(0.332)

***, **, ***indicates significance at the 90%, 95%, and 99% level, respectively. R-squared are reported in parentheses.**

2.3.4.3 Waist to Height ratio

In the overall cohort, WHtR had the strongest association with the L12SAT (with R2 of 23%, β coefficient of 0.196); L23SAT (with R2 of 19.3%, β coefficient of 0.153); and L45SAT (with R2 of 18.8%, β coefficient of 0.14). None of the associations was statistically significant in the three ethnic groups (**Table 2-5**).

Table 2-5 Regression Result for Ethnicity-Specific Associations Between WHtR and fat depositions

	L12SAT	*L23SAT*	*L34SAT*	*L45SAT*	*L12VAT*	*L23VAT*	*L34VAT*	*L45VAT*
Unadjusted								
Total	0.235***	0.187***	0.159***	0.167***	0.069	0.063	0.078*	0.098*
	(0.044)	(0.041)	(0.043)	(0.040)	(0.053)	(0.049)	(0.046)	(0.052)
NZ European	0.0170***	0.148***	0.134***	0.158***	0.028	0.001	0.007	-0.015
	(0.055)	(0.047)	(0.050)	(0.043)	(0.054)	(0.052)	(0.048)	(0.058)
Māori/PI	0.200***	0.205***	0.187***	0.194***	-0.172	-0.092	-0.059	0.056
	(0.066)	(0.061)	(0.068)	(0.063)	(0.117)	(0.102)	(0.108)	(00.110)
Asian	0.087	0.027	0.035	0.035	0.042	0.009	0.040	0.094
	(0.102)	(0.084)	(0.074)	(0.074)	(0.098)	(0.096)	(0.079)	(0.081)
Adjusted for age and sex								
Total	0.150**	0.160**	0.149**	0.263***	0.078	0.070	0.110	0.059
	(0.057)	(0.058)	(0.054)	(0.122)	(0.028)	(0.027)	(0.041)	(0.023)
NZ European	0.091	0.034	0.038	0.086	0.032	0.031	0.059	-0.054
	(-0.017)	(-0.041)	(-0.040)	(-0.011)	(-0.041)	(-0.041)	(-0.229)	(-0.033)
Māori/PI	0.120	-0.016	0.073	-0.001	-0.109	-0.091	-0.029	0.003
	(0.007)	(-0.018)	(-0.006)	(-0.018)	(0.010)	(0.010)	(-0.016)	(-0.018)
Asian	-0.024	-0.052	-0.009	0.017	-0.002	-0.023	0	0.017
	(-0.108)	(-0.076)	(-0.114)	(-0.111)	(-0.115)	(-0.106)	(-0.115)	(-0.108)
***, **, ***indicates significance at the 90%, 95%, and 99% level, respectively.**								
R-squared are reported in parentheses.								

2.3.5 Ethnicity-specific predictive equations

Due to the weak correlation between PAT and LAT deposition and anthropometric indices, ethnicity-specific equations were only constructed to estimate the relationship between anthropometric indices and different level VAT depositions. In NZ European, age, sex and BMI were significantly correlated with each layer of VAT (**Table 2-6**). The derived equation in NZ European was calibrated with each MRI-derived VAT deposition, the R^2 value were 0.236, 0.263, 0.325 and 0.486 for L12VAT, L23VAT, L34VAT, L45VAT respectively. In Māori/PI, BMI and sex are both significant factors that associated with all levels of VAT deposition except L12VAT (**Table 2-7**). The calibrated R^2 value were 0.282, 0.336 and 0.383 respectively. In Asian, there is no significant association between VAT and anthropometric indices which enable a predictive equation.

Table 2-6 Ethnicity-Specific Equations to Estimate VAT depositions for NZ European

	VIF	Equation
Age, years	1.061*	L12VAT=0.405 (Age)-0.565(sex)+0.347(BMI) L23VAT=0.460 (Age)-0.603(sex)+0.373(BMI) L34VAT=0.571(Age)-0.612(sex)+0.348(BMI) L45VAT=0.464(Age)-0.558(sex)+0.346(BMI)
Sex	2.987*	
BMI, kg/m2	1.679*	
WC, cm	1.953	
WHtR	3.306	

* is statistical significance (P< 0.05). In the equation. Sex-men=1, women=0. BMI: body mass index; WC: waist circumference; WHtR: waist to height ratio; PI: Pacific Islanders; VAT: visceral adipose tissue; VIF: variance inflation factor of VAT.

Table 2-7 Ethnicity-Specific Equations to Estimate VAT depositions for Māori/PI

	VIF	Equation
Age, years	1.057	L23VAT=0.615(BMI)-0.34(sex) L34VAT=0.518(BMI)-0.27(sex) L45VAT=0.642(BMI)-0.31(sex)
Sex	2.987*	
BMI, kg/m2	1.679*	
WC, cm	1.953	
WHtR	3.306	

* is statistical significance (P< 0.05). In the equation. Sex-men=1, women=0. BMI: body mass index; WC: waist circumference; WHtR: waist to height ratio; PI: Pacific Islanders; VAT: visceral adipose tissue; VIF: variance inflation factor of VAT.

Chapter 3. An adipose tissue phantom to determine the theoretical accuracy for both artificial and automatic measurement of fat deposition in MRI

3.1 Introduction

The distribution of adipose tissues, especially the visceral fat is a crucial determinant of health risks associated with metabolic diseases such as type 2 diabetes, certain types of cancer and cardiovascular disease. (Cheng et al. 2010, Coe et al. 2018, Singh et al. 2019, Sreedhar et al. 2020) Diabetes affects approximately 8.5% of the adult population worldwide, (Cheng et al. 2010) and is the key driver of early morbidity and mortality and health care costs. (Coe et al. 2018) The pancreas plays a vital role in maintaining glucose homeostasis and energy metabolism. More and more clues in recent years suggests that type 2 diabetes, the most common form of diabetes, is caused by reduction in pancreatic volume and physiological changes of visceral adipose tissues, especially ectopic fat deposition in the pancreas. (Singh et al. 2019, Sreedhar et al. 2020, Ashwell et al. 2012, Shen et al. 2003) Thus, quantification of such pancreatic changes provides huge potential in terms of diagnosis and treatment to prevent and type 2 diabetes.

The accurate detection and measurement of pancreatic fat deposition were challenging in the 20th century because of its retroperitoneal location in the body. However, within the next decade, the great progress of magnetic resonance imaging (MRI) and magnetic resonance spectroscopy (MRS) techniques have enabled an accurate investigation of the organ. MRI is now regarded as well-suited for fat quantification because it is a non-invasive and does not utilize ionizing radiation. Furthermore, it also provides sensitive mechanisms for identifying fat from lean tissues based on T1 relaxation and chemical-shift properties. (Longo et al. 1995) MRI allows not only the detection of the abnormalities of the pancreas structure but also the quantification of the dimension and composition of the organ based on various imaging parameters. On the other hand, MRS is generally regarded as the gold standard non-invasive technique for in vivo fat and its metabolic quantification in clinical trials. It has been used for the measurement of liver fat (Kim et al. 2008, Thomsen et al. 1994), tissue composition (Machann et al. 2003), myocellular adipose tissue (Ren et al. 2008), and brain metabolites. Further, over the past 20 years, there is a significant improvement of Dixon's reconstruction algorithms enabled an advanced 3-dimensional (3D) imaging technique called Iterative

Decomposition with Echo Asymmetry and Least-squares estimation (IDEAL) for MRI images. (Hardy et al. 1995, Xiang 2006) IDEAL provides more reliable resonance offsets of separating fat and water images by optimizing their signal-to-noise ratio, which could have been difficult to calculate due to the impact of magnetic field nonuniformity. (Reeder et al. 2005)

Both IDEAL and MRS are based on the chemical-shift principles, where the resonant frequencies of protons in water and the primary methylene groups (-CH_2-) n of triglyceride fatty acid chains are separated at around 3.4 p.p.m. in the magnetic field. The water is characterized by a single spectral peak, whereas the fat tissue includes several continuous minor peaks, which represent methyl, olefinic, and carboxyl groups respectively. These peaks have slightly different chemical shifts with respect to water.(Brix et al. 1993) Compared with MRS, the multi-fat-peak T^*_2-IDEAL is a 3D images technique that presents spatial information and yields a fat-to-water ratio by systematically evaluating the transverse relaxation and intravoxel dephasing effects on the acquired MRI signal. These enabled a more accurate measure of the proton ratio between fat and water underlying tissues. (Yu et al. 2008)

However, quantification of the fat deposition inside relatively small organs such as the pancreas is still challenging given the variable and sometimes ambiguous borders of this organ. Currently, the extremely time-consuming manual fat segmentation of MRI images by experienced experts is regarded as the gold standard method for pancreatic volume and fat quantification. (Al-Mrabeh et al. 2017). In this study we describe how we trained convolutional neural networks (CNN) to determine the pancreatic and visceral fat deposition from abdominal MRI and assessed the method's performance using different external datasets in comparison with the time-consuming, manual gold-standard method.

In this study, we designed a phantom validation to 1). set a scale reference for both manual operation and machine learning of measuring pancreatic fat fraction for our future clinical studies, and 2). prospectively compare and evaluate the effectiveness of T^*_2-IDEAL, MRS, and expert manual operation in terms of measuring the MRI-derived hepatic fat fractions (HFFs) and intrapancreatic fat fractions (PFFs).

3.2 Method

In this study, all participants underwent MRI at the Center of Advanced MRI (University of Auckland) with a field strength of 3.0 Tesla MAGNETOM Skyra scanner (Siemens, Erlangen, Germany). Phantom experiment data were from a single channel transmit/receive abdominal coil. Participants' data were acquired with an eight-channel receive-only abdominal array. The axial T_1-weighted volumetric interpolated breath-hold examination Dixon sequence was used in this study. The study was approved by the Health and Disability Committee and followed all informed consent guide-lines. The HISTO (high-speed T_2-corrected multi-echo single voxel spectroscopy) protocol in the Siemens Skyra 3.0 software was used to determine the intra-hepatic fat. It ran with 5 TEs ranging from 12 to 72 ms and a voxel of size 3 x 3 x 3 cm^3, which was placed in the liver avoiding major vessels and ducts. Proton Density Fat Fraction (PDFF) was derived and corrected for fat and water transverse relaxation. The sequence was a 15 second breath-hold spectroscopy sequence for each patient. The HISTO automatic inline processing integrated the water and fat parts of the spectrum for individual echoes and performed a T_2 relaxation correction. The fat signal was expressed as a percentage. A spectrum of the shortest TE and a list of quantification values for the individual echoes were added for quality control of the signal fitting.

3.2.1 IDEAL fat-water MRI

The latest 3D IDEAL is a water *W* and fat *F* content separating method based on the Dixon technique.(Dixon 1984) In this study, we built up fat spectrum modelling (Yu et al. 2008) based on the signal model by the following equation (a):

$$s(t) = (W + F \sum a_i \cdot e^{j2\pi t\,(\Delta fi)})\, e^{j2\pi t\,\psi - (t/T^*2)}$$

where, *s(t)* is the signal at time t in each voxel, Δfi and a_i represents the relative amplitude and spectral frequency of the i^{th} peak of *F* relative to *W*, phi is the magnetic field inhomogeneity, *j* is the imaginary number ($\sqrt{-1}$), and T^*_2 is the transverse relaxation and intravoxel dephasing of the signal. The unknown parameters (W, F, ψ, T^*_2) were solved with six measurements of *s(t)*. The IDEAL fat fraction was computed from the separated water and fat signals in equation (b):

$$Fat\ Fraction\ (FF_{IDEAL}) = \frac{F}{(W+F)} \times 100\%$$

3.2.2 MRS

In this study, MRS data were acquired by the point-resolved spectroscopy method (27), which requires placing a single large voxel in an anatomical region-of-interest. MRS generally involves noise filtering, apodization, phase correction, and signal fitting of the peaks within the acquired spectra, the area of each spectral peak of interest of water at 4.7 p.p.m., methylene fat at 1.3 p.p.m. was obtained by integration. The software of MRUI was utilized for analysis for spectral quantification. The fat fraction in MRS was defined by equation (c)

$$Fat\ Fraction\ (FF_{MRS}) = \frac{\text{area under fat peaks}}{\text{area under fat and water peaks}} \times 100\%$$

3.2.3 Phantom validation

We used vegetable (soy) oil and distilled and undoped water to make a homogeneous emulsions series to evaluate the accuracy of each type of quantification result. We added 0-100% fat volume fractions and lecithin (1% by weight from sigma) in 100-ml bottles. To stabilize the emulsions, agar gel (3% by weight) and dioctyl sulfosuccinate sodium salt were applied to the system. The emulsions were prepared slowly over a heat-stir plate and subsequently cooled down to room temperature allowing the suspension to stay evenly distributed. The bottles were then placed in a container with solid agar and conducted in the MRI machine under the following parameters: In 3D IDEAL spoiled-gradient-echo pulse sequence: repetition time=10ms, echo times= 2.0, 2.4, 2.8, 3.2, 3.6, 4.0 ms, flip angle=5°, receiver bandwidth=±125kHz, 2mm in-plane spatial resolution, eight 5-mm slices and single signal average. Single voxel MRS was performed on ten emulsions with a fat fraction of 10-100% fat with the same scan parameters as repetition time=4s, echo time=23ms, bandwidth= 2.5kHz.

3.2.4 Clinical participants for validation

The cohort MRI images of 16 asymptomatic subjects were acquired from our clinical study (6 males, 10 females, age range 20-55 years, the details of participants were summarized in **Table 3-1**). Each subject underwent the MRI scan involving a single axial 3D IDEAL spoiled-gradient-echo acquisition encompassing the right lobe of the liver and pancreas. The parameter of MRI imaging was set similarly to the phantom study, except resolution in-plane was set at a range of 2-2.75mm, based on the body habitus, and 12 slices were obtained. Six echoes spacing 0.8ms were acquired in total with the first echo between 1.0-1.5ms. The IDEAL scans

were conducted under giving the patients instruction of 20s breath-hold section. Each MRS scan took 3-4 mins to complete with no breath-holding. MRS were conducted on the liver and pancreas with the same parameters as the phantom, no water suppression, and eight signal averages. For the liver, a voxel of 20×20×20 mm^3 was targeted to the right lobe avoiding the vascular and biliary noises. For the pancreas, the voxel was placed inside the organ and avoided including any visceral fat surrounding the pancreas.

Table 3-1. Summary of anthropological details of 16 participants in this study.

Participant ID	***Gender***	***Age***	***Weight (kg)***	***Height (m)***	***BMI***	***Ethnicity***
1	Male	20	71.5	1.82	21.6	NZ European
2	Male	28	88.8	1.79	27.7	NZ European
3	Male	35	106.7	1.88	30.2	NZ European
4	Male	32	89.7	1.75	29.3	Pacific Islander
5	Male	22	78.7	1.83	23.5	Pacific Islander
6	Male	55	93.4	1.69	32.7	Māori
7	Female	38	86.4	1.58	34.6	Māori
8	Female	43	94.3	1.77	30.1	NZ European
9	Female	52	83.8	1.68	29.7	NZ European
10	Female	48	75.7	1.72	25.6	NZ European
11	Female	21	81.1	1.56	33.3	Pacific Islander
12	Female	29	74.7	1.67	26.8	Pacific Islander
13	Female	33	68.2	1.55	28.4	Pacific Islander
14	Female	39	46.2	1.58	18.5	Asian
15	Female	46	59.1	1.65	21.7	Asian
16	Female	32	62.7	1.63	23.6	Asian

The pancreas fat fraction was also segmented manually by experts under the guidance of the method of our previous published studies. (Al-Mrabeh et al. 2017, Yang et al. 2020, Al-Mrabeh et al. 2021) The process of segmentation was shown in **Figure. 3-1**. We compared the results of this method with the ones derived from MRS and IDEAL.

3.2.5 Data and Statistical Analysis

Fat fractions calculated from IDEAL and MRS were compared against true fat volume fraction in the phantom study in linear regression. Pixel length was converted into millimetres for further application on manual operation and machine learning. From the in vivo studies, expert manually derived pancreas fat fraction (PFF_{MANUAL}) based on phantom scale was compared with the methods of IDEAL (PFF_{IDEAL}) and MRS (PFF_{MRS}) for validation. Linear correlation and Pearson's correlation coefficient (r) were applied in those comparisons. The linear regression was analysed by identifying the gradient difference derived by the t-test. For box-and-whisker plots were drawn from paired t-tests to test whether there were statistical differences among methods. $P<0.05$ was used to claim statistical significance and 95% confidence intervals are provided for the *in vivo* experiments.

3.3 Results

3.3.1 Summary of phantom experiment

The results of the phantom experiment were summarized in **Fig. 3-1.** where the separated water, fat, and fat fraction gradient heatmap from IDEAL are demonstrated. The gradient of each phantom emulsions was plotted linearly and compared with the true fat volume fraction. The **Fig.3-1** d showed excellent correlation between true fat volume fraction and the fat fraction both from IDEAL (slope=0.99, R^2=0.99, $P<0.001$) and from MRS (slope=0.95, R^2=0.99, $P<0.001$). Compared with the zero-intercept, IDEAL (0.24) was less biased than MRS (0.69). This is likely because, in IDEAL, the fat fraction operation in Eq. (b) utilized magnitude values of F and W, which balanced the impacts from both the intrinsic noise in the separated fat-water images and phase errors due to eddy currents from the magnet hardware. This also suggested that the IDEAL technique is more robust in fat-water separation and accurate in fat content quantification.

The pixel length was converted to length in millimetre through measuring tools in the app of image J. We measured the real size of the diameter (42mm) of the bottle by tape and, the result matched the one received from the software. We also measure the length of the container for reference shown in Fig.2 c. The result was concluded in the table, and the average convert ratio was 0.76.

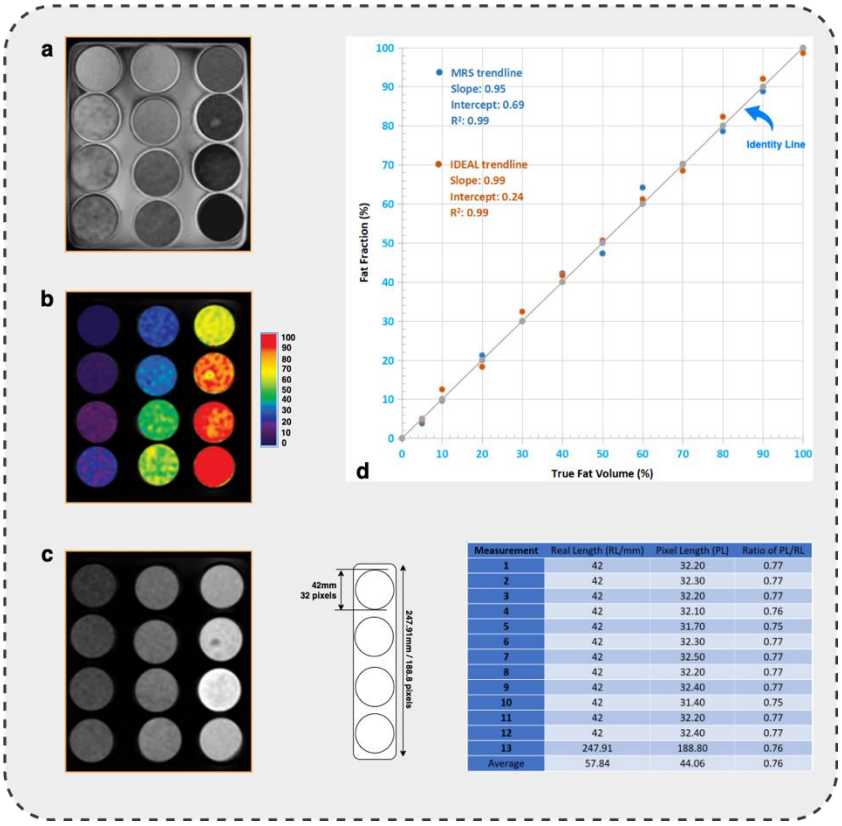

Measurement	Real Length (RL/mm)	Pixel Length (PL)	Ratio of PL/RL
1	42	32.20	0.77
2	42	32.30	0.77
3	42	32.20	0.77
4	42	32.10	0.76
5	42	31.70	0.75
6	42	32.30	0.77
7	42	32.50	0.77
8	42	32.20	0.77
9	42	32.40	0.77
10	42	31.40	0.75
11	42	32.20	0.77
12	42	32.40	0.77
13	247.91	188.80	0.76
Average	57.84	44.06	0.76

Figure 3-1 Phantom results from oil-water emulsion experiment a.) the water image. b.) the heatmap of fat fraction gradient. c.) the fat images with the result of pixel to millimetre length conversion measurement. d.) correlation of true fat volume fraction against the mean fat fraction computed from IDEAL and MRS.

3.3.2 Illustrate HFF results of IDEAL and MRS from patients

The HFF results from two subjects that read from both IDEAL and MRS was illustrated in **Fig. 3-2 a**. One subject had a lean liver (top) with the HFF_{IDEAL} reading of 5.32% and HFF_{MRS} reading of 4.94%, respectively. The other had a relative fattier liver (bottom) with the HFF_{IDEAL} reading of 34.28% and HFF_{MRS} reading of 35.61%, respectively. **Fig 3-2.** b summarized the paired t-test result between the HFF_{IDEAL} and the HFF_{MRS} from all 16 MRI scans. The result showed that there was no significant difference between the two readings (P=0.239). The Pearson's correlation result (P<0.01) showed that a strong agreement between the HFF_{IDEAL} and the HFF_{MRS}. (**Fig 3-2**.c) The regression results further proved that the fat fraction readings from IDEAL and MRS were highly matched. The slope was 0.9787, the intercept was 0.0632, the R^2 was 0.99, respectively.

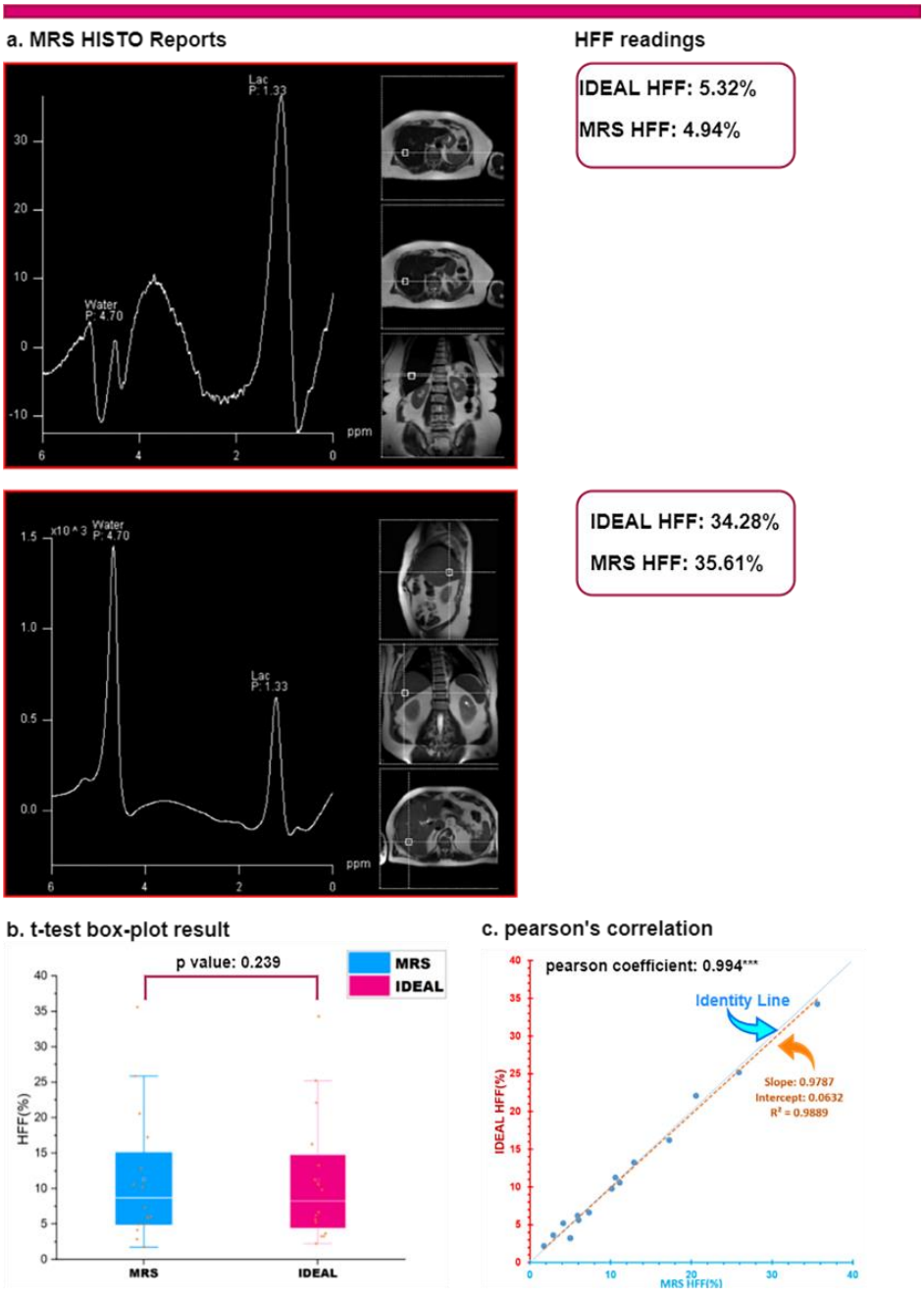

Figure 3-2 Hepatic fat fraction (HFF) results from IDEAL and MRS. a.) MRS HISTO Report from MRI machine. b.) t-test box-plot result showed that the HFF of IDEAL has no difference with HFF of MRS, p=0.239. c.) Pearson's correlation and regression of HFF between IDEAL and MRS in 16 studies.

3.3.3 Validation of PFF results from patients

3.3.3.1 PFF results of IDEAL and MRS from patients

The PFF results from two subjects that read from both IDEAL and MRS was showed in **Fig. 3-3 a**. One subject had a lean pancreas (top) with the PFF_{IDEAL} reading of 4.32% and PFF_{MRS} reading of 6.88%, respectively. The other had a relative fattier pancreas (bottom) with the PFF_{IDEAL} reading of 14.23% and PFF_{MRS} reading of 22.36%, respectively. **Fig.3-3** b illustrated the paired t-test result between the PFF_{IDEAL} and the PFF_{MRS} from all 16 MRI scans. The result showed that there was a significant difference between the two readings ($P<0.02$). The Pearson's correlation result ($P<0.05$) indicated that there was a relatively similar trend between the PFF_{IDEAL} and the PFF_{MRS}. (**Fig. 3-3** .c) However, the regression results showed that the fat fraction readings from IDEAL and MRS were not agreed with each other. The slope was 0.5884, the intercept was 0.7324, the R^2 was 0.92, respectively.

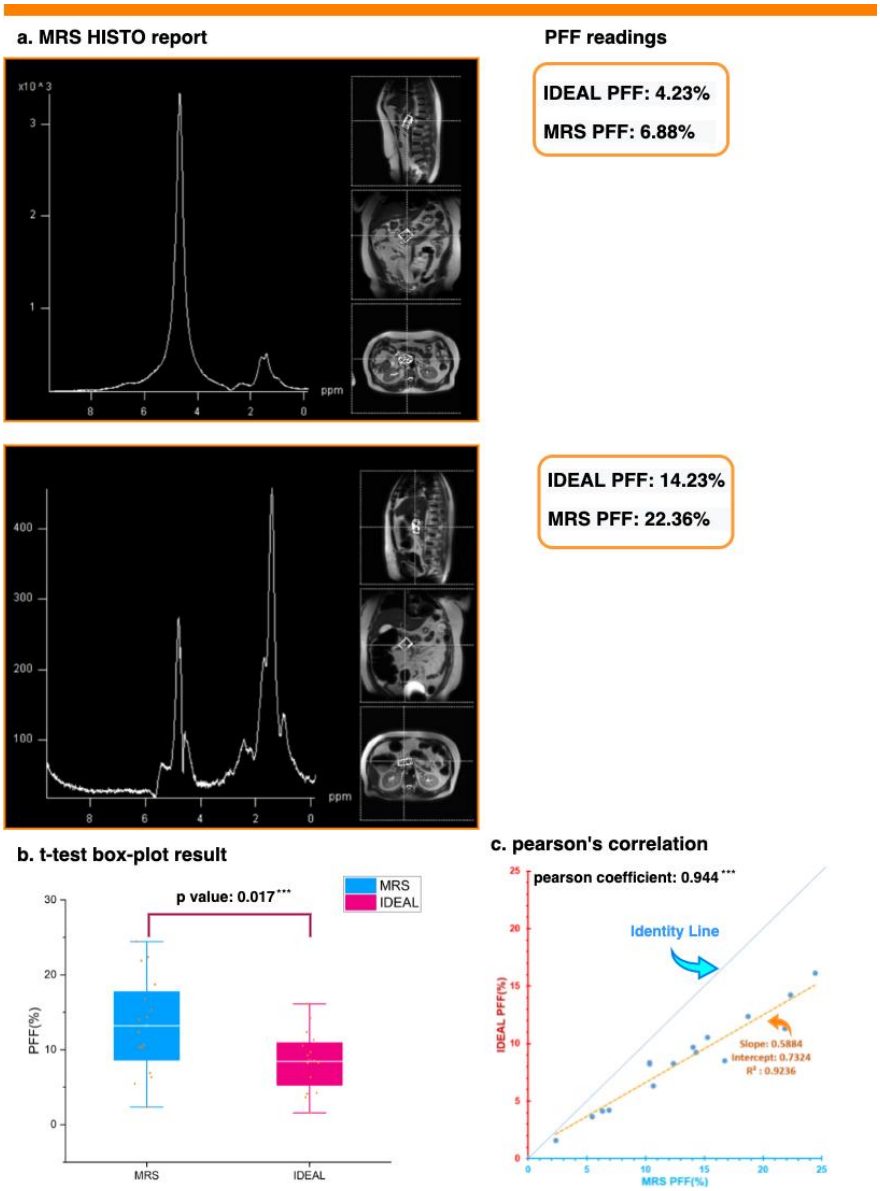

Figure 3-3 Pancreatic fat fraction (PFF) results from IDEAL and MRS. a.) MRS HISTO Report from MRI machine. b.) t-test box-plot result showed that the PFF of IDEAL was significantly different from PFF of MRS with p value of 0.017. c.) Pearson's correlation and regression of PFF between IDEAL and MRS in 16 studies.

3.3.3.2 PFF validation by manual operation

The PFF_{IDEAL} and PFF_{MRS} were compared with the manually derived PFF results, which were shown in **Fig 3-4** a. b. The regression correlation between PFF_{MANUAL} and PFF_{MRS} was 0.2703 with the interception of 1.4005, and R^2 of 0.7397. The regression correlation between PFF_{MANUAL} and PFF_{IDEAL} was 0.4516 with the interception of 1.1308, and R^2 of 0.7738. The regression gradient of both readings of PFF_{MRS} and PFF_{IDEAL} and PFF_{MANUAL} has sloped away from the identity line, which means the PFF readings from the artificial method was not agree with the MRI machine. The t-test result also showed there was a significant difference between PFF_{MANUAL} and PFF_{MRS} with $p<0.01$ and between PFF_{MANUAL} and PFF_{IDEAL} with $p<0.01$. The general pancreatic fat deposition range was reported as 1.8%-10.4% with a mean of 4.5% (Wong et al. 2014),which was shown on the box-plot graph by a dashed line.

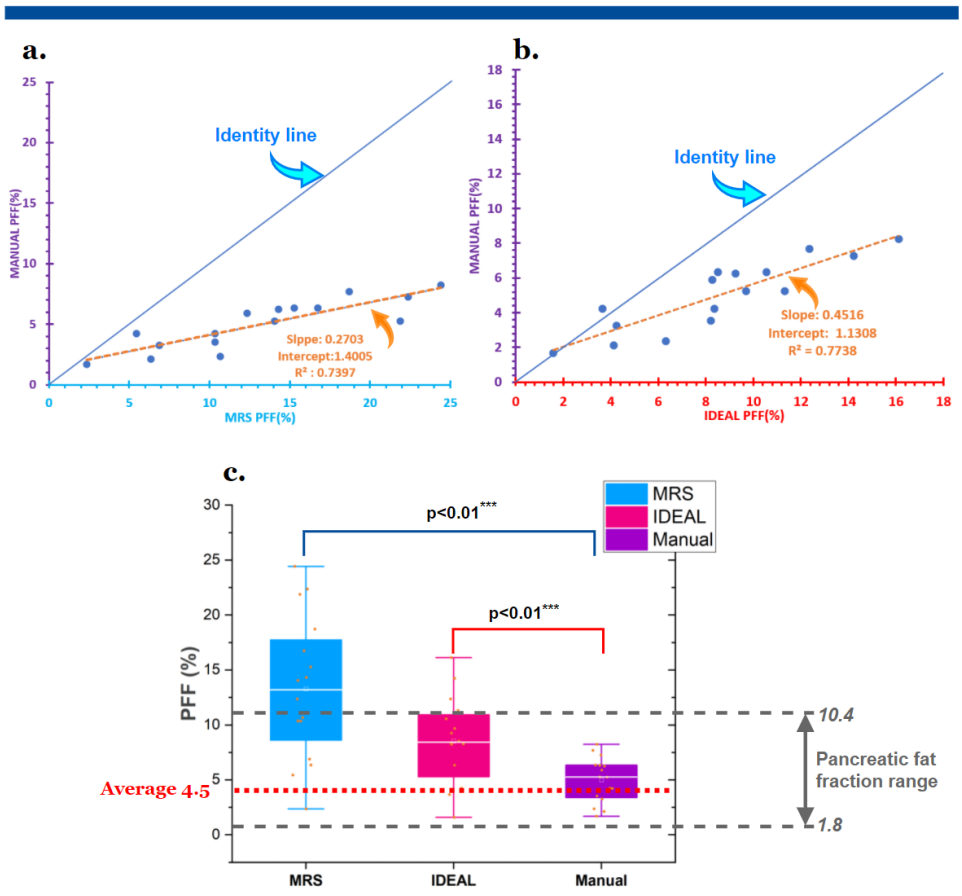

Figure 3-4 Correlation of the manually and machine derived PFF. a.) Regression of MRS PFF and manually derived PFF b.) Regression of IDEAL PFF and manually derived PFF c.) t-test box-plot results between MRS PFF, IDEAL PFF and Manually derived PFF. The general pancreatic fat fraction range and mean value were noted with dash line.

Chapter 4. An in Clinical Multi-protocol Magnetic Resonance Images: a retrospective study with multi-ethnic external validation

In part of my study, I established a novel CNN based on U-net and designed a new method for CNN architecture to recognize pancreas and work out pancreatic fat deposition based on the expert manual segmentation process. Most of the MR images used for building up the automatic pancreatic segmentation were from the previous clinical research. Only the data for the validation of novel CNN was from the newly recruited patients who was conducted bariatric surgery. The data was collected from both before and after their surgeries. For the patient recruitment, it is a single centre, prospective, randomised, double blind procedure, both of their pre-surgery and post-surgery followed a same protocol with our previous clinical research. There were 156 participants in total from different ethnicities in New Zealand with more than 3000 qualified MR images involved in this study. We further enrolled 10 more individual patients for validation purpose.

4.1 Introduction

Diabetes is a disorder of glucose metabolism which is an increasingly prevalent chronic disease(Nazir et al. 2018), with high morbidity and mortality, that can be reduced by early diagnosis and treatment (DeSouza et al. 2018b). The pancreas plays a critical physiological role in maintaining glucose homeostasis. Recently, mendelian randomization studies have documented a causal role for pancreatic fat (and volume) in type 2 diabetes (Martin et al. 2021), after several reports describing an association between reduced pancreas volume and type 2 diabetes (Goda et al. 2001b, Burute et al. 2014, Desouza et al. 2018a, Macauley et al. 2015), or increase in ectopic fat deposition in the pancreas in individuals with T2DM (Garcia et al. 2017, Garcia et al. 2018, Singh et al. 2019, Singh et al. 2017a, Singh et al. 2017c, Singh et al. 2017b, Al-Mrabeh et al. 2016).Thus, precise characterization of the pancreas has the potential for improving diabetes risk stratification and treatment selection. Traditional intra-organ investigating techniques such as computed tomography (CT) has lower response sensitivity of fat tissue gradient in pancreas (Patel et al. 2013a, Kim et al. 2014b). MRI offers highly sensitive mechanisms for identifying fat from lean tissues based on T_1 relaxation chemical-shift properties.

Over the past 20 years, the development of reconstruction algorithms have dramatically improved the MRI techniques and enabled advanced fat fraction quantification function, which is called proton density fat fraction mapping (PDFF) (Stine et al. 2021). PDFF, which is currently regarded as the most practical and meaningful MR-based biomarker of tissue fat fraction (Reeder et al. 2012), provides a reliable fat fraction result by exploiting the difference in resonance frequencies of protons in water and fat(Mashhood et al. 2013). However, quantification of the fat deposition inside relatively small organs such as the pancreas by MRI-PDFF is still challenging as it is based on delineating tissues entirely within the pancreas. The relative softness of the pancreas makes it easy to be squeezed by its surrounding organs, which reduces the demarcation of the boundaries of the pancreas, which collapse with other non-pancreatic soft tissues, such as the small intestine, blood vessels, and visceral adipose tissues of abdomen. Consequently, measurements of pancreatic volume and fat deposition by MRI in humans are highly variable (Szczepaniak et al. 2013b, Lingvay et al. 2009b, Hu et al. 2010b, Pinnick et al. 2008). Manual fat segmentation on MRI images by experienced evaluators is regarded as the gold standard. (Al-Mrabeh et al. 2017) In order to reduce inter-observer and intra-observer variability, one traditional manual pancreatic fat segmentation method quantifies 100mm^2 regions of interest (ROI) within the entire pancreas, and excludes pixels with fat percentage values of <1% and >20% which represent histological verified blood vessels, ducts or visceral fat (termed MR-opsy) (Al-Mrabeh et al. 2017). However, this method is still time consuming and is unable to calculate pancreatic volume.

Rapid development of Convolutional Neural Networks (CNNs), such as full convolutional network (FCN) and conditional random fields (CRF)(Ronneberger et al. 2015, Long et al. 2015, Krähenbühl and Koltun 2011, Roth et al. 2018, Zhou et al. 2017) has advanced much of medical image analysis, by enabling computers to learn organ segmentation tasks from large MRI datasets including heart, liver, kidney and spleen (Alom et al. 2018, Cai et al. 2016). However, automatic pancreas segmentation has rarely been reported to date due to the high inter-observer variation of this retroperitoneal organ. Furthermore, additional information shown from 3D MRI scans compared to 2D images, makes it more complicated to establish 3D models by using the classical Atlas model(Wolz et al. 2013) for context learning due to the limitation of current GPU memory. While there are flaws in each method, updated, 2D and 3D networks have been developed, and strategies such as coarse-to-fine framework, recurrent and ensemble learning have been applied to improve accuracy of segmentation results (Li et al. 2019, Zeng and Zheng 2019, Yu et al. 2018, Zhu et al. 2018).

This study describes the development and validation of a modified coarse-to-fine 2D framework for auto pancreas segmentation and pancreatic fat fraction measurement. This framework was built around the traditional clinical manual operation. The development included two consecutive stages: localization stage and refinement stage. We selected more than 3000 MR water images with clear characteristic of pancreas from 156 individuals for this work. 2800 of these images for training and 200 for testing the CNN. The pancreas boundary was labelled using LabelMe(Russell et al. 2005) from MR images by one experienced operator for training purposes. After the CNN established, we applied it to identify the fat MR images. To standardize the fat pixel segmentation, we conducted phantom study which help setting up both real dimension and the fat percentage scale. The fat pixel information on phantom images were converted into digital signal for the machine to exclude any pixels of <1% and >20% fat depositions in the pancreas. The area measurement of pancreas and fat pixels within it on each image slice of one participant was stacked together to calculate the volume of pancreas and pancreatic fat. We then validated the state-of-art network on 10 more participants by employing both traditional clinical manual calculation and our CNN.

To solve the problem of the discontinuity of the grey pixel value and the ambiguity edge between pancreatic and other tissues in the localization stage, we employed super pixel segmentation, which is a shallow learning model that initially clusters image pixels based on their local structural features and spatial characteristics between them. This method aggregates image pixels into a series of adjacent pixel blocks with similar colour, brightness, and texture, which enhances the boundary contrast between super pixels. An overview of the segmentation framework is illustrated in **Fig. 4-1**. To date, this is the first idea to propose such a method to segment pancreatic fat content.

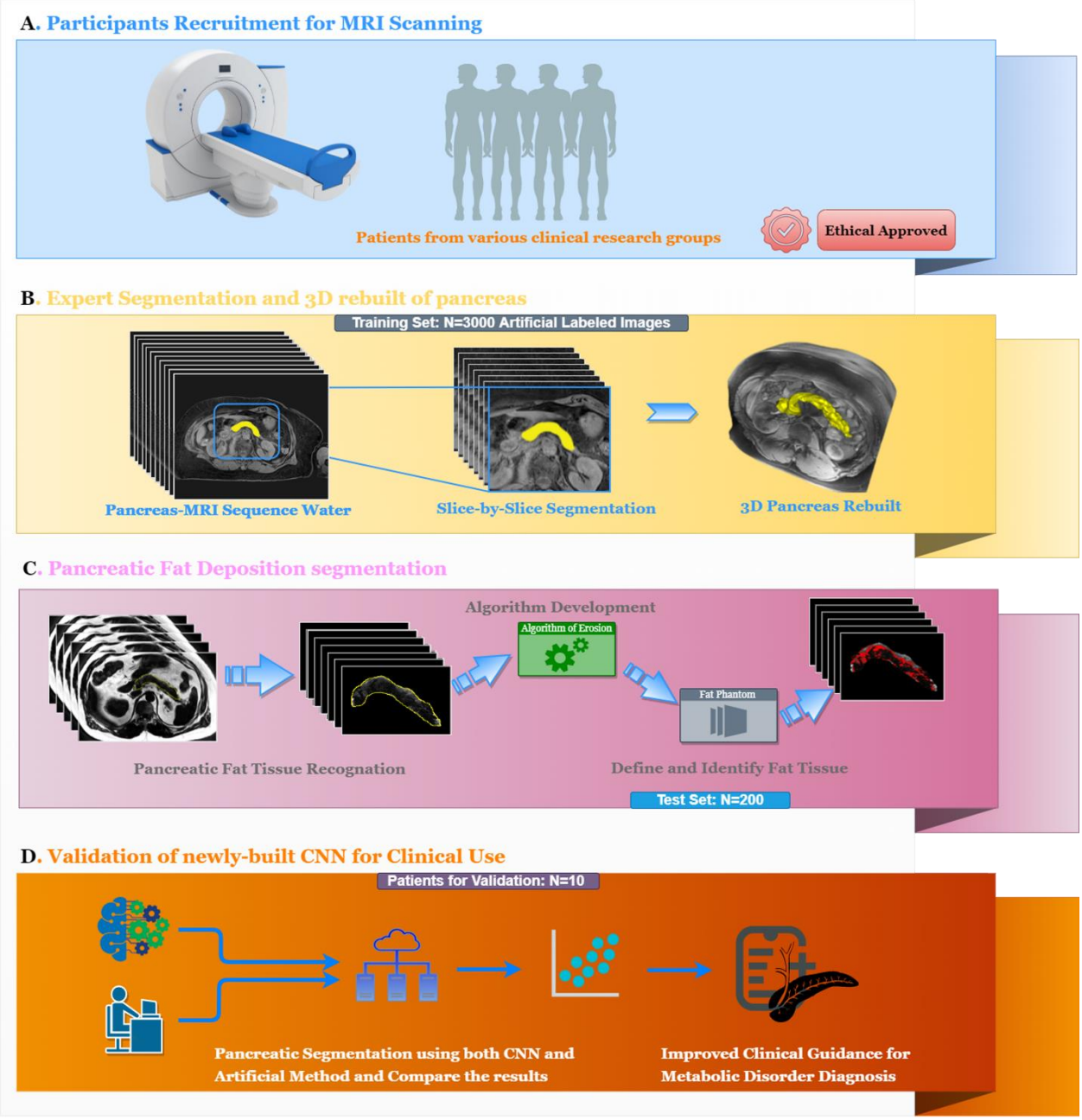

Figure 4-1 The overall workflow of the pancreatic volume and fat tissues segmentation. A) Clinical MRI scanners were used to acquire raw data for machine learning. Patients were recruited from our other research groups for metabolic disorders. B) The pancreas was manually segmented in a slice-by-slice manner by experts to obtain labels of the pancreas. The 3D geometry can be obtained from stacking 2D segmentation together. C) Improved algorithm of CNN for the segmentation of fat tissue in the pancreas. Fat Phantom was conducted with the same MRI machine to establish the criteria boundary for fat pixel selection. D) Validation of the newly built CNN with 10 patients from an isolated obesity-related research project

4.2 Materials and Method

4.2.1 Sample Size and details

Among the 156 participants, 38 of them were with prediabetes, 36 were in diabetes, and 82 of them were normoglycemic. These patients were from different ethnicities in New Zeeland with the age range of 18-84 y (average of 47.2 y) Investigation of health and ethnic background was conducted all patients before they went through MRI to make sure that they had no drug history and no malignancy, coeliac disease, cystic fibrosis, chronic pancreatitis, pregnancy, or symptoms of upper abdominal pain and nausea. They also had no endocrine disorders, nor any history of acute infectious or inflammatory conditions requiring medical evaluation or treatment in the 3 months prior to the study date. All participants included in the study provided informed consent. Participants were excluded if they were unable to give informed consent and unwilling to commit to follow-up or had general contraindications for MRI (such as metallic foreign body or electronic device implantation).

The validation MR images were from the patients in another clinical research category at the same hospital. These participants have the metabolic conditions and will conduct bariatric surgery. We totally involved 10 volunteers for novel CNN validation. After receiving verbal consent, all patients were required to complete a survey form which includes age, height, weight, race, smoking and alcoholic history, bowel motion, the frequency of defecation and medical history. Participants were grouped into NZ Europeans, Asians, and Māori/Pacific Islanders (PI). The questionnaire we used is attached as (Appendix C).

4.2.2 Image pre-processing and development of the automated pancreatic segmentation model

The MRI scan resolution was 512×512, average thickness was 3mm, and the MRI images were converted from DICOM into PNG files using MicroDicom for the convenient using purpose. The measurement of images was conducted on Image J from phantom study, we then converted the pixel length to real length accordingly.

The MRI images were then selected to discard the cluster images which were not suitable for automated segmentation, and around 3000 choice images were included with minimum reserve of 7 images for each participant. Images with clear pancreas was labelled by LabelMe(Russell

et al. 2008) for deep learning. Of the 3000 image files, 2800 were selected randomly for training and the remaining 200 images were reserved for testing.

MRI imaging modality presents more details in soft tissues due to the slow imaging speed and the relatively low resolution of MRI images often introduces more boundary artifacts for the pancreas. So, it is important to pre-process the images to strengthen the contrast between the tissues in organs. Super pixel segmentation is the method that gathers the reduced dimensionality pixels with similar colour, brightness, texture to generate a visual summary image. This enhances the contrast between the boundaries of different tissues and dramatically increases the accuracy of pancreas recognition. The image pre-processing includes two stages: super pixel segmentation and image dimensionality reduction.

4.2.2.1. Super pixel segmentation

There were rarely seen reports that establish pancreatic segmentation CNN using the super pixel method. The linear spectral clustering (LSC) method can be regarded as the best performing super pixel segmentation acting on three-channel natural images (Chen, Li and Huang 2017). However, the MRI medical images have only one-grey-channel that cannot be directly segmented by LSC. The simple linear iterative clustering 0 (SLIC0) can be regarded as the latest and optimum method for super pixel segmentation of medical images(Qiao et al. 2021). Thus, we adjusted the method of distance measurement in LSC to enable super pixel segmentation of the MRI images based on SLIC0. Only grey scale distance was measured to get the pixel distance in medical images.

$$\boldsymbol{W}(p,q) = c_s^2\left(cos\frac{\pi}{2}(x_p - x_q) + cos\frac{\pi}{2}(y_p - y_q)\right) + c_c^2\left(cos\frac{\pi}{2}(g_p - g_q)\right)$$

In the formula, $\boldsymbol{W}$ represents the distance between pixels, p and q are 2 different pixels, c_s is the spatial proximity, c_c is the colour similarity, x and y are the spatial positions of pixels, g is the gray scale value of pixels.

Compare this with the pixel distance measurement formula in original LSC,

$$d_s = cos\frac{\pi}{2}(x_p - x_q) + cos\frac{\pi}{2}(y_p - y_q)$$

We keep the same pixel spatial distance value d_s and change the pixel colour distance value from

$$d_{C_1} = cos\frac{\pi}{2}(l_p - l_q) + 2.55^2\left(cos\frac{\pi}{2}(a_p - a_q) + cos\frac{\pi}{2}(b_p - b_q)\right)$$

to

$$d_{C_2} = \cos\frac{\pi}{2}(g_p - g_q)$$

To get better pancreas segmentation, the variables *l*, *a*, *b* in these formulae which represent the colour scale values of pixels were replaced by grey scale values. By adjusting the ratio, r, of c_s and c_c, the improved LSC method can generate super pixels with higher compactness (CP) and boundary recall (BR).

$$r = c_s / c_c$$

The larger the r value, the closer the spatial pixels cluster together, which generate super pixels with high CP but low BR. Conversely, low r values generate pixels with low CP but high BR. In order to get the super pixels with both high CP and BR, we propose a new index as follows:

$$I = 1 - BR/CP$$

The CP and BR would be balanced when *I* reaches a minimum positive value. In this study, we used simulated annealing (SA) method to get r value.

4.2.2.2. Comparison of improved LSC and SLIC0 method

We compared the performance of our improved LSC with SLIC0 using the evaluation index of super pixel segmentation. They are under segmentation error (UE), boundary recall (BR), and achievable segmentation accuracy (ASA)(Schick, Fischer and Stiefelhagen 2014). These indexes can be derived from the following formulas:

Formula for UE:

$$UE = \frac{Us}{Rs+Os}$$

In this formula, O_S represents the observed number of segmented pixels which should not have been presented; R_S is the theoretical number of pixels; U_S is the number of pixels that did not appear in the actual segmented image which should have presented theoretically.

Formula for BR:

$$BR(S,G) = \frac{TP(S,G)}{TP(S,G)+FN(S,G)}$$

When given a ground truth, G and S represent the reference and real boundaries of super pixel segmented images, respectively. The maximum distance d=1. TP is the true value of the pixel number of S that overlaps G within the range of d. FN is the value of the opposite of TP.

Formula for ASA:

$$ASA = \left(1 - \frac{|Rs-Ts|}{Rs}\right) \times 100\%$$

R_s represents the manually segmented reference area that is marked by the expert; T_s is the area from the trained CNN.

4.2.2.3. Dimensionality Reduction of Images

Based on super pixel segmentation, we adjusted the images by reducing dimensionality and generated their visual summary maps that only showed the structural features between super pixels. Combined with the idea of average pooling in deep learning, we input CNN a calculation of averaging grey values of all pixels in each super pixel, and then reassigned values to each grey value to generate a schematic diagram the pre-processed abdominal schematic diagram enhanced the display of the separability between organs and tissues, which is conducive to the segmentation of the pancreas.

4.2.3 The Design of Convolutional Neural Networks.

The MRI machine responds to water and fat content in opposed phase due to the uniqueness of their chemical structure. Thus, each slice of the pancreatic MRI image was produced in both water and fat images that are shown in **Fig.3-1**. Manually, experts segmented the pancreas area based on water images and which correspondingly reflected the boundary for its fat series, where the fat tissue pixels could be exposed by adjusting the threshold on clinical software. We previously have published the details of the manual clinical pancreatic segmentation(Yang et al. 2020). Based on this technique, we proposed the framework of our novel CNN.

We fine-tuned an existing U-net model and trained a new CNN architecture from scratch (Roth et al. 2015) to converge based on a large amount of artificially labelled training data of MRI water images, which was obtained from our previous clinical research. To increase CNN accuracy, we transferred learned kernels in the bottom layers of the VGG-16 network to our domain (Simonyan and Zisserman 2014), which have been proved to be highly discriminative with a stable training convergence (Girshick et al. 2014). U-net models have produced extraordinary results in the area of medical image segmentation combining the information from low and high medical image layers which help to improve accuracy and extract complex features, respectively. In our study, we applied ideas of super pixel to make the identification of pancreas on 2D MR images more accurate. The overview of the process was summarized in **Fig 4-2**.

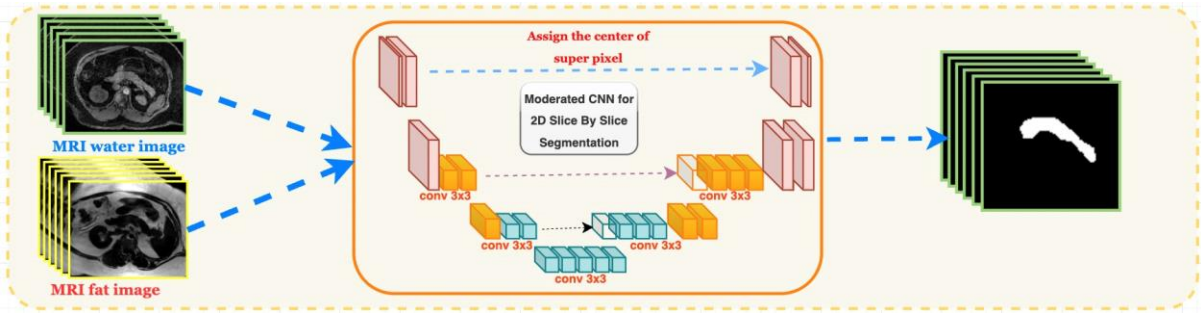

Figure 4-2 The overview of modified CNN process for pancreas volume and fat deposition

We improved the CNN by adding the super pixel method for pancreatic image segmentation. In the last layer of traditional CNN, it performs 1×1 convolutional classification, which significantly slows its inference procedure. To address this problem, we proposed an acceleration method shown in **Fig 4-3**, which only performs convolutional classification on the labelled super pixel at the centre position that represents the same pixel cluster with identical characteristics. This method ensured both the network speed and its classification performance.

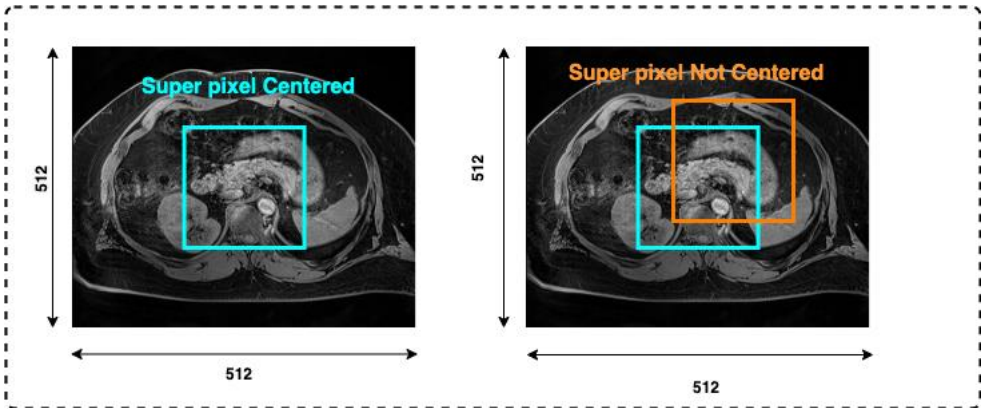

Figure 4-3 Super pixel cantered MR Image VS offset

4.2.4 Strategy of determining pancreas volume and pancreatic fat deposition

We further fine-adjusted and enabled the CNN with the function of measuring pancreas volume and pancreatic fat deposition based on the artificial measurement method.

Overall, the segmental volume was calculated as the product of area of each pancreatic slice (generally there were 6-9 pancreatic MRI images for each patient) and the thickness (3mm), as indicated by the Cavalieri principle: (Sahin et al. 2003)

$$Volume\ in\ vivo = \sum Volumes\ of all\ pancreatic\ slices$$

We input the water phase MRI images into the well-trained CNN and segmented the pancreas for accumulating the total volume. **(Fig 4-2)** On the one hand, the corresponding fat MRI images can be segmented with a redundant boundary. The pancreatic fat was distributed within the inner area of the images shown by the point pixels in **Fig. 4-4.** To calculate the inner pancreatic fat accurately, we applied an erosion algorithm to remove and adjust the extra boundary in the segmented images until we got the ideal result as shown in **Fig 4-4**. OpenCV provided a support method which is used to perform erosion on the images, which erodes away the boundaries of the foreground object. A pixel in the original image (either 1 or 0) will be considered 1 only if all the pixels under the kernel is 1, otherwise it is eroded (made to zero). In clinical manual operation, the threshold of the pancreatic fat image was adjusted in Image J to get the ideal fat pixel for accumulation. On average, the ideal threshold range, when converted into fat percentage, was at 1%-20%. Thus, we made the modified CNN recognize the fat pixels within the fat percentage range for accumulation. We assigned the values for the kernel until the CNN got a similar performance as artificial segmentation and measured the fat pixels in the segmented images.

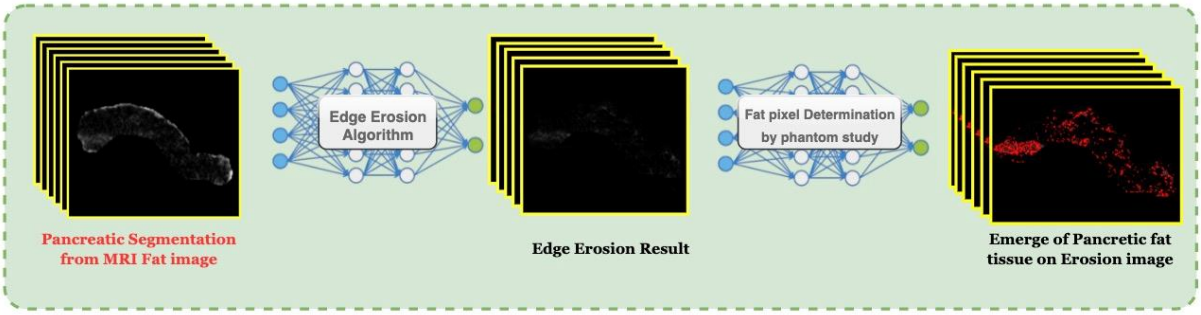

Figure 4-4 Method of pancreatic volume and fat deposition

4.2.5 Training and validating the novel CNN

4.2.5.1 Training Process

Training was conducted on a workstation with Inter i9-11900k CPU 2080 NVIDIA Ti GPU using Python 3.6.0 and packages TensorFlow and Keras. The CNN training process included continuous iterations of forward followed by backward propagation. The forward propagation involves feeding input images and ultimately returning corresponding output sets of per-pixel predictions of being within an aneurysm. The segmentation accuracy of each sample was evaluated by the Dice Similarity Coefficient (Dice Score), which measures the overlap between the user-annotated aneurysm and the CNN-predicted masks (shown as X and Y respectively):

$$Dice\ Score = \frac{2\times|X\cap Y|}{|X|+|Y|}$$

4.2.5.2 Novel CNN validation

To further validate the novel CNN, we also applied it to 10 more patients with prediabetes from our latest clinical research targeted at detecting the change of pancreas features before and after bariatric surgery. Their MRI images were obtained under the same condition as described in the training process. Two independent experienced researchers segmented pancreatic volume and fat fraction by the method we published (Yang et al. 2020) and the their results were averaged. The data was then compared with the results derived from the machine. The time consumption and how closely those two sets of results are related were observed.

4.3 Results

In this study, the MR images were collected from three independent clinical research projects in order to satisfy the images amount for built up novel CNN. Some images have been used in our previous publication.(Yang et al. 2020) The number of MR images has been increasing due to on-going participants recruitment. Thus, some results that were drawn from different stages will be notified the details in this part.

4.3.1 Testing the improved CNN

4.3.1.1 Results of the comparison between improved LSC and SLIC0 method

Based on SLIC0, we adjusted our LSC with the new method of distance measurement. The performance comparison results of improved LSC and SLIC0 are shown in **Fig. 4-5**, through which we can see the improved LSC method performed better than SLIC0 in terms of UE, BR, and ASA indexes. The results showed that the LSC method better satisfied the actual requirements of super pixel segmentation of medical images.

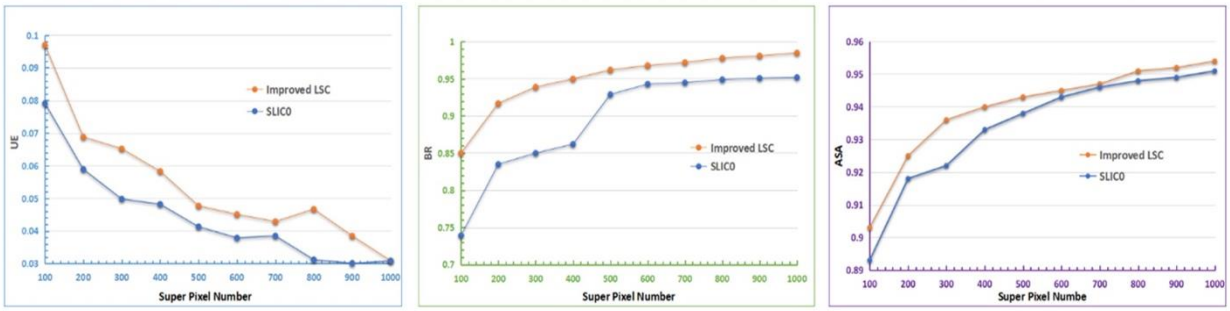

Figure 0-5 Comparison between improved LSC and SLIC0 by various evaluation index

4.3.1.2 Request r value by improved LSC method

Based on the poor segmentation feature of medical images, the segmented result of super pixel on medical images should have both high BR and CP values. To achieve this target, we adjusted the ratio of CS and CC values by the improved LSC method. According to the result of simulated annealing, we selected the r value range at [0.05,1], and calculated the *I* value correspondingly. The correlations of different *r* values of super pixel segmentation and *I* values are shown in **Fig 4-6**, from which we can see the optimum and minimum *I* value was derived when r=0.25 that achieved balance between CP and BR values.

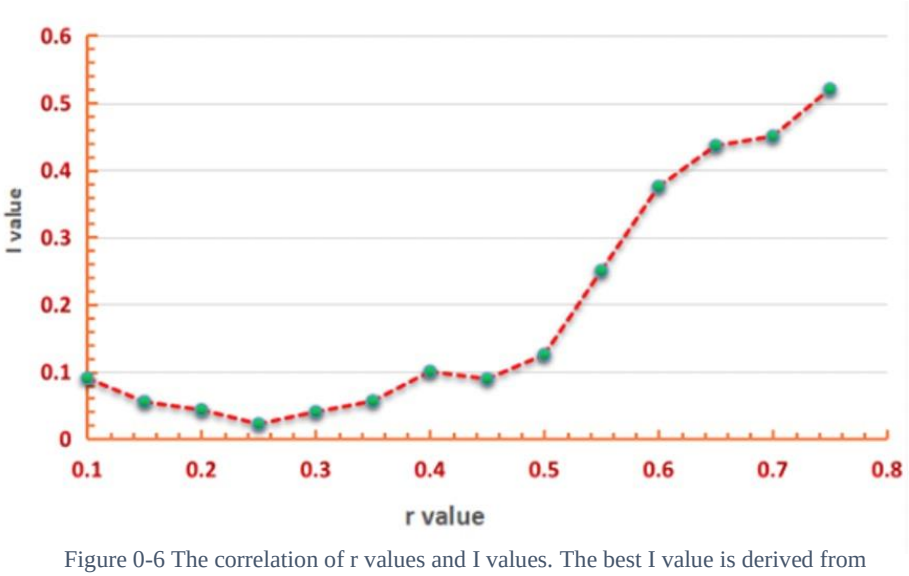

Figure 0-6 The correlation of r values and I values. The best I value is derived from the r-value. The best I value was at the r=0.25.

4.3.1.3 Result of super pixel Segmentation and generation of schematic images by improved LSC

Before we input the images into the novel CNN, we coded a pre-processing process which help with dealing with the MR images from original state to a schematic image. With the pre-testing, we get the optimum condition for generating the schematic images was to segment the images into 2500 super pixel and do algorithm of regeneration. The result of the segmentation and schematic generation was shown in **Fig 4-7**. The schematic images were clearer with the boundaries and make it easy to be distinguished from other duct and fat tissues. The method can also be applied to other types of images such as CT.

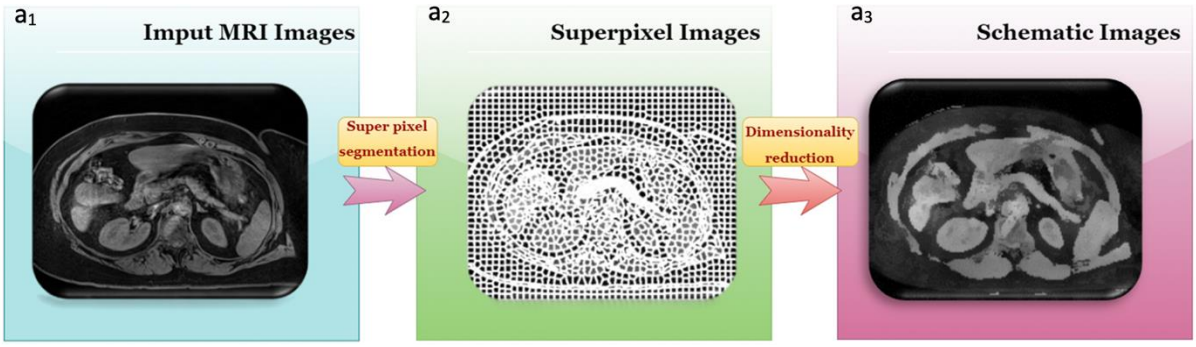

Figure 4-7 Result of super pixel segmentation and generation of schematic images by improved LSC.a_1 is the original images, a_2 is the segmented images with 2500 super pixels; a_3 is the schematic images

4.3.2 Performance Evaluation of the improved CNN

To get the best pancreas segmentation result, we pre-processed the medical images and got their corresponding super pixel schematic images. Then the processed images were input into the CNN for training and testing. We applied the standard cross-validation to complete the segmentation and trained our CNN with 2800 and tested on a set of 200 images. Dice value of each sample was calculated.

The number of super pixels was also regarded as a crucial factor that has an impact on the segmentation result. So, under the condition of training CNN for 20 epochs, we adjusted the number of super pixels on pre-processing images at 500, 1000, 1500, 2000, 2500, 3000, and 3500, respectively. The result shown in **Fig. 4-8**. suggested that Dice Score values tend to be stable when the number of super pixels is larger than 2500.

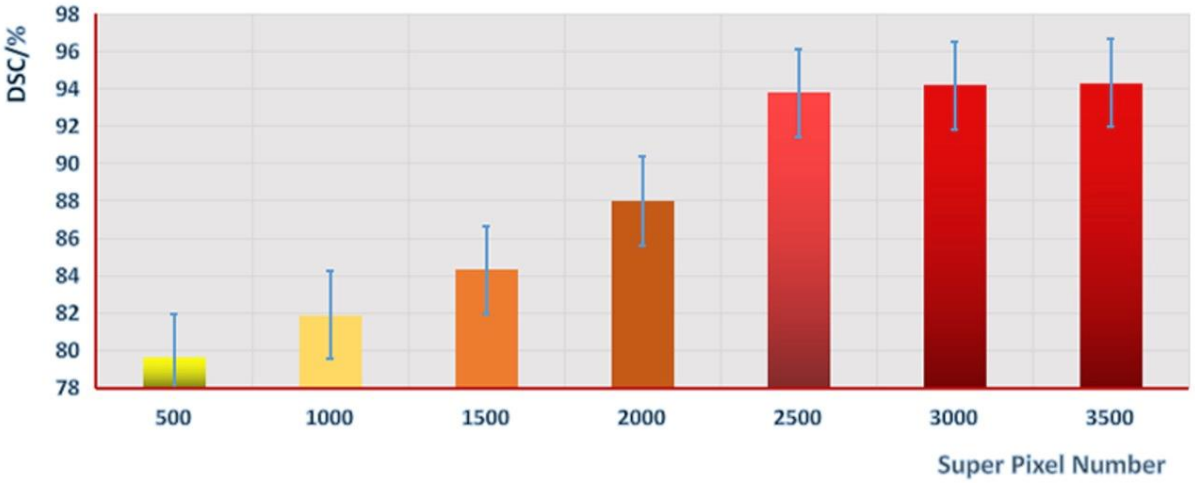

Figure 4-8 Optimum super pixel number for ideal DSC%. Correlation of the average performance and different super pixel numbers. The higher Dice scores were relatively stable after the super pixel number reached 2500

We compared the average Dice Score value of our CNN with and without pre-processing images at 1, 10, and 20 epochs; the results showed that higher average Dice Score values came out from the CNN with inputting the pre-processed images. (**Fig 4-9** A). The Loss curve based

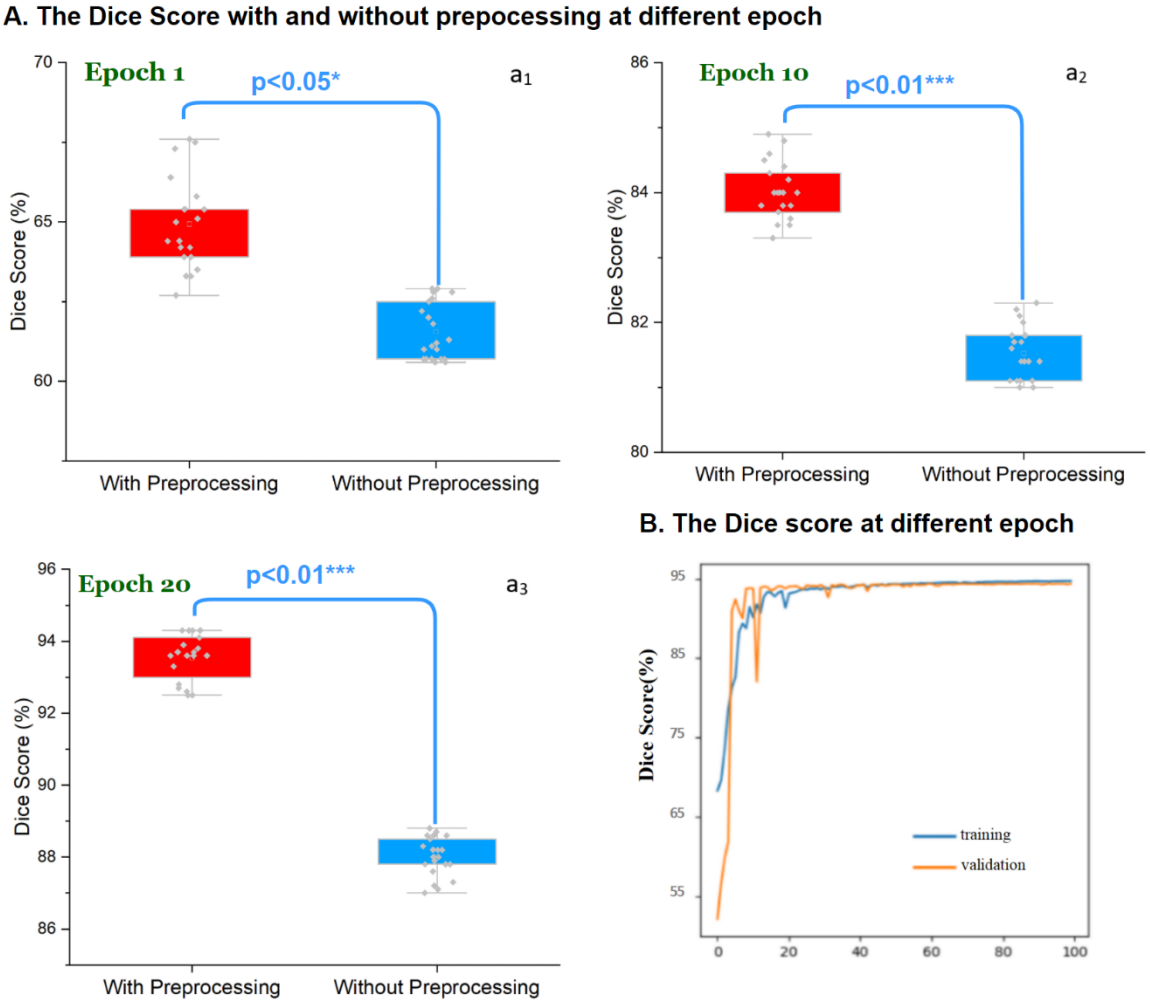

Figure 4-9 Comparison of the Performance of modified CNN at different epoch with and without pre-processing of super pixel segmentation. A) The Dice Score comparison at different epochs. a1) is at one epoch. a2) is at 10 epochs. a3) is at 20 epochs. B) The Dice score at different epoch. After 20 epochs, the segmentation became stable

on Dice score showed that the weighted network became stable after 20 epochs, which is shown in **Fig 4-9** B. In consideration of saving time, we set the optimum conditions for our CNN as training for 20 epochs with the number of super pixels at 2500.

We further compared the segmentation performance between super pixel centred and not centred, the result is shown in **Fig 4-10**. The results illustrated that centred super pixel on images can significantly increase the Dice score of the CNN, with the significance $p<0.05$.

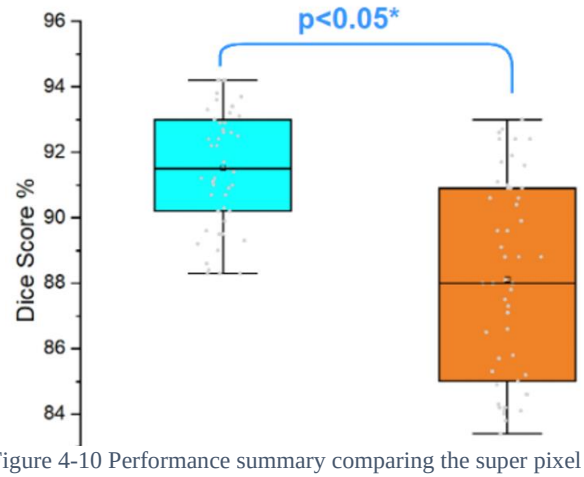

Figure 4-10 Performance summary comparing the super pixel segmentation methods of pancreas centred and non-centred

In the trail, we applied erosion algorithm to calculate the pancreatic fat deposition. By adjusting the kernel values, we trained the machine to recognize the edge of the pancreas with the pixel fade away gradually. When the image showed best performance, we used that value into our novel CNN. The evaluation of the effectiveness of the erosion algorithms shown in **Fig 4-11** The result showed that the stability of the highest performance was established when the kernel value was adjusted to 5. The corresponding Dice Score for 20 epochs reached up to 94.3%.

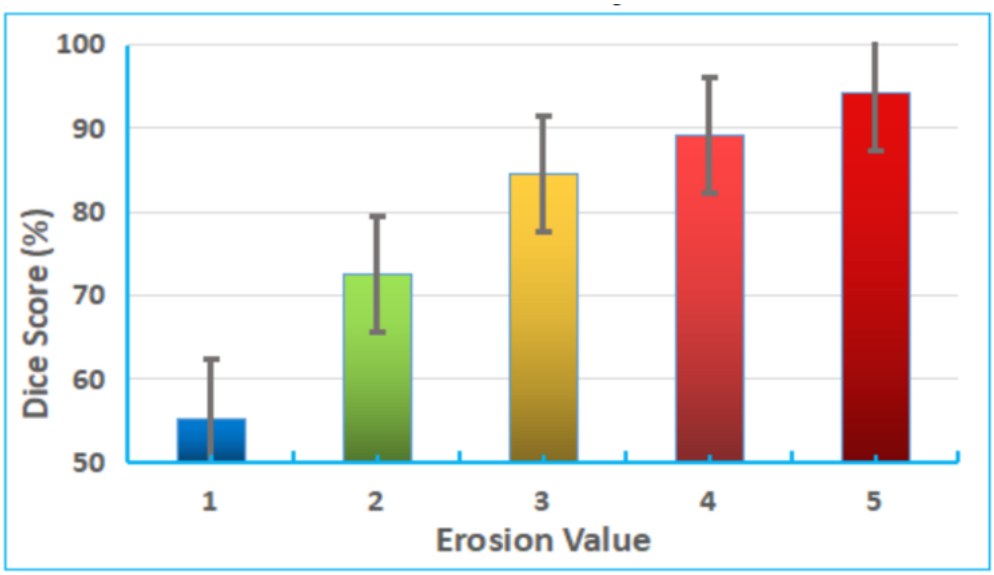

Figure 4-11 Correlation between Erosion algorithm kernel values adjusting and Dice Score

In order to exclude the unwanted pixel on image, which was smaller than 1% and larger than 20%, we also turned the gradient from phantom fat deposition into the digital signals for the machine. We trained the machine to recognize the brightness in the fat phantom. The signal can then be turned to visible colours series which was shown in **Fig 4-12.**

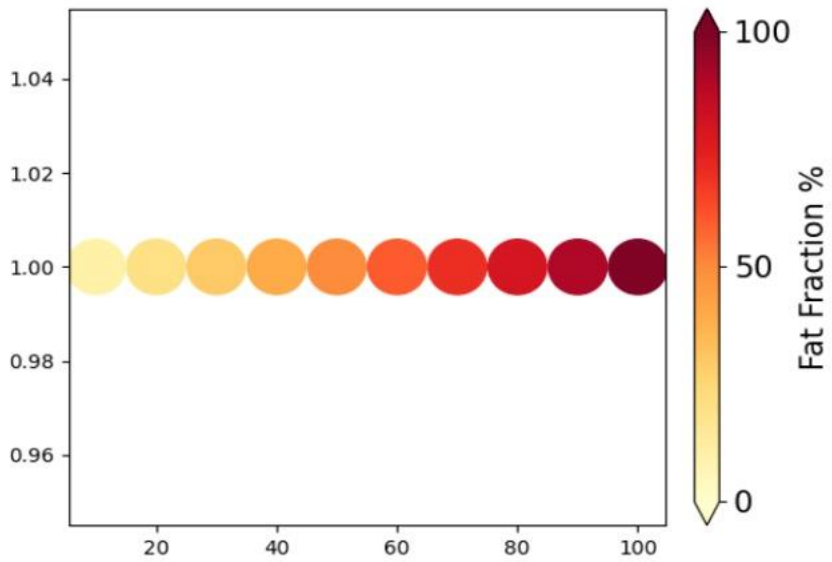

Figure 4-12 Fat fraction gradient from CNN based on phantom

Overall, when everything was ready to build up the CNN, we run the code and make it recognize pancreas on MR images. The Dice Score value from the novel CNN met the actual requirements, and the integrity of the pancreatic organ from testing images is shown in **Fig. 4-13**. We got the images directly from MRI and made comparison with the expert free hand drawing result. The high similarity can be observed from the figure.

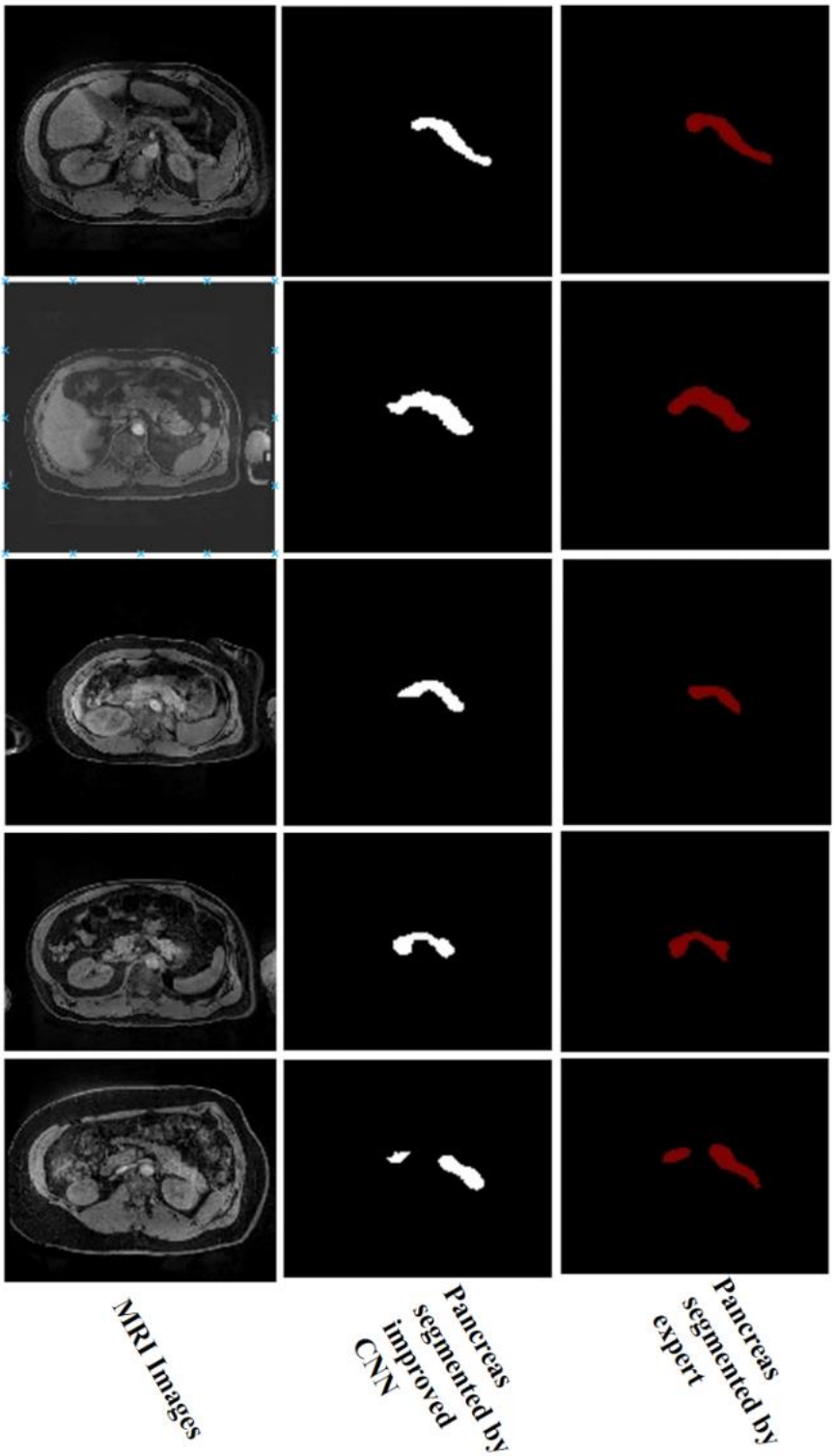

Figure 4-13 Novel CNN performance on recognition of pancreas. The original MRI images, CNN segmentation result and expert hand drawing results were listed together for comparison

After we got adequate 2D segmented images, we tried to rebuilt the pancreas organ of one of our patients to 3-dimensional image via 3DSOM, the result was shown in **Fig 4-14**.

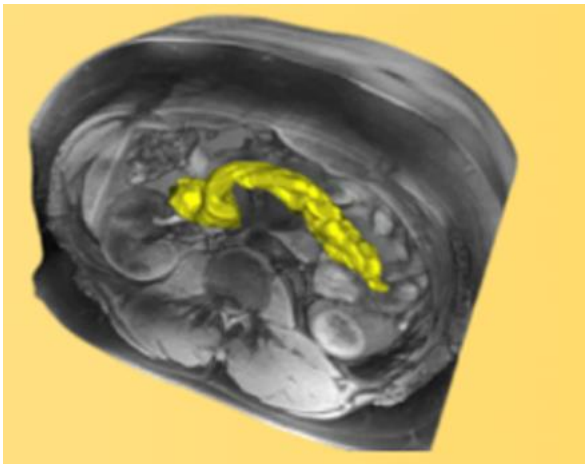

Figure 4-14 3D rebuilt result of pancreas of one patient

In recent years, there were some research groups tried to build up the CNN for pancreas segmentation. The building up ideas were different end with different recognition results. We also compared the segmentation results between our CNN and other state-of-the-art neural networks published in recent years, and the results showed that the pancreatic segmentation performance of our CNN was better than the others in terms of the mean Dice Score value (**Table 4-1**).

Table 4-1 Comparison of different pancreatic

Method	Mean Dice Score/%
Attention U-net (Oktay et al. 2018)	81.5
3D FCN (Roth et al. 2018)	76.8
RSTN (Yu et al. 2018)	84.5
Graph-based decision fusion (Cai et al. 2016)	76.1
Lightweight DCNN modules (Zhang et al. 2021)	85.6
Spatial aggregation (Zhou et al. 2017)	81.3
Fixed-Point (Chen et al. 2017)	83.2
Bayesian Model (Ma et al. 2018)	85.3
Our CNN	91.2

4.3.3 Clinical validation of the novel CNN

In order to further validate the novel CNN, a cohort of 10 more obesity patients who were assigned to do bariatric surgery was enrolled for the study (6 male, 4 female, age range: 21-55 y). The details were summarized in Table 4-2.

Table 4-2. Summary of details of 10 participants in validation.

Characteristics	**Total**	**NZ European**	Māori/**Pl**	**Asian**
No. of participants	10	3	6	1
Age (years)	46	40	44	55
Sex				
Male	6	2	3	1
Female	4	1	3	0
Height (cm)	174	179.4	172.8	172
Weight (kg)	101	107.4	112	85.6
WC (cm)	111	110	115.5	108.3
BMI (kg/ m^2)	33.3	33.4	37.5	29
LAT (Single slice)	9.6	8.3	12.8	7.6
PAT (cm^3)	2706	1890	3480	2748

Each subject underwent twice MRI examinations before and after their surgeries with consistent conditions as described in method. The validation of the segmentation results of pancreas volume and pancreatic fat fraction by the artificial method and novel established CNN are shown in the regression graph in **Fig 4-15**. The R^2 values of pancreas volume and fat fraction were 0.9764 and 0.9675, respectively. From the graph, we can claim that the segmentation results derived by the newly built CNN were reliable compared with the manual operation. Further, the state-of-the-art CNN shortened the time consumption dramatically. The average noted time utilized for the measurement of each patient was from an average 1.5 hour via manual operation to 5 seconds on our machine.

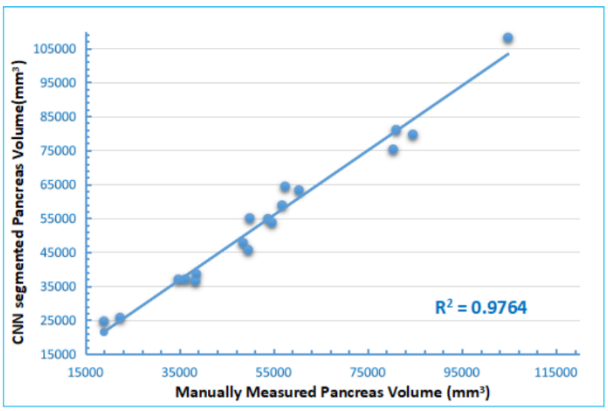

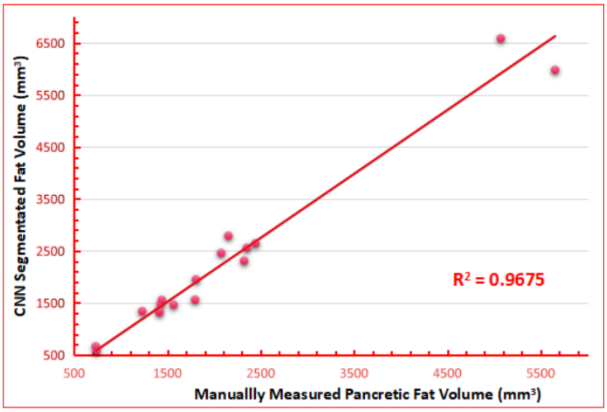

Figure 4-15 Validation of the integrity of trained CNN. Performance validation between expert manual operation and trained CNN segmentation in terms of pancreas volume and pancreatic fat volume. The R^2 values were 97.64% and 96.75 respectively

Chapter 5 Discussion

5.1 The usefulness of different fat tissues among various ethnicities

The study reported four key findings. Firstly, both SAT and VAT volume in Māori/PI was significantly higher than in the other two ethnic groups. Asian had a VAT fat volume similar to Māori/PI, especially in low abdominal slices, but lower SAT fat volume. The Asian group had the highest PAT and LAT volume. Secondly, the correlation results showed some significant ethnicity-specific relationships between anthropometric indices and fat depositions. Ethnicity-specific equations which predict MRI-derived VAT depositions from anthropometric indices were developed. Thirdly, the study showed no correlation between traditional anthropometric indices and intra-hepatic and intra-pancreatic fat depositions. Lastly, the power of the usefulness of fat deposition from different lumbar spine was varied between ethnic groups in terms of associating with anthropometric indices, which means ethnicity-specific evaluation should be fully weighted when diagnostic models establish. This MRI imaging study investigated the differences in distribution of adult adipose tissues between specific ethnicity groups - New Zealand European, Māori/PI and Asian. State-of-the-art method was used in the present study that derives the fat and water volume from MRI images using threshold pixel contrast (which is different from previously published studies that used VAT and SAT areas but not their volume). Although using areas of VAT and SAT is timesaving, it lacks accuracy comparing with using volumes. In this study, the correlations between anthropometric indices (BMI, WC and WHtR) and SAT, VAT from all intervals of lumbar discs (L12SAT, L23AT, L34AT, L45AT, L12VAT, L23VAT, L34VAT and L45VAT) and the intra-organ fat content from liver and pancreas (LAT and PAT) were studied. Results were both age- and sex-unadjusted and adjusted.

A notable finding of this study was that VAT volume in the Māori/PI group and Asian group are similar and are significantly higher than in the NZ European group (despite having nearly the same SAT volume). The intra-hepatic fat deposition was higher in Asian and intra-pancreatic fat deposition was higher in Māori/PI. There were no statistically significant differences in SAT volume between the ethnicities. It is well established that SAT's function is absorbing excess circulating free fatty acid and glycerol and storing them triglycerides in adipocytes.(Fain et al. 2004) Once SAT is full of its lipid storage, fat begins to accumulate in fat compartments (especially VAT).(Freedland 2004) It is believed that people with relatively

higher VAT volume have higher risk of developing metabolic disorders.(Singh et al. 2019, Preis et al. 2010) Furthermore, intra-pancreatic fat deposition has a negative correlation with insulin secretion, and it promises to become a novel and more accurate biomarker for metabolic disorders.(Heni et al. 2010, Ozturk et al. 2018, Cho, Ye and Kim 2016) Previous studies also showed that genetic mutation has an impact on the lipid storage and end with more accumulation of VAT(Heid et al. 2010, Schweiger et al. 2009), which may interact with the ethnicity-specific VAT volume. Other similar studies of African Americans and Asians(Cardel et al. 2011, Wang et al. 2016) also demonstrated that the ethnic diversity is associated with specific genetic background, which has considerable impact on the pattern of fat distribution. The result of this study is consistent with the investigation by the New Zealand Ministry of Health, according to which, 1 in 3 New Zealand adults were confirmed as obese (2019), and Māori and Pacific Islander had the highest rate of obesity (66.5% PI and 48.2% Māori), following by NZ European (29.1%) and Asian (13.8%) (New Zealand Health Survey. Ministry of Health. 2019). We showed that Māori and PI have significantly higher VAT and PAT volume, comparing with the other two groups. This suggests that visceral and intra-pancreatic fat depositions are likely to be the key at depots that are be highly correlated with the morbidity of metabolic diseases. Genetic studies are now warranted to investigate metabolism-related gene expression patterns in Māori and PI.

The present study also investigated the strength of correlation between each fat deposition and anthropometric indices in the three groups. In addition to the two traditional indexes (BMI and WC), we also evaluated Waist to Height ratio (WHtR) as the third index as there are published studies showing that WHtR is a better anthropometrical index than BMI and WC.(Ashwell et al. 2012, Savva et al. 2000) The results of this study do not support that and show that, in the overall cohort, WHtR has the weakest association with each SAT level. BMI was correlated with both SAT and VAT (and better with SAT than VAT) but did not correlate with LAT and PAT. WC correlated with SAT only - this finding is in line with studies in African Americans and Filipinos. (Camhi et al. 2011, Araneta and Barrett‐Connor 2005) The above findings suggest that the anthropometric indices can roughly evaluate the adipose tissue distribution in people (mainly SAT) but do not have enough accuracy in estimating visceral adiposity across all ethnic groups. It is worth mentioning that growing evidence shows that intra-pancreatic fat is strongly associated with obesity, metabolic syndrome, type 2 diabetes mellitus, pancreatic exocrine dysfunction, acute pancreatitis, pancreatic cancer.(van Geenen et al. 2010, Smits and

Van Geenen 2011, Garcia et al. 2018, Meyer et al. 2016) Unfortunately, our study showed that there is no correlation between any anthropometric index and PAT. This highlights the need to develop a more accurate method to estimate intra-pancreatic and visceral fat deposition, taking into account different ethnic backgrounds. Given that deep machine learning holds promise in biomedical research(Michael et al. 2018, Mamoshina et al. 2016) (including medical image recognition(Erickson et al. 2017)), future studies will likely focus on developing integral machine learning system to recognize the fat depositions and their links with metabolic disorders.

In conclusion, VAT and PAT depositions in Māori/PI are significantly higher than in NZ European and Asian. Intra-hepatic fat volume in Asian is higher than in the other two groups, whereas VAT and intra-pancreatic fat depositions are comparatively higher than in NZ European. BMI appears to be the most useful anthropometric indices in this study. All the studied anthropometric indices reflect only abdominal fat compartments in ethnic groups and have different correlations, but not intra-organ fat depositions. VAT and intra-pancreatic fat may be the most important fat compartments for predicting the risk of metabolic disorders in New Zealanders.

5.2 The feasibility of applying CNN for pancreatic parameters determination

In this study, we compared and evaluate the effectiveness of IDEAL and MRS in terms of measuring the MRI-derived HFFs and PFFs. The resulting PFF_{IDEAL} and PFF_{MRS} data for each proccing approach were compared with the manually derived PFF data to assess the efficiency of these approaches in pancreatic fat fraction quantification.

In our phantom study in a set of emulsion standards, we have shown that both IDEAL and MRS fat fractions were strongly correlated with the underlying fat volume fraction (**Fig. 3-1**). Other studies have also verified this robust relationship. (Bydder et al. 2008, Reeder et al. 2009) We also converted the pixel length (PL) to real length in millimetres (RL) for future study. The conversion ratio of PL and RL was averaged as 0.76. In the *in vivo* experiment, the IDEAL algorithm was employed six echoes for transverse relaxation and intravoxel dephasing (T_2, T_2^*)(Sharma et al. 2009). Because the T_2 correction involved additional echo times that could have been saved at the expense of scan time for MRS, we used a single echo time of 23ms for our MRS protocol. As the results showed, we got excellent agreement between the HFF_{IDEAL}

and HFF_{MRS} (**Fig.**3-2). However, in the measurement of PFF, only a moderate correlation was obtained between PFF_{IDEAL} and PFF_{MRS} (**Fig.**3-3). From the t-test result, we can derive that the readings between them were significantly different. Nearly all the MRS estimates were greater than the IDEAL readings. We also noticed that in our data, there were some extremely large MRS estimates up to 62.8% due to intravoxel field inhomogeneity in the MRS voxel. This MRS data was absurd and abandoned to use in our study. This did not appear in IDEAL readings.

The poor PFF correlation between each reading can be attributed to two reasons. Firstly, MRS voxel placement requires operator expertise, because the pancreas is a small organ that elongate its shape and burry it in the duct. These factors increased the difficulties to localize the pancreas. Voxel prescription is performed on localizer images which were scanned after the patients were placed into the MRI tunnel. Pancreas MRS was conducted several minutes after the localizer, which means the slight motion of the patients could have caused a spatial mismatch between the prescribed voxel and the physiological structure during the gap. Secondly, respiration caused the abdominal organs to shift readily (Nehrke et al. 2001). The diaphragm motion between inhalation and exhalation makes the pancreas shift around 15mm along the superior-inferior axis, which lead to enormous fat signal contamination from the abundance of visceral fat around the pancreas and reflect on MRS spectra. In contrast, voxel can be placed easier on the liver and remain confidently with it throughout the respiration cycle.

IDEAL-MRI performed better than MRS in terms of PFF readings. The IDEAL does not require a high-level of operator expertise in voxel prescription and operated within the period of breath-hold of patients. Further, IDEAL images were reconstructed, and fat fraction was computed on the scanner host computer for 2-3 mins after the data acquisition. The manual segmentation of HFF and PFF was operated on fat fraction images directly, which help to avoid a large amount of background noise of vessels and non-fat structures. This advantage was also recognized by parallel validation studies that included large patient cohorts. (Yokoo et al. 2009, Yokoo et al. 2011, Reeder et al. 2009) However, IDEAL also have intrinsic limitations. Firstly, IDEAL depends on the respiration restriction of the patient multiple times, which is not always realistic in certain patients. Secondly, based on Eq (a), we must assign the values of Δf_i and a_i, which are determined by subcutaneous adipose tissue to reconstruct an accurate model of the fat spectra. The inaccuracies may appear if the signal of triglycerides in organs is significantly different from that of subcutaneous fat tissue. Thirdly, the values of T^*_2 were assigned for both

water and fat components, which should have been adopted. This can be addressed by enlarging the acquisition echoes; however, long time operation also takes potential inaccuracies.

In the study, the manual pancreatic fat fraction method was employed to address the difference performance between IDEAL and MRS and to get a more accurate PFF reading. We used the Image J Polygon tool to cycle the region of interest in the parenchymal tissue of the head, body, and tail of the pancreas. The region was selected carefully and avoid any possible contamination of the surrounding visceral fat. (**Fig.** 2-1) The threshold was adjusted until satisfied fat pixels were exposed. Pixels within the threshold range were selected and accumulated to acquire the total area of each slice of the pancreas. The ratio of the pancreatic fat area and total pancreas area were noted and counted into the PFF_{MANUAL}. The method was conducted by two experienced operators and average their results. Based on the result in **Fig.** 3-4 c, we can claim that our manual operation performed better than IDEAL and MRS in terms of PFF reading. The results were exactly laid on the reported general pancreatic fat fraction range (1.8%-10.4% with the mean of 4.5%).(Majumder et al. 2017)

The knowledge acquired from our study will be utilized in our future work to focus on the feasibility and reliability of MRI quantification and developed machine learning system to determine the pancreatic and hepatic fat depositions and try to link them with metabolic disorders. Another interesting area we would like to focus on application of MRI on pancreas whose irregular shape is a problem for localized MRS.

5.3 The prospect of the new CNN

Fat quantification of pancreas by MRI is significantly affected by the method of sampling. In general, The MRI measurement for water/fat decomposition is a valuable method for hepatic and pancreatic fat fraction quantification. Based on my study, I have demonstrated a strong advantage of the artificial pancreatic fat fraction derived method as a pancreatic fat quantification tool. And propose this method as a valuable tool for our future machine learning establishment for automatically diagnose obesity and metabolic diseases.

Fat deposition and volume in pancreas have been demonstrated in many controlled experiments to be important indicators of metabolic disease(Singh et al. 2017b, DeSouza et al. 2018b). Due to the special clinical features of the pancreas, which is comparatively small and hard to localize because of the complexity of ducts in and around it, the measurement of pancreas volume and

its fat fraction is regarded as more difficult compared with other organs (Virostko 2020, Williams et al. 2020). To date, the most efficient measuring protocol utilized in scaling the pancreas volume and its fat fraction is software-based manual segmentation which was developed from 3D IDEAL MRI scans(Al-Mrabeh et al. 2017). It is a clinical expert-based method that requires freehand drawing round an area to be within the substance of the pancreas. The advantage of this method was more accuracy and practicality than the direct reading from MRS (Al-Mrabeh et al. 2017). However, it was a time-consuming task, and cannot be performed without the specialist. To expand the measurement method for wider use, I copied and improved the measurement approach into one new trained Convolutional Neural Network. Prior work has shown that CNNs can achieve considerable medical image segmentation tasks on heart, liver, and kidney, but studies have rarely to our knowledge been seen on the pancreas in terms of fat deposition and volume due to high variability in size and location among patients (Litjens et al. 2017, Heller et al. 2021). The present work, to our knowledge, is the first to demonstrate one way of enabling CNN to derive pancreas fat deposition and volume based on the method of artificial segmentation of medical images. I introduced the method of super pixel segmentation to our CNN and preprocessed the medical images. I innovated the calculation index of pixel to improve the LSC algorithm based on SLIC0 which turned super pixel segmentation acting on three-channel natural images to only one-grey-channel MRI images and adapted it to the evaluation of medical images. The results showed that the super pixel clarified the boundary of the pancreas which made the recognition easier for CNN. The comparison results of user-based and automatic segmentation showed that our CNN was particularly well-suited to this task since it computes pancreas presence and location on a super pixel basis with a multi-resolution approach with a U-net-base architecture. Extension to three-dimensional volume predictions is anticipated to be straightforward, with stacked areas of irregular shape of pancreatic MRI image layers, which was strictly loyal to the clinical manipulation of pancreatic measurement. Compared with the user-performed segmentation, this method was distinct within acceptable error range and saved a large amount of time on counting and summation. It would be feasible to measure pancreatic fat deposition and size for data sets numbering in the thousands that could power large studies and, more importantly, the method avoids time and labor consuming manual tracing of pancreatic borders. This undoubtedly will also enhance opportunities for future clinical application because it is most important to characterize pancreatic images from those with prediabetes to normoglycemia accurately before biochemical and other clinical risk factors become abnormal.

More meaningfully, I collected the MRI images from clinical patients with different ethnic backgrounds and different clinical preconditions at Auckland City Hospital to train our CNN. This undoubtedly enhanced the pancreas recognition variability for the machine and ensure more accuracy segmentation. In future research, based on extending our current work to 3D CNNs with higher training sets, the pancreas volume could be correlated more specifically with some metabolic conditions, such as glycemia and diabetes.

Chapter 6 Conclusion, limitations and future recommendations

6.1 Conclusion

Currently, the prevalence of obesity and type 2 diabetes are increasing dramatically. There is an abundance of literature which demonstrates a correlation between the risk of metabolic disease, such as T2D, and obesity. (Goda et al. 2001a, Burute et al. 2014, DeSouza et al. 2018b, Macauley et al. 2015) Since fat deposition varies among different ethnicities and body parts, it is vital to get an accurate target as a biomarker which accurately reflects the physiological shift for prognosis. From our previous investigation, it was shown that significant changes can lead to the development of metabolic disorders, so I proposed the hypothesis that the change of pancreatic volume and fat fraction can be a potential biomarker for metabolic disease prognosis. Based on this hypothesis, our team targeted the patients who underwent bariatric surgery and designed a pilot clinical study to investigate the potential of the shifted biomarkers before and after the bariatric surgery. Our previous research showed that after bariatric surgery, remission of diabetes immediately occurred in patients even before they lost weight. Previous studies showed the changes in fatty acids and some types of hormones, such as leptin, ghrelin, FGF19. Notably, the changes of hormones are primarily located in alimentary canals. (Turnbaugh et al. 2009) The most likely explanation for this change is the functional shift of pancreas. (Macauley et al. 2015, Gaborit et al. 2015b, Goda et al. 2001a, Saisho et al. 2007) However, there have been few studies which have investigated the correlation between traditional anthropometric measurements and pancreatic fat fraction. In the first part of this study, we designed a method that used statistical analysis to derive the linkage between the fat deposition in the pancreas to traditional anthropometric indices, such as WC and BMI. This is also the first study that looks into the relationship between anthropometric measurement and pancreatic and hepatic fat fractions. I also took the SAT and VAT into consideration and linked them to anthropometric measurements, building up an equation for the two variables to give further guidance in clinical use. Previous studies have rarely focused on gathering data from various ethnicities, and as our data was collected from Auckland Central Hospital, New Zealand, it was the first time Māori and Pacific Islanders were included in this field of research, which broadens the observation samples for future studies.I separated our data using 3D slicer software in different lumbar disc layers (L12, L23, L34, and L45), and draw conclusions respectively. Previous publications were more focused on a single layer. I made a comparison of the effectiveness of the correlation between these disc layers and traditional anthropometric measurements.

The second significant contribution of this study was that it was the first study to construct a novel convolutional neural network (CNN) to measure the pancreatic volume and pancreatic fat fraction using the state-of-art manual segmentation method. Since the MRS measurement of fat deposition in tiny organs like intra-pancreas has an error reading of up to 40% according to our phantom study, the alternative manual segmentation method comparatively has more accurate results in terms of fat fraction prediction on MRI images because the recognition of duct and fat tissues are better done by experienced observers. The method turns the pixelated information into digital information after selection by Image J and excludes the unwanted pixels outside the range of 1%-20%, which facilitates the final estimation of the fat fraction inside the pancreas. This artificial pancreatic segmentation process includes the traditional method and MR-opsy method, both methods using the same calculation process. The traditional method chose the entire area of the pancreas as the measuring region of interest (ROI), while the MR-opsy method only chose three distinct areas in the head, body, and tail as ROIs. These manual segmentation methods provide a new path towards accurate measurements of pancreatic fat fraction, which will be used for further clinical prognosis for metabolic diseases such as T2DM.

The novel auto pancreatic segmentation neural network includes two innovative algorithms. One is the super pixel, which helps to build up the clearness of the pancreas boundary on MRI images. It facilitates machine recognition of the shape of the pancreas and accurately segments it out. The other is erosion, which helps to reduce the numbers of pixels on the pancreas image boundary, and is currently considered the most accurate artificial intelligence model in measuring pancreas volume and fat deposition using CNN. We proposed an improved pancreatic image segmentation method combining U-NET and the super pixel algorithm, which made the near-indistinguishable pancreatic boundary recognition easier. The overall mean DSC is 91.2%, which is the highest known CNN of the same type. Future work will focus on 3D data sets and getting more training data to improve accuracy, which will lead to large-scale automated processes of pancreas volume and fat deposition calculation in research and clinical applications. A cloud service will be set up to both attract data and provide service to research and clinical communities. This study provides proof of concept that CNN-based analysis of pancreatic fat and pancreatic volume among participants of different adult ages, BMI, and ethnicities achieves a greater accuracy in comparison to manual grading, and is obtained at a much greater speed (5 seconds for CNN analysis vs 1.5 hours for manual

grading). Because the test sets and training and validation sets shared no common participants, the excellent performance of the CNN could not be attributed to overfitting. Ethnicity and BMI are key factors that influence the imaging characteristics of the pancreas, including pancreatic fat. (Szczepaniak et al. 2005, Szczepaniak et al. 2012b, Lê et al. 2011) In order to ascertain the potential generalizability of CNN in recognizing pancreatic fat and volume in people of different ethnicities and of different body sizes, we tested the CNN trained on a multi-ethnic group of participants (BMI range 18.28 to 46.56) with an external dataset of participants. These participants differed substantially from the initial training set of data as they had a higher BMI (ranging from 36.78 to 52.13). MR images were taken 3 days before and after bariatric surgery when type 2 diabetes was present and then absent, respectively, showing a correlation to significant reductions in pancreatic fat and volume. The excellent performance of the CNN on the external dataset suggests good representation of BMI and ethnicity in the training set images.

6.2 Limitations

6.2.1 Limitation for chapter 2

In this study there are limitations which need to be acknowledged. For the first part of the study, the main limitations were as follows. Firstly, age and sex - the crucial determinant of adipose distribution - were not evenly distributed between the groups. However, they were adjusted statistically with specific models in this study, which were shown in Tables 3.4-3.6. Secondly, the sizes of groups were imbalanced. The number of participants from the NZ European group was significantly higher than the other two groups. However, the current study represented an analysis of consecutive unselected participants who met the study eligibility criteria. Thereby, our study cohort was representative of the ethnic ratio of the general population in New Zealand. The presented analyses should be viewed as exploratory and hypothesis-generating. The conclusion of the study will be used to inform the design and power calculation of future purpose-designed studies on ethnic variations in abdominal fat depositions. Thirdly, diet and physical exercise - common factors that influence fat accumulation - were not considered. However, to the best of our knowledge, no published study investigated them as confounders in ethnicities-specific analyses. Fourthly, this study did not study genetic variations between the groups.[316] Future studies should also focus on the correlation between genetic variations and patterns of fat deposition in different ethnic groups. Lastly, the present study did not directly

establish a correlation between the relevant metabolism milieus and fat deposition. This warrants investigations in the future.

6.2.2 Limitations for Chapter 3

For the phantom study, some major limitations came from using the manual method. Firstly, the manual method lacks a gold standard for non-invasive quantitation of fat solely within the parenchymal tissue of the pancreas. With the development of imaging techniques, optimized images with better differentiation between parenchymal tissue and ductal or small vascular structures may be possible in the near future, such as with the T_2-SPAIR sequence. (Dalto et al. 2020) Secondly, the resolution of pancreas imaging in a shorter period needs to be improved. The breath-hold duration was low for a lot of patients thereby lowering the resolution of the images. Sparse scanning techniques may fill this gap soon. (Mann et al. 2016) Nonetheless, the artificial method remains useful because threshold adjusting can exclude areas of visceral fat invasion effectively and the accuracy can be improved dramatically by examining the detail of the pancreas when conducting the selection of regions of interest.

6.2.3 Limitations for Chapter 4

For building up the CNN, we developed the most accurate artificial intelligence model to date in order to measure the pancreas volume and fat deposition. We proposed an improved pancreatic image segmentation method combining U-NET and super pixel algorithm, which made the near indistinguishable pancreatic boundary recognition easier. The overall mean DSC was 91.2%, which is the highest known CNN of the same type. Future work will focus on 3D data sets and getting more training data to improve accuracy, which will lead to large-scale automated processes of pancreas volume and fat deposition in research and clinical applications. A cloud service will be set up to both compile data and provide service to the research and clinical communities. There were four main shortcomings of our image captures. The first was that medical images showed various shapes for the pancreas, due to the different spatial structures of this organ, which made deep learning a difficult process regarding pancreatic recognition – this will require more data to overcome. The accuracy needs to be improved by more inputting data to resolve ambiguities. Secondly, more pancreatic MRI slices should have been included to increase the result's accuracy. However, due to the restriction of the MRI machine, only 12 slices could be taken for each patient. I will collect more data from different centres to improve results in future studies. The third shortcoming is that while this study

developed a novel CNN based on two-dimensional (2D) data which strictly mimics clinical artificial operation, it could have been upgraded to 3D prediction by adjusting the models. Again, more clinical data is needed for the network to build accurate correlations with 3D predictions. Future work will involve fully 3D MRI image stacks (which will be based on this study) in order to be more useful clinically and in research. Finally, I came up with an excellent solution called the erosion algorithm which will be used to work out the fat deposition in the pancreas; however, a larger training set could provide the CNN with stability and efficiency. As stated above, in order to obtain better results false negatives, need to be balanced against the interference of false positives for future clinical and research practice.

6.2.4 Limitations of other aspects

The participant's recruitment was seriously affected by Covid-19. The pandemic made the research rougher than it used to. The data for building up the CNN and the phantom validation were all from the previous clinical study, which makes the project as retrospective research. Only obese patients in PAT project were used for the machine learning validation. However, the CNN was built up for a general purpose, which has already uploaded the information from various types of samples. This makes the validation meaningful and solidate.

The table 4-1 was summarized the DCS values from different models. Some of them were built on 3D model, which makes the comparison a little bit improper. However, the pancreatic model on the market were rarely seen in 2D base for MRI. I believe with the development of CNN and more brilliant ideas come in the field; more models will appear in the future. I hope my research can play a role for initiation of the pancreatic fat detection and measurement.

6.3 Future Study Recommendation

Future study should also aim to have a greater number of patients in order to grow the MRI data bank and make the CNN result more significant. The amount of the image data collected is regarded as one of the largest limitations of the study. The future CNN can be moderated into the formation of 3D for greater accuracy of volume measurement, which can be regarded as an important direction to build up machine learning. The new algorithm can be inserted into the CNN for better pixel measurement. Further comparison of the measurement of MRS, DXA scans and machine learning need be conducted. Validation among the different pancreatic measurements should be done. We have already derived the conclusion that the fat fraction

measurement by MRS in small organs, such as the pancreas, varies among different measurements. However, with the development of MRI techniques, new algorithms will be used to upgrade the detection efficiency in the future. The body fat fraction measured by DXA can be compared further with novel MRS, the traditional manual method, and automatic measurement. Molecular biology tests require further improvements, especially in regards to the taking of blood samples from patients who were scanned using MRI before and after bariatric surgery. Venous blood will be collected three days prior to the start of the procedure, and ELISA kits will be used to measure some of our listed serum biomarkers related to type 2 diabetes mellitus, including: insulin, glucose, FGF21, leptin, irisin, gastrin, secretin, and ghrelin. Additionally, the bile acid levels will be determined by Liquid Chromatograph Mass Spectrometer (LC-MS/MS). The bile acids in the serum will be extracted by acetonitrile and isotopically labelled as internal standards. A C8 column will be used for baseline separation of the bile acid. By using spectrometry in negative ion mode, multiple reaction detection was used to measure the level of bile acids.

In conclusion, fat quantification of the pancreas by MRI is significantly affected by the method of sampling. In general, the MRI measurement for water/fat deposition is a valuable method for hepatic and pancreatic fat fraction quantification. Based on our study, I have demonstrated a strong advantage of the artificial pancreatic fat fraction derived method as a pancreatic fat quantification tool, and propose that this method is a valuable tool for future machine learning in automatically diagnosing obesity and metabolic diseases.

References

Abadi, M., A. Agarwal, P. Barham, E. Brevdo, Z. Chen, C. Citro, G. S. Corrado, A. Davis, J. Dean & M. Devin (2016) Tensorflow: Large-scale machine learning on heterogeneous distributed systems. *arXiv preprint arXiv:1603.04467*.

Abate, N., D. Burns, R. M. Peshock, A. Garg & S. M. Grundy (1994) Estimation of adipose tissue mass by magnetic resonance imaging: validation against dissection in human cadavers. *Journal of lipid research,* 35**,** 1490-1496.

Al-Mrabeh, A., K. G. Hollingsworth, S. Steven & R. Taylor (2016) Morphology of the pancreas in type 2 diabetes: effect of weight loss with or without normalisation of insulin secretory capacity. *Diabetologia,* 59**,** 1753-1759.

Al-Mrabeh, A., K. G. Hollingsworth, S. Steven, D. Tiniakos & R. Taylor (2017) Quantification of intrapancreatic fat in type 2 diabetes by MRI. *PloS one,* 12**,** e0174660.

Al-Mrabeh, A., C. Peters, K. G. Hollingsworth & R. Taylor (2021) Measurement of intraorgan fat and hepatic output of triglycerides in human type 2 diabetes by magnetic resonance and intralipid infusion techniques. *STAR protocols,* 2**,** 100355.

Al-Muhtaresh, H. A. & G. Al-Kafaji (2018) Evaluation of two-diabetes related microRNAs suitability as earlier blood biomarkers for detecting prediabetes and type 2 diabetes mellitus. *Journal of clinical medicine,* 7**,** 12.

Al-Rfou, R., G. Alain, A. Almahairi, C. Angermueller, D. Bahdanau, N. Ballas, F. Bastien, J. Bayer, A. Belikov & A. Belopolsky (2016) Theano: A Python framework for fast computation of mathematical expressions. *arXiv e-prints***,** arXiv: 1605.02688.

Alom, M. Z., M. Hasan, C. Yakopcic, T. M. Taha & V. K. Asari (2018) Recurrent residual convolutional neural network based on u-net (r2u-net) for medical image segmentation. *arXiv preprint arXiv:1802.06955*.

Amitani, M., A. Asakawa, H. Amitani & A. Inui (2013) The role of leptin in the control of insulin-glucose axis. *Frontiers in neuroscience,* 7**,** 51.

Angelin, B., T. E. Larsson & M. Rudling (2012) Circulating fibroblast growth factors as metabolic regulators—a critical appraisal. *Cell metabolism,* 16**,** 693-705.

Araneta, M. R. G. & E. Barrett-Connor (2005) Ethnic differences in visceral adipose tissue and type 2 diabetes: Filipino, African-American, and white women. *Obesity research,* 13**,** 1458-1465.

Arnold, T. B. (2017) kerasR: R Interface to the Keras Deep Learning Library. *J. Open Source Softw.,* 2**,** 296.

Arslanian, S., F. Bacha, S. Caprio, R. Goland, M. W. Haymond, L. Levitsky, K. J. Nadeau, N. H. White & S. M. Willi (2017) Adiponectin, insulin sensitivity, β-cell function, and racial/ethnic disparity in treatment failure rates in TODAY. *Diabetes care,* 40**,** 85-93.

Ashwell, M., P. Gunn & S. Gibson (2012) Waist-to-height ratio is a better screening tool than waist circumference and BMI for adult cardiometabolic risk factors: systematic review and meta-analysis. *Obesity reviews,* 13**,** 275-286.

Atzmon, G., X. Yang, R. Muzumdar, X. Ma, I. Gabriely & N. Barzilai (2002) Differential gene expression between visceral and subcutaneous fat depots. *Hormone and metabolic research,* 34**,** 622-628.

Baglioni, S., G. Cantini, G. Poli, M. Francalanci, R. Squecco, A. Di Franco, E. Borgogni, S. Frontera, G. Nesi & F. Liotta (2012) Functional differences in visceral and subcutaneous fat pads originate from differences in the adipose stem cell. *PLoS one,* 7**,** e36569.

Bagust, A. & S. Beale (2003) Deteriorating beta-cell function in type 2 diabetes: A long-term model. *Quarterly Journal of Medicine,* 96**,** 281-288.

Banerjee, J., V. Nema, Y. Dhas & N. Mishra (2017) Role of microRNAs in type 2 diabetes and associated vascular complications. *Biochimie,* 139**,** 9-19.

Bazata, D. D., J. G. Robinson, K. M. Fox, S. Grandy & S. S. Group (2008) Affecting Behavior Change in Individuals With Diabetes Findings From the Study to Help Improve Early Evaluation and Management of Risk Factors Leading to Diabetes (SHIELD). *The Diabetes Educator,* 34**,** 1025-1036.

Benedetti, G., G. Mingrone, S. Marcoccia, M. Benedetti, A. Giancaterini, A. V. Greco, M. Castagneto & G. Gasbarrini (2000) Body composition and energy expenditure after weight loss following bariatric surgery. *Journal of the American College of Nutrition,* 19**,** 270-274.

Bevilacqua, S., R. Bonadonna, G. Buzzigoli, C. Boni, D. Ciociaro, F. Maccari, M. A. Giorico & E. Ferrannini (1987) Acute elevation of free fatty acid levels leads to hepatic insulin resistance in obese subjects. *Metabolism,* 36**,** 502-506.

Birbrair, A., T. Zhang, Z.-M. Wang, M. L. Messi, G. N. Enikolopov, A. Mintz & O. Delbono (2013) Role of pericytes in skeletal muscle regeneration and fat accumulation. *Stem cells and development,* 22**,** 2298-2314.

Boden, G. & G. Shulman (2002) Free fatty acids in obesity and type 2 diabetes: defining their role in the development of insulin resistance and β-cell dysfunction. *European journal of clinical investigation,* 32**,** 14-23.

Bonfante, I. L. P., M. P. T. Chacon-Mikahil, D. T. Brunelli, A. F. Gáspari, R. G. Duft, A. G. Oliveira, T. G. Araujo, M. J. A. Saad & C. R. Cavaglieri (2017) Obese with higher FNDC5/Irisin levels have a better metabolic profile, lower lipopolysaccharide levels and type 2 diabetes risk. *Arch Endocrinol Metab,* 61**,** 524-33.

Borkan, G. A., S. G. Gerzof, A. H. Robbins, D. Hults, C. Silbert & J. Silbert (1982) Assessment of abdominal fat content by computed tomography. *The American journal of clinical nutrition,* 36**,** 172-177.

Brix, G., S. Heiland, M. E. Bellemann, T. Koch & W. J. Lorenz (1993) MR imaging of fat-containing tissues: valuation of two quantitative imaging techniques in comparison with localized proton spectroscopy. *Magnetic resonance imaging,* 11**,** 977-991.

Brodie, D., H. Vicki Moscrip MSC & R. Hutcheon (1998) Body composition measurement: a review of hydrodensitometry, anthropometry, and impedance methods. *Nutrition,* 14**,** 296-310.

Brookheart, R. T., C. I. Michel & J. E. Schaffer (2009) As a matter of fat. *Cell metabolism,* 10**,** 9-12.

Brown, J. C., M. O. Harhay & M. N. Harhay (2017) Anthropometrically-predicted visceral adipose tissue and mortality among men and women in the third national health and nutrition examination survey (NHANES III). *American Journal of Human Biology,* 29**,** e22898.

Buchwald, H., Y. Avidor, E. Braunwald, M. D. Jensen, W. Pories, K. Fahrbach & K. Schoelles (2004) Bariatric surgery: A systematic review and meta-analysis. *JAMA,* 292**,** 1724-1737.

Buchwald, H. & D. M. Oien (2013) Metabolic/bariatric surgery worldwide 2011. *Obesity surgery,* 23**,** 427-436.

Burute, N., R. Nisenbaum, D. J. Jenkins, A. Mirrahimi, S. Anthwal, E. Colak & A. Kirpalani (2014) Pancreas volume measurement in patients with Type 2 diabetes using magnetic resonance imaging-based planimetry. *Pancreatology,* 14**,** 268-274.

Butler, A. E., J. Janson, S. Bonner-Weir, R. Ritzel, R. A. Rizza & P. C. Butler (2003a) β-cell deficit and increased β-cell apoptosis in humans with type 2 diabetes. *Diabetes,* 52**,** 102-110.

Butler, E. A., J. Janson, S. Bonner-Weir, R. Ritzel, A. R. Rizza & C. P. Butler (2003b) β-cell deficit and Increased β-cell apoptosis in humans with type 2 diabetes. *Diabetes,* 52**,** 102-110.

Bydder, M., T. Yokoo, G. Hamilton, M. S. Middleton, A. D. Chavez, J. B. Schwimmer, J. E. Lavine & C. B. Sirlin (2008) Relaxation effects in the quantification of fat using gradient echo imaging. *Magnetic resonance imaging,* 26**,** 347-359.

Cai, J., L. Lu, Z. Zhang, F. Xing, L. Yang & Q. Yin. 2016. Pancreas segmentation in MRI using graph-based decision fusion on convolutional neural networks. In *International Conference on Medical Image Computing and Computer-Assisted Intervention*, 442-450. Springer.

Cali, A. M. G., C. D. Man, C. Cobelli, J. Dziura, A. Seyal, M. Shaw, K. Allen, S. Chen & S. Caprio (2009) Primary defects in β-Cell function further exacerbated by worsening of insulin resistance mark the development of impaired glucose tolerance in obese adolescents. *Diabetes Care,* 32**,** 456-461.

Camastra, S., A. Vitali, M. Anselmino, A. Gastaldelli, R. Bellini, R. Berta, I. Severi, S. Baldi, B. Astiarraga & G. Barbatelli (2017) Muscle and adipose tissue morphology, insulin sensitivity and beta-cell function in diabetic and nondiabetic obese patients: effects of bariatric surgery. *Scientific reports,* 7**,** 9007.

Camhi, S. M., G. A. Bray, C. Bouchard, F. L. Greenway, W. D. Johnson, R. L. Newton, E. Ravussin, D. H. Ryan, S. R. Smith & P. T. Katzmarzyk (2011) The relationship of waist circumference and BMI to visceral, subcutaneous, and total body fat: sex and race differences. *Obesity,* 19**,** 402-408.

Cardel, M., P. Higgins, A. Willig, A. Keita, K. Casazza, B. Gower & J. Fernandez (2011) African genetic admixture is associated with body composition and fat distribution in a cross-sectional study of children. *International journal of obesity,* 35**,** 60-65.

Catanzaro, R., B. Cuffari, A. Italia & F. Marotta (2016) Exploring the metabolic syndrome: Nonalcoholic fatty pancreas disease. *World journal of gastroenterology,* 22**,** 7660.

Chang-Chen, K., R. Mullur & E. Bernal-Mizrachi (2008) β-cell failure as a complication of diabetes. *Reviews in Endocrine and Metabolic Disorders,* 9**,** 329-343.

Chen, J., Z. Li & B. Huang (2017) Linear spectral clustering superpixel. *IEEE Transactions on image processing,* 26**,** 3317-3330.

Chen, Y., J. Zhu, P. Y. Lum, X. Yang, S. Pinto, D. J. MacNeil, C. Zhang, J. Lamb, S. Edwards & S. K. Sieberts (2008) Variations in DNA elucidate molecular networks that cause disease. *Nature,* 452**,** 429-435.

Cheng, S., J. M. Massaro, C. S. Fox, M. G. Larson, M. J. Keyes, E. L. McCabe, S. J. Robins, C. J. O'Donnell, U. Hoffmann & P. F. Jacques (2010) Adiposity, cardiometabolic risk, and vitamin D status: the Framingham Heart Study. *Diabetes,* 59**,** 242-248.

Cho, J.-Y., S.-Y. Ye & D.-H. Kim (2016) The study on risk factor of metabolic diseases in pancreatic steatosis. *Journal of radiological science and technology,* 39**,** 81-88.

Chui, P. C., P. J. Antonellis, H. A. Bina, A. Kharitonenkov, J. S. Flier & E. Maratos-Flier (2010) Obesity is a fibroblast growth factor 21 (FGF21)-resistant state. *Diabetes,* 59**,** 2781-2789.

Coe, P. O., S. R. Williams, D. M. Morris, E. Parkin, M. Harvie, A. G. Renehan & D. A. O'Reilly (2018) Development of MR quantified pancreatic fat deposition as a cancer risk biomarker. *Pancreatology,* 18**,** 429-437.

Cohen, M., C. Syme, M. Deforest, G. Wells, G. Detzler, H. L. Cheng, B. McCrindle, A. Hanley & J. Hamilton (2014) Ectopic fat in youth: The contribution of hepatic and pancreatic fat to metabolic disturbances. *Obesity,* 22**,** 1280-1286.

Collaborators, G. O. (2017) Health effects of overweight and obesity in 195 countries over 25 years. *New England Journal of Medicine,* 377**,** 13-27.

Collobert, R., K. Kavukcuoglu & C. Farabet. 2011. Torch7: A matlab-like environment for machine learning. In *BigLearn, NIPS workshop*.

Committee, I. E. (2009) International Expert Committee report on the role of the A1C assay in the diagnosis of diabetes. *Diabetes care,* 32**,** 1327-1334.

Coppack, S. W. (2001) Pro-inflammatory cytokines and adipose tissue. *Proceedings of the Nutrition Society,* 60**,** 349-356.

Coppell, K. J., J. I. Mann, S. M. Williams, E. Jo, P. L. Drury, J. C. Miller & W. R. Parnell (2013) Prevalence of diagnosed and undiagnosed diabetes and prediabetes in New Zealand: findings from the 2008/09 Adult Nutrition Survey. *NZ Med J,* 126**,** 23-42.

Cornelissen, J. P., S. A. Haslam & J. M. Balmer (2007) Social identity, organizational identity and corporate identity: Towards an integrated understanding of processes, patternings and products. *British journal of management,* 18**,** S1-S16.

Crandall, J. P., W. C. Knowler, S. E. Kahn, D. Marrero, J. C. Florez, G. A. Bray, S. M. Haffner, M. Hoskin & D. M. Nathan (2008) The prevention of type 2 diabetes. *Nature clinical practice Endocrinology & metabolism,* 4**,** 382-393.

Cummings, P. B. THE ENDOCRINE SYSTEM AND PHYSIOLOGICAL COMMUNICATION. *Our Marvelous Bodies***,** 200.

Dalto, V. F., R. L. Assad, M. M. Lorenzato, M. D. Crema, P. Louzada-Junior & M. H. Nogueira-Barbosa (2020) Comparison between STIR and T2-weighted SPAIR sequences in the evaluation of inflammatory sacroiliitis: diagnostic performance and signal-to-noise ratio. *Radiologia Brasileira,* 53**,** 223-228.

de Vries, M. A., B. Klop, H. W. Janssen, T. L. Njo, E. M. Westerman & M. C. Cabezas (2014) Postprandial inflammation: targeting glucose and lipids. *Oxidative Stress and Inflammation in Non-communicable Diseases-Molecular Mechanisms and Perspectives in Therapeutics***,** 161-170.

Deng, Y. & P. E. Scherer (2010) Adipokines as novel biomarkers and regulators of the metabolic syndrome. *Annals of the New York Academy of Sciences,* 1212**,** E1-E19.

Desouza, S., H. Yoon, R. Singh & M. Petrov (2018a) Quantitative determination of pancreas size using anatomical landmarks and its clinical relevance: a systematic literature review. *Clinical Anatomy,* 31**,** 913-926.

DeSouza, S. V., R. G. Singh, H. D. Yoon, R. Murphy, L. D. Plank & M. S. Petrov (2018b) Pancreas volume in health and disease: a systematic review and meta-analysis. *Expert Review of Gastroenterology & Hepatology,* 12**,** 757-766.

Després, J.-P. & I. Lemieux (2006) Abdominal obesity and metabolic syndrome. *Nature,* 444**,** 881-887.

Deurenberg, P., M. Deurenberg-Yap & S. Guricci (2002) Asians are different from Caucasians and from each other in their body mass index/body fat per cent relationship. *Obesity reviews,* 3**,** 141-146.

Dhaliwal, S. S. & T. A. Welborn (2009) Central obesity and multivariable cardiovascular risk as assessed by the Framingham prediction scores. *The American journal of cardiology,* 103**,** 1403-1407.

DiBaise, J. K. & A. E. Foxx-Orenstein (2013) Role of the gastroenterologist in managing obesity. *Expert review of gastroenterology & hepatology,* 7**,** 439-451.

Dixon, W. T. (1984) Simple proton spectroscopic imaging. *Radiology,* 153**,** 189-194.

ELDerawi, W. A. 2017. The Effectivenes of Oral Magnesium Supplementation on the Glycemic control in Type II diabetic Patients.

Erickson, B. J., P. Korfiatis, Z. Akkus & T. L. Kline (2017) Machine learning for medical imaging. *Radiographics,* 37**,** 505-515.

Erickson, H. P. (2013) Irisin and FNDC5 in retrospect: an exercise hormone or a transmembrane receptor? *Adipocyte,* 2**,** 289-293.

Fain, J. N., A. K. Madan, M. L. Hiler, P. Cheema & S. W. Bahouth (2004) Comparison of the release of adipokines by adipose tissue, adipose tissue matrix, and adipocytes from visceral and subcutaneous abdominal adipose tissues of obese humans. *Endocrinology,* 145**,** 2273-2282.

Fazeli Farsani, S., M. Van Der Aa, M. Van Der Vorst, C. Knibbe & A. De Boer (2013) Global trends in the incidence and prevalence of type 2 diabetes in children and adolescents: a systematic review and evaluation of methodological approaches. *Diabetologia,* 56**,** 1471-1488.

Fedorov, A., R. Beichel, J. Kalpathy-Cramer, J. Finet, J.-C. Fillion-Robin, S. Pujol, C. Bauer, D. Jennings, F. Fennessy & M. Sonka (2012) 3D Slicer as an image computing platform for the Quantitative Imaging Network. *Magnetic resonance imaging,* 30**,** 1323-1341.

Fitness, B. Belly Fat in Women Over 50: Why It Happens| How to Lose It Belly Fat in Women Over 50: Why It Happens| How to Lose It.

Fornari, F., M. Ferracin, D. Trerè, M. Milazzo, S. Marinelli, M. Galassi, L. Venerandi, D. Pollutri, C. Patrizi & A. Borghi (2015) Circulating microRNAs, miR-939, miR-595, miR-519d and miR-494, identify cirrhotic patients with HCC. *PloS one,* 10**,** e0141448.

Freedland, E. S. (2004) Role of a critical visceral adipose tissue threshold (CVATT) in metabolic syndrome: implications for controlling dietary carbohydrates: a review. *Nutrition & metabolism,* 1**,** 12.

Freidenberg, G., D. Reichart, J. Olefsky & R. Henry (1988) Reversibility of defective adipocyte insulin receptor kinase activity in non-insulin-dependent diabetes mellitus. Effect of weight loss. *The Journal of clinical investigation,* 82**,** 1398-1406.

Gaborit, B., I. Abdesselam, F. Kober, A. Jacquier, O. Ronsin, O. Emungania, N. Lesavre, M.-C. Alessi, J. Martin & M. Bernard (2015a) Ectopic fat storage in the pancreas using 1 H-MRS: importance of diabetic status and modulation with bariatric surgery-induced weight loss. *International journal of obesity,* 39**,** 480-487.

Gaborit, B., I. Abdesselam, F. Kober, A. Jacquier, O. Ronsin, O. Emungania, N. Lesavre, M. Alessi, J. Martin & M. Bernard (2015b) Ectopic fat storage in the pancreas using 1 H-MRS: importance of diabetic status and modulation with bariatric surgery-induced weight loss. *International journal of obesity,* 39**,** 480.

Gaborit, B., M. Bernard, A. Dutour, I. Abdesselam, F. Kober, A. Jacquier, O. Ronsin, O. Emungania, N. Lesavre, M. C. Alessi & J. C. Martin (2015c) Ectopic fat storage in the

pancreas using 1H-MRS: Importance of diabetic status and modulation with bariatric surgery-induced weight loss. *International Journal of Obesity* 39**,** 480-487.

Gaborit, B., M. Bernard, A. Dutour, A. Jacquier, F. Kober, I. Abdesselam, T. Cuisset, S. Boullu-Ciocca, O. Emungania, M.-C. Alessi & K. Clément (2012) Effects of bariatric surgery on cardiac ectopic fat. *Journal of the American College of Cardiology,* 60**,** 1381-1389.

Garcia, B. C., Y. Wu, E. B. Nordbeck, S. Musovic, C. S. Olofsson, P. Rorsman & I. W. Asterholm. 2018. Pancreatic Adipose Tissue in Diet-Induced Type 2 Diabetes. Am Diabetes Assoc.

García Torres, D., M. F. Castellanos González, R. Cedeño Morales, M. Benet Rodríguez & I. Ramírez Arteaga (2017) Adipose tissue as an endocrine gland. pathophysiological implications. *Revista de Enfermedades no Transmisibles Finlay,* 7**,** 131-151.

Garcia, T. S., T. H. Rech & C. B. Leitão (2017) Pancreatic size and fat content in diabetes: a systematic review and meta-analysis of imaging studies. *PloS one,* 12**,** e0180911.

Gerhard, G. S., A. M. Styer, G. C. Wood, S. L. Roesch, A. T. Petrick, J. Gabrielsen, W. E. Strodel, C. D. Still & G. Argyropoulos (2013) A role for fibroblast growth factor 19 and bile acids in diabetes remission after Roux-en-Y gastric bypass. *Diabetes care,* 36**,** 1859-1864.

Gillies, N., S. A. Pendharkar, V. M. Asrani, J. Mathew, J. A. Windsor & M. S. Petrov (2016) Interleukin-6 is associated with chronic hyperglycemia and insulin resistance in patients after acute pancreatitis. *Pancreatology,* 16**,** 748-755.

Girshick, R., J. Donahue, T. Darrell & J. Malik. 2014. Rich feature hierarchies for accurate object detection and semantic segmentation. In *Proceedings of the IEEE conference on computer vision and pattern recognition*, 580-587.

Goda, K., E. Sasaki, K. Nagata, M. Fukai, N. Ohsawa & T. Hahafusa (2001a) Pancreatic volume in type 1 and type 2 diabetes mellitus. *Acta diabetologica,* 38**,** 145-149.

Goda, K., E. Sasaki, K. Nagata, M. Fukai, N. Ohsawa & T. Hahafusa (2001b) Pancreatic volume in type 1 und type 2 diabetes mellitus. *Acta diabetologica,* 38**,** 145-149.

Goulding, A., A. M. Grant, R. W. Taylor, S. M. Williams, W. R. Parnell, N. Wilson & J. Mann (2007) Ethnic differences in extreme obesity. *Journal of Pediatrics,* 151**,** 542-4.

Grant, A. K. & L. Golden (2019) Technological advancements in the management of type 2 diabetes. *Current diabetes reports,* 19**,** 1-5.

Guilherme, A., J. V. Virbasius, V. Puri & M. P. Czech (2008) Adipocyte dysfunctions linking obesity to insulin resistance and type 2 diabetes. *Nature reviews Molecular cell biology,* 9**,** 367.

Hardy, P. A., R. S. Hinks & J. A. Tkach (1995) Separation of fat and water in fast spin-echo MR imaging with the three-point Dixon technique. *Journal of Magnetic Resonance Imaging,* 5**,** 181-185.

Heid, I. M., A. U. Jackson, J. C. Randall, T. W. Winkler, L. Qi, V. Steinthorsdottir, G. Thorleifsson, M. C. Zillikens, E. K. Speliotes & R. Mägi (2010) Meta-analysis identifies 13 new loci associated with waist-hip ratio and reveals sexual dimorphism in the genetic basis of fat distribution. *Nature genetics,* 42**,** 949-960.

Heller, N., F. Isensee, K. H. Maier-Hein, X. Hou, C. Xie, F. Li, Y. Nan, G. Mu, Z. Lin & M. Han (2021) The state of the art in kidney and kidney tumor segmentation in contrast-enhanced ct imaging: Results of the kits19 challenge. *Medical Image Analysis,* 67**,** 101821.

Heni, M., J. Machann, H. Staiger, N. F. Schwenzer, A. Peter, F. Schick, C. D. Claussen, N. Stefan, H. U. Häring & A. Fritsche (2010) Pancreatic fat is negatively associated with

insulin secretion in individuals with impaired fasting glucose and/or impaired glucose tolerance: a nuclear magnetic resonance study. *Diabetes/metabolism research and reviews,* 26**,** 200-205.

Hens, W., J. Taeymans, J. Cornelis, J. Gielen, L. Van Gaal & D. Vissers (2016) The effect of lifestyle interventions on excess ectopic fat deposition measured by noninvasive techniques in overweight and obese adults: a systematic review and meta-analysis. *Journal of Physical Activity and Health,* 13**,** 671-694.

Hens, W., D. Vissers, D. Hansen, S. Peeters, J. Gielen, L. Van Gaal & J. Taeymans (2017) The effect of diet or exercise on ectopic adiposity in children and adolescents with obesity: a systematic review and meta-analysis. *Obesity Reviews,* 18**,** 1310-1322.

Holst, J. J., S. Madsbad, K. N. Bojsen-Møller, M. S. Svane, N. B. Jørgensen, C. Dirksen & C. Martinussen (2018) Mechanisms in Bariatric Surgery: Gut Hormones, Diabetes Resolution and Weight loss. *Surgery for Obesity and Related Diseases*.

Horng-Yih, O., W. Chih-Yuan, Y. Yi-Ching, C. Ming-Fong & C. Chih-Jen (2013) The association between nonalcoholic fatty pancreas disease and diabetes. *PLoS One* 8**,** e62561.

Horton, E. S. (1988) Role and management of exercise in diabetes mellitus. *Diabetes care,* 11**,** 201-211.

Hu, H. H., H.-W. Kim, K. S. Nayak & M. I. Goran (2010a) Comparison of Fat-Water MRI and Single-voxel MRS in the Assessment of Hepatic and Pancreatic Fat Fractions in Humans. *Obesity,* 18**,** 841-847.

Hu, H. H., H. W. Kim, K. S. Nayak & M. I. Goran (2010b) Comparison of fat–water MRI and single-voxel MRS in the assessment of hepatic and pancreatic fat fractions in humans. *Obesity,* 18**,** 841-847.

Huxley, R., F. Barzi, R. Stolk, I. Caterson, T. Gill, T. H. Lam, A. Omari, M. Woodward, C. Obesity in Asia & C. Obesity in Asia (2005) Ethnic comparisons of obesity in the Asia-Pacific region: Protocol for a collaborative overview of cross-sectional studies. *Obesity Reviews,* 6**,** 193-198.

Ibrahim, M. M. (2010) Subcutaneous and visceral adipose tissue: structural and functional differences. *Obesity reviews,* 11**,** 11-18.

Inzucchi, S. E., R. M. Bergenstal, J. B. Buse, M. Diamant, E. Ferrannini, M. Nauck, A. L. Peters, A. Tsapas, R. Wender & D. R. Matthews (2012) Management of hyperglycemia in type 2 diabetes: a patient-centered approach: position statement of the American Diabetes Association (ADA) and the European Association for the Study of Diabetes (EASD). *Diabetes care,* 35**,** 1364-1379.

Irlbeck, T., J. Massaro, F. Bamberg, C. O'donnell, U. Hoffmann & C. Fox (2010) Association between single-slice measurements of visceral and abdominal subcutaneous adipose tissue with volumetric measurements: the Framingham Heart Study. *International journal of obesity,* 34**,** 781-787.

Irving, B. A., C. K. Davis, D. W. Brock, J. Y. Weltman, D. Swift, E. J. Barrett, G. A. Gaesser & A. Weltman (2008) Effect of exercise training intensity on abdominal visceral fat and body composition. *Medicine and science in sports and exercise,* 40**,** 1863.

Jastrzębska-Mierzyńska, M., L. Ostrowska, H. R. Hady, J. Dadan & E. Konarzewska-Duchnowska (2015) The impact of bariatric surgery on nutritional status of patients. *Videosurgery and Other Miniinvasive Techniques* 10**,** 115-124.

Jensen, M. D., D. H. Ryan, C. M. Apovian, J. D. Ard, A. G. Comuzzie, K. A. Donato, F. B. Hu, V. S. Hubbard, J. M. Jakicic & R. F. Kushner (2014) 2013 AHA/ACC/TOS guideline for the management of overweight and obesity in adults: a report of the American College

of Cardiology/American Heart Association Task Force on Practice Guidelines and The Obesity Society. *Journal of the American college of cardiology,* 63**,** 2985-3023.

Jeremic, N., P. Chaturvedi & S. C. Tyagi (2017) Browning of white fat: novel insight into factors, mechanisms, and therapeutics. *Journal of cellular physiology,* 232**,** 61-68.

Jiao, Z., X. Gao, Y. Wang & J. Li (2016) A deep feature based framework for breast masses classification. *Neurocomputing,* 197**,** 221-231.

Jonas, J.-C., M. Bensellam, J. Duprez, H. Elouil, Y. Guiot & S. Pascal (2009) Glucose regulation of islet stress responses and β-cell failure in type 2 diabetes. *Diabetes, obesity and metabolism,* 11**,** 65-81.

Joshy, G., P. Dunn, M. Fisher & R. Lawrenson (2009) Ethnic differences in the natural progression of nephropathy among diabetes patients in New Zealand: hospital admission rate for renal complications, and incidence of end-stage renal disease and renal death. *Diabetologia,* 52**,** 1474-1478.

Kadowaki, T., A. Sekikawa, K. Murata, H. Maegawa, T. Takamiya, T. Okamura, A. El-Saed, N. Miyamatsu, D. Edmundowicz & Y. Kita (2006) Japanese men have larger areas of visceral adipose tissue than Caucasian men in the same levels of waist circumference in a population-based study. *International journal of obesity,* 30**,** 1163-1165.

Kagawa, M., N. M. Byrne, N. A. King, S. Pal & A. P. Hills (2009) Ethnic differences in body composition and anthropometric characteristics in Australian Caucasian and urban indigenous children. *British Journal of Nutrition,* 102**,** 938-946.

Karastergiou, K., S. R. Smith, A. S. Greenberg & S. K. Fried (2012) Sex differences in human adipose tissues–the biology of pear shape. *Biology of sex differences,* 3**,** 13.

Kashyap, S. Daud, K. Kelly, A. Gastaldelli, H. Win, S. Brethauer, J. Kirwan & P. Schauer (2010) Acute effects of gastric bypass versus gastric restrictive surgery on β-cell function and insulinotropic hormones in severely obese patients with type 2 diabetes. *International journal of obesity,* 34**,** 462-471.

Kashyap, M. Gupta, J. P. Kirwan, P. R. Schauer, D. L. Bhatt, K. Wolski, R. M. Watanabe, M. Abdul-Ghani, B. Abood, C. E. Pothier, S. Brethauer & S. Nissen (2013) Metabolic effects of bariatric surgery in patients with moderate obesity and type 2 diabetes: Analysis of a randomized control trial comparing surgery with intensive medical treatment. *Diabetes Care,* 36**,** 2175-2182.

Kershaw, E. E. & J. S. Flier (2004) Adipose tissue as an endocrine organ. *The Journal of Clinical Endocrinology & Metabolism,* 89**,** 2548-2556.

Kim, H.-S. Han, H. S. Kang, H. Kim, J. Y. Cho, S. Lim, K. Cha, K. H. Lee, Y. H. Kim, J. H. Kim & Y.-S. Yoon (2014a) Quantitative assessment of pancreatic fat by using unenhanced CT: Pathologic correlation and clinical implications. *Radiology,* 271**,** 104-112.

Kim, H. K. Kim, E. H. Kim, S. J. Bae & J. Y. Park (2012) Impact of body mass index on the predictive ability of body fat distribution for Type 2 diabetes risk in Koreans. *Diabetic Medicine,* 29**,** 1395-1398.

Kim, H., S. E. Taksali, S. Dufour, D. Befroy, T. R. Goodman, K. F. Petersen, G. I. Shulman, S. Caprio & R. T. Constable (2008) Comparative MR study of hepatic fat quantification using single-voxel proton spectroscopy, two-point dixon and three-point IDEAL. *Magnetic Resonance in Medicine: An Official Journal of the International Society for Magnetic Resonance in Medicine,* 59**,** 521-527.

Kim, S. Y., H. Kim, J. Y. Cho, S. Lim, K. Cha, K. H. Lee, Y. H. Kim, J. H. Kim, Y.-S. Yoon & H.-S. Han (2014b) Quantitative assessment of pancreatic fat by using unenhanced CT: pathologic correlation and clinical implications. *Radiology,* 271**,** 104-112.

King, H., M. Rewers & W. A. H. D. R. Group (1993) Global estimates for prevalence of diabetes mellitus and impaired glucose tolerance in adults. *Diabetes care,* 16**,** 157-177.

Kitabchi, A. E., G. E. Umpierrez, J. M. Miles & J. N. Fisher (2009) Hyperglycemic crises in adult patients with diabetes. *Diabetes care,* 32**,** 1335-1343.

Kosteli, A., E. Sugaru, G. Haemmerle, J. F. Martin, J. Lei, R. Zechner & A. W. Ferrante (2010) Weight loss and lipolysis promote a dynamic immune response in murine adipose tissue. *The Journal of clinical investigation,* 120**,** 3466-3479.

Krähenbühl, P. & V. Koltun (2011) Efficient inference in fully connected crfs with gaussian edge potentials. *Advances in neural information processing systems,* 24**,** 109-117.

Kreel, L., M. Haertel & D. Katz (1977) Computed tomography of the normal pancreas. *Journal of Computer Assisted Tomography,* 1**,** 290-299.

Krizhevsky, A., I. Sutskever & G. E. Hinton (2012) Imagenet classification with deep convolutional neural networks. *Advances in neural information processing systems,* 25.

Kuk, J. L., T. S. Church, S. N. Blair & R. Ross (2006) Does measurement site for visceral and abdominal subcutaneous adipose tissue alter associations with the metabolic syndrome? *Diabetes care,* 29**,** 679-684.

Lê, K.-A., E. E. Ventura, J. Q. Fisher, J. N. Davis, M. J. Weigensberg, M. Punyanitya, H. H. Hu, K. S. Nayak & M. I. Goran (2011) Ethnic differences in pancreatic fat accumulation and its relationship with other fat depots and inflammatory markers. *Diabetes care,* 34**,** 485-490.

Leahy, J. L., I. B. Hirsch, K. A. Peterson & D. Schneider (2010) Targeting β-cell function early in the course of therapy for type 2 diabetes mellitus. *The Journal of Clinical Endocrinology & Metabolism,* 95**,** 4206-4216.

Li, Q., W. Cai, X. Wang, Y. Zhou, D. D. Feng & M. Chen. 2014. Medical image classification with convolutional neural network. In *2014 13th international conference on control automation robotics & vision (ICARCV)*, 844-848. IEEE.

Li, Y., Z. Zhu, Y. Zhou, Y. Xia, W. Shen, E. K. Fishman & A. L. Yuille. 2019. Volumetric Medical Image Segmentation: A 3D Deep Coarse-to-Fine Framework and Its Adversarial Examples. In *Deep Learning and Convolutional Neural Networks for Medical Imaging and Clinical Informatics*, 69-91. Springer.

Liang, W. & D. dong Ye (2019) The potential of adipokines as biomarkers and therapeutic agents for vascular complications in type 2 diabetes mellitus. *Cytokine & growth factor reviews,* 48**,** 32-39.

Liang, Y. Z., J. J. H. Li, H. B. Xiao, Y. He, L. Zhang & Y. X. Yan (2020) Identification of stress-related microRNA biomarkers in type 2 diabetes mellitus: A systematic review and meta-analysis. *Journal of diabetes,* 12**,** 633-644.

Lingvay, I., V. Esser, J. L. Legendre, A. L. Price, K. M. Wertz, B. Adams-Huet, S. Zhang, R. H. Unger & L. S. Szczepaniak (2009a) Noninvasive quantification of pancreatic fat in humans. *The Journal of clinical endocrinology and metabolism,* 94**,** 4070-4076.

Lingvay, I., V. Esser, J. L. Legendre, A. L. Price, K. M. Wertz, B. Adams-Huet, S. Zhang, R. H. Unger & L. S. Szczepaniak (2009b) Noninvasive quantification of pancreatic fat in humans. *The Journal of Clinical Endocrinology & Metabolism,* 94**,** 4070-4076.

Litjens, G., T. Kooi, B. E. Bejnordi, A. A. A. Setio, F. Ciompi, M. Ghafoorian, J. A. Van Der Laak, B. Van Ginneken & C. I. Sánchez (2017) A survey on deep learning in medical image analysis. *Medical image analysis,* 42**,** 60-88.

Long, J., E. Shelhamer & T. Darrell. 2015. Fully convolutional networks for semantic segmentation. In *Proceedings of the IEEE conference on computer vision and pattern recognition*, 3431-3440.

Longo, R., P. Pollesello, C. Ricci, F. Masutti, B. J. Kvam, L. Bercich, L. S. Croce, P. Grigolato, S. Paoletti & B. De Bernard (1995) Proton MR spectroscopy in quantitative in vivo determination of fat content in human liver steatosis. *Journal of Magnetic Resonance Imaging,* 5**,** 281-285.

Lovejoy, J. C., A. Jacques, M. Klemperer & R. Tulley (1996) Abdominal fat distribution and metabolic risk factors: effects of race. *Metabolism,* 45**,** 1119-1124.

Luppino, F. S., L. M. de Wit, P. F. Bouvy, T. Stijnen, P. Cuijpers, B. W. Penninx & F. G. Zitman (2010) Overweight, obesity, and depression: a systematic review and meta-analysis of longitudinal studies. *Archives of general psychiatry,* 67**,** 220-229.

Ma, J., F. Lin, S. Wesarg & M. Erdt. 2018. A novel bayesian model incorporating deep neural network and statistical shape model for pancreas segmentation. In *International Conference on Medical Image Computing and Computer-Assisted Intervention*, 480-487. Springer.

Macauley, M., K. Percival, P. E. Thelwall, K. G. Hollingsworth & R. Taylor (2015) Altered volume, morphology and composition of the pancreas in type 2 diabetes. *PloS one,* 10**,** e0126825.

Machann, J., O. P. Bachmann, K. Brechtel, D. B. Dahl, B. Wietek, B. Klumpp, H. U. Häring, C. D. Claussen, S. Jacob & F. Schick (2003) Lipid content in the musculature of the lower leg assessed by fat selective MRI: intra-and interindividual differences and correlation with anthropometric and metabolic data. *Journal of Magnetic Resonance Imaging: An Official Journal of the International Society for Magnetic Resonance in Medicine,* 17**,** 350-357.

Maggio, A. B. R., P. Mueller, J. Wacker, M. Viallon, D. C. Belli, M. Beghetti, N. J. Farpour-Lambert & V. A. McLin (2012) Increased pancreatic fat fraction is present in obese adolescents with metabolic syndrome. *Journal of Pediatric Gastroenterology and Nutrition* 54**,** 720-726.

Majumder, S., N. A. Philip, N. Takahashi, M. J. Levy, V. P. Singh & S. T. Chari (2017) Fatty pancreas: should we be concerned? *Pancreas,* 46**,** 1251.

Mamoshina, P., A. Vieira, E. Putin & A. Zhavoronkov (2016) Applications of deep learning in biomedicine. *Molecular pharmaceutics,* 13**,** 1445-1454.

Mancuso, P. (2016) The role of adipokines in chronic inflammation. *ImmunoTargets and therapy,* 5**,** 47.

Mann, L. W., D. M. Higgins, C. N. Peters, S. Cassidy, K. K. Hodson, A. Coombs, R. Taylor & K. G. Hollingsworth (2016) Accelerating MR imaging liver steatosis measurement using combined compressed sensing and parallel imaging: a quantitative evaluation. *Radiology,* 278**,** 247-256.

Mantziari, S., A. Dayer, C. Duvoisin, N. Demartines, P. Allemann, J.-M. Calmes, L. Favre, P. Fournier & M. Suter (2020) Long-term weight loss, metabolic outcomes, and quality of life at 10 years after Roux-en-Y gastric bypass are independent of patients' age at baseline. *Obesity surgery,* 30**,** 1181-1188.

Marchal, J., S. Blanc, J. Epelbaum, F. Aujard & F. Pifferi (2012) Effects of chronic calorie restriction or dietary resveratrol supplementation on insulin sensitivity markers in a primate, Microcebus murinus. *PLoS One,* 7**,** e34289.

Maresky, H. S., Z. Sharfman, T. Ziv-Baran, J. Gomori, L. Copel & S. Tal (2015) Anthropometric assessment of neck adipose tissue and airway volume using multidetector computed tomography: an imaging approach and association with overall mortality. *Medicine,* 94.

Martin, B. D. & E. Schwab (2013) Current usage of symbiosis and associated terminology. *International Journal of Biology,* 5**,** 32.

Martin, S., E. P. Sorokin, E. L. Thomas, N. Sattar, M. Cule, J. D. Bell & H. Yaghootkar (2021) Estimating the effect of liver and pancreas volume and fat content on risk of diabetes: A Mendelian randomization study. *Diabetes Care*.

Mashhood, A., R. Railkar, T. Yokoo, Y. Levin, L. Clark, S. Fox-Bosetti, M. S. Middleton, J. Riek, E. Kauh & B. J. Dardzinski (2013) Reproducibility of hepatic fat fraction measurement by magnetic resonance imaging. *Journal of Magnetic Resonance Imaging,* 37**,** 1359-1370.

Maskarinec, G., A. Grandinetti, G. Matsuura, S. Sharma, M. Mau, B. E. Henderson & L. N. Kolonel (2009) Diabetes prevalence and body mass index differ by ethnicity: The multiethnic cohort. *Ethnicity & Disease,* 19**,** 49-55.

Mathers, C. D., T. Boerma & D. Ma Fat (2009) Global and regional causes of death. *British medical bulletin,* 92**,** 7-32.

Matsha, T. E., A. P. Kengne, S. Hector, D. L. Mbu, Y. Y. Yako & R. T. Erasmus (2018) MicroRNA profiling and their pathways in South African individuals with prediabetes and newly diagnosed type 2 diabetes mellitus. *Oncotarget,* 9**,** 30485.

Mattiuzzi, C. & G. Lippi (2020) Cancer statistics: a comparison between world health organization (WHO) and global burden of disease (GBD). *European journal of public health,* 30**,** 1026-1027.

Mazurek, T., L. Zhang, A. Zalewski, J. D. Mannion, J. T. Diehl, H. Arafat, L. Sarov-Blat, S. O'Brien, E. A. Keiper & A. G. Johnson (2003) Human epicardial adipose tissue is a source of inflammatory mediators. *Circulation,* 108**,** 2460-2466.

Meyer, K. A., C. K. Neeley, N. A. Baker, A. R. Washabaugh, C. G. Flesher, B. S. Nelson, T. L. Frankel, C. N. Lumeng, C. A. Lyssiotis & M. L. Wynn (2016) Adipocytes promote pancreatic cancer cell proliferation via glutamine transfer. *Biochemistry and biophysics reports,* 7**,** 144-149.

Michael, K. Y., J. Ma, J. Fisher, J. F. Kreisberg, B. J. Raphael & T. Ideker (2018) Visible machine learning for biomedicine. *Cell,* 173**,** 1562-1565.

Mingrone, G., A. DeGaetano, A. Greco, E. Capristo, G. Benedetti, M. Castagneto & G. Gasbarrini (1997) Reversibility of insulin resistance in obese diabetic patients: role of plasma lipids. *Diabetologia,* 40**,** 599-605.

Ministry of Health. 2004. *Tracking the Obesity Epidemic: New Zealand 1977-2003*. Wellington: Ministry of Health.

Misra, A., J. S. Wasir & N. K. Vikram (2005) Waist circumference criteria for the diagnosis of abdominal obesity are not applicable uniformly to all populations and ethnic groups. *Nutrition,* 21**,** 969-976.

Mitsiopoulos, N., R. Baumgartner, S. Heymsfield, W. Lyons, D. Gallagher & R. Ross (1998) Cadaver validation of skeletal muscle measurement by magnetic resonance imaging and computerized tomography. *Journal of applied physiology,* 85**,** 115-122.

Mokdad, A. H., E. S. Ford, B. A. Bowman, W. H. Dietz, F. Vinicor, V. S. Bales & J. S. Marks (2003) Prevalence of obesity, diabetes, and obesity-related health risk factors, 2001. *Jama,* 289**,** 76-79.

Morimoto, Y., G. Maskarinec, S. M. Conroy, U. Lim, J. Shepherd & R. Novotny (2012) Asian ethnicity is associated with a higher trunk/peripheral fat ratio in women and adolescent girls. *Journal of Epidemiology,* 22**,** 130-135.

Moses, H., D. H. Matheson, E. R. Dorsey, B. P. George, D. Sadoff & S. Yoshimura (2013) The anatomy of health care in the United States. *Jama,* 310**,** 1947-1964.

Nagai, M., H. Komiya, Y. Mori, T. Ohta, Y. Kasahara & Y. Ikeda (2010) Estimating visceral fat area by multifrequency bioelectrical impedance. *Diabetes care,* 33**,** 1077-1079.

Nakayama, K., Y. Oshiro, R. Miyamoto, K. Kohno, K. Fukunaga & N. Ohkohchi (2017) The effect of three-dimensional preoperative simulation on liver surgery. *World journal of surgery,* 41**,** 1840-1847.

Nazir, M. A., L. AlGhamdi, M. AlKadi, N. AlBeajan, L. AlRashoudi & M. AlHussan (2018) The burden of diabetes, its oral complications and their prevention and management. *Open access Macedonian journal of medical sciences,* 6**,** 1545.

Nehrke, K., P. Bornert, D. Manke & J. C. Bock (2001) Free-breathing cardiac MR imaging: study of implications of respiratory motion—initial results. *Radiology,* 220**,** 810-815.

Niraj, S. P., M. R. Peterson, G. Y. Lin, A. Feldstein, B. Schnabl, R. Bettencourt, E. Seki, C. B. Sirlin & R. Loomba (2013) Insulin resistance increases MRI-estimated pancreatic fat in nonalcoholic fatty liver disease and normal controls. *Gastroenterology Research and Practice,* 2013**,** 1-8.

Nishimura, T., Y. Nakatake, M. Konishi & N. Itoh (2000) Identification of a novel FGF, FGF-21, preferentially expressed in the liver1. *Biochimica et Biophysica Acta (BBA)-Gene Structure and Expression,* 1492**,** 203-206.

O'Connor, M., J. Ryan & S. Foley (2015) Best single-slice location to measure visceral adipose tissue on paediatric CT scans and the relationship between anthropometric measurements, gender and VAT volume in children. *The British journal of radiology,* 88**,** 20140711.

Ohkawara, K., S. Tanaka, M. Miyachi, K. Ishikawa-Takata & I. Tabata (2007) A dose–response relation between aerobic exercise and visceral fat reduction: systematic review of clinical trials. *International journal of obesity,* 31**,** 1786-1797.

Ohshima, S. (2014) Volume analyzer SYNAPSE VINCENT for liver analysis. *Journal of Hepato-Biliary-Pancreatic Sciences,* 21**,** 235-238.

Oktay, O., J. Schlemper, L. L. Folgoc, M. Lee, M. Heinrich, K. Misawa, K. Mori, S. McDonagh, N. Y. Hammerla & B. Kainz (2018) Attention u-net: Learning where to look for the pancreas. *arXiv preprint arXiv:1804.03999*.

Organization, W. H. 2011. Use of glycated haemoglobin (HbA1c) in diagnosis of diabetes mellitus: abbreviated report of a WHO consultation. World Health Organization.

Ouchi, N., J. L. Parker, J. J. Lugus & K. Walsh (2011) Adipokines in inflammation and metabolic disease. *Nature reviews immunology,* 11**,** 85-97.

Owen, B. M., D. J. Mangelsdorf & S. A. Kliewer (2015) Tissue-specific actions of the metabolic hormones FGF15/19 and FGF21. *Trends in Endocrinology & Metabolism,* 26**,** 22-29.

Ozturk, K., T. Dogan, S. Celikkanat, A. Ozen, H. Demirci, O. Kurt, T. Turker, Y. Yilmaz & A. Uygun (2018) The association of fatty pancreas with subclinical atherosclerosis in nonalcoholic fatty liver disease. *European journal of gastroenterology & hepatology,* 30**,** 411-417.

Park, A. (2009) Fat-Bellied Monkeys Suggest Why Stress Sucks. *Time. Retrieved***,** 08-08.

Paskze, A. & S. Chintala. 2017. Tensors and Dynamic neural networks in Python with strong GPU acceleration.

Patel, N., M. Peterson, D. Brenner, E. Heba, C. Sirlin & R. Loomba (2013a) Association between novel MRI-estimated pancreatic fat and liver histology-determined steatosis and fibrosis in non-alcoholic fatty liver disease. *Alimentary pharmacology & therapeutics,* 37**,** 630-639.

Patel, N. S., M. R. Peterson, D. A. Brenner, E. Heba, C. Sirlin & R. Loomba (2013b) Association between novel MRI-estimated pancreatic fat and liver histology-determined steatosis and fibrosis in non-alcoholic fatty liver disease. *Alimentary Pharmacology & Therapeutics,* 37**,** 630-639.

Peng, S., L. D. Plank, J. L. McCall, L. K. Gillanders, K. McIlroy & E. J. Gane (2007) Body composition, muscle function, and energy expenditure in patients with liver cirrhosis: a comprehensive study. *The American journal of clinical nutrition,* 85**,** 1257-1266.

Pereira, S., A. Pinto, V. Alves & C. A. Silva (2016) Brain tumor segmentation using convolutional neural networks in MRI images. *IEEE transactions on medical imaging,* 35**,** 1240-1251.

Petrov, M. S. 2018. Harnessing analytic morphomics for early detection of pancreatic cancer. LWW.

Pezeshkian, M., M. Noori, H. Najjarpour-Jabbari, A. Abolfathi, M. Darabi, M. Darabi, M. Shaaker & G. Shahmohammadi (2009) Fatty acid composition of epicardial and subcutaneous human adipose tissue. *Metabolic syndrome and related disorders,* 7**,** 125-132.

Pinnick, K. E., S. C. Collins, C. Londos, D. Gauguier, A. Clark & B. A. Fielding (2008) Pancreatic ectopic fat is characterized by adipocyte infiltration and altered lipid composition. *Obesity,* 16**,** 522-530.

Porter, S. A., J. M. Massaro, U. Hoffmann, R. S. Vasan, C. J. O'Donnel & C. S. Fox (2009) Abdominal subcutaneous adipose tissue: a protective fat depot? *Diabetes care,* 32**,** 1068-1075.

Pratley, R., M. Nauck, T. Bailey, E. Montanya, R. Cuddihy, S. Filetti, A. Garber, A. Thomsen, H. Hartvig & M. Davies (2011) One year of liraglutide treatment offers sustained and more effective glycaemic control and weight reduction compared with sitagliptin, both in combination with metformin, in patients with type 2 diabetes: a randomised, parallel-group, open-label trial. *International journal of clinical practice,* 65**,** 397-407.

Preis, S. R., J. M. Massaro, S. J. Robins, U. Hoffmann, R. S. Vasan, T. Irlbeck, J. B. Meigs, P. Sutherland, R. B. D'Agostino Sr & C. J. O'donnell (2010) Abdominal subcutaneous and visceral adipose tissue and insulin resistance in the Framingham heart study. *Obesity,* 18**,** 2191-2198.

Prevention, C. f. D. C. a. 2018. Diabetes Report Card 2017. Atlanta, GA: Centers for Disease Control and Prevention, US Dept of Health and Human Services.

Puhl, R. M. & C. A. Heuer (2010) Obesity stigma: important considerations for public health. *American journal of public health,* 100**,** 1019-1028.

Qiao, N., C. Sun, J. Sun & C. Song. 2021. Superpixel Combining Region Merging for Pancreas Segmentation. In *2021 36th Youth Academic Annual Conference of Chinese Association of Automation (YAC)*, 276-281. IEEE.

Rahier, J., Y. Guiot, R. M. Goebbels, C. Sempoux & J. C. Henquin (2008) Pancreatic beta-cell mass in European subjects with type 2 diabetes. *Diabetes, Obesity and Metabolism,* 10**,** 32-42.

Randle, P., P. Garland, C. Hales & E. Newsholme (1963) The glucose fatty-acid cycle its role in insulin sensitivity and the metabolic disturbances of diabetes mellitus. *The Lancet,* 281**,** 785-789.

Ranzato, M. A., G. Hinton & Y. LeCun (2015) Guest editorial: Deep learning. *International Journal of Computer Vision,* 113**,** 1-2.

Reeder, S., C. Hines, H. Yu, C. McKenzie & J. Brittain. 2009. On the definition of fat-fraction for in vivo fat quantification with magnetic resonance imaging. In *Proceedings of the 17th Annual Meeting of ISMRM*, 211.

Reeder, S. B., H. H. Hu & C. B. Sirlin (2012) Proton density fat-fraction: a standardized MR-based biomarker of tissue fat concentration. *Journal of magnetic resonance imaging: JMRI,* 36**,** 1011.

Reeder, S. B., A. R. Pineda, Z. Wen, A. Shimakawa, H. Yu, J. H. Brittain, G. E. Gold, C. H. Beaulieu & N. J. Pelc (2005) Iterative decomposition of water and fat with echo asymmetry and least-squares estimation (IDEAL): application with fast spin-echo imaging. *Magnetic Resonance in Medicine: An Official Journal of the International Society for Magnetic Resonance in Medicine,* 54**,** 636-644.

Ren, J., I. Dimitrov, A. D. Sherry & C. R. Malloy (2008) Composition of adipose tissue and marrow fat in humans by 1H NMR at 7 Tesla. *Journal of lipid research,* 49**,** 2055-2062.

Reynolds, N., J. Neidig, A. Wu, A. Gifford & W. Holmes (2006) Balancing disfigurement and fear of disease progression: Patient perceptions of HIV body fat redistribution. *Aids Care,* 18**,** 663-673.

Rhodes, C. J. (2005) Type 2 diabetes-a matter of ß-cell life and death? *Science,* 307**,** 380-384.

Roden, M., T. B. Price, G. Perseghin, K. F. Petersen, D. L. Rothman, G. W. Cline & G. I. Shulman (1996) Mechanism of free fatty acid-induced insulin resistance in humans. *Journal of Clinical Investigation,* 97**,** 2859.

Rome, S. (2013) Are extracellular microRNAs involved in type 2 diabetes and related pathologies? *Clinical biochemistry,* 46**,** 937-945.

Ronneberger, O., P. Fischer & T. Brox. 2015. U-net: Convolutional networks for biomedical image segmentation. In *International Conference on Medical image computing and computer-assisted intervention*, 234-241. Springer.

Ross, R., D. Dagnone, P. J. Jones, H. Smith, A. Paddags, R. Hudson & I. Janssen (2000) Reduction in obesity and related comorbid conditions after diet-induced weight loss or exercise-induced weight loss in men: a randomized, controlled trial. *Annals of internal medicine,* 133**,** 92-103.

Ross, R. & J. Rissanen (1994) Mobilization of visceral and subcutaneous adipose tissue in response to energy restriction and exercise. *The American journal of clinical nutrition,* 60**,** 695-703.

Rossi, A. P., M. Zamboni, F. Fantin, G. A. Zamboni, G. Mazzali, C. A. Rinaldi, M. Del Giglio, V. Di Francesco, M. Barillari & R. Pozzi Mucelli (2011) Predictors of Ectopic Fat Accumulation in Liver and Pancreas in Obese Men and Women. *Obesity,* 19**,** 1747-1754.

Rotella, F. & E. Mannucci (2013) Depression as a risk factor for diabetes: a meta-analysis of longitudinal studies. *The Journal of clinical psychiatry,* 74**,** 4231.

Roth, G. A., G. A. Mensah, C. O. Johnson, G. Addolorato, E. Ammirati, L. M. Baddour, N. C. Barengo, A. Z. Beaton, E. J. Benjamin & C. P. Benziger (2020) Global burden of cardiovascular diseases and risk factors, 1990–2019: update from the GBD 2019 study. *Journal of the American College of Cardiology,* 76**,** 2982-3021.

Roth, H. R., L. Lu, A. Farag, H.-C. Shin, J. Liu, E. B. Turkbey & R. M. Summers. 2015. Deeporgan: Multi-level deep convolutional networks for automated pancreas segmentation. In *International conference on medical image computing and computer-assisted intervention*, 556-564. Springer.

Roth, H. R., L. Lu, N. Lay, A. P. Harrison, A. Farag, A. Sohn & R. M. Summers (2018) Spatial aggregation of holistically-nested convolutional neural networks for automated pancreas localization and segmentation. *Medical image analysis,* 45**,** 94-107.

Russell, B. C., A. Torralba, K. P. Murphy & W. T. Freeman (2005) LabelMe: a database and web-based tool for image. *Int. J. of Computer Vision,* 77.

--- (2008) LabelMe: a database and web-based tool for image annotation. *International journal of computer vision,* 77**,** 157-173.

Russo, V., C. Yu, P. Belliveau, A. Hamilton & L. E. Flynn (2014) Comparison of human adipose-derived stem cells isolated from subcutaneous, omental, and intrathoracic adipose tissue depots for regenerative applications. *Stem cells translational medicine,* 3**,** 206-217.

Rynders, C. A., E. A. Thomas, A. Zaman, Z. Pan, V. A. Catenacci & E. L. Melanson (2019) Effectiveness of intermittent fasting and time-restricted feeding compared to continuous energy restriction for weight loss. *Nutrients,* 11**,** 2442.

Sadeghabadi, Z. A., F. Lotfi, S. S. Moheb, R. Abbasalipourkabir, M. T. Goodarzi & N. Ziamajidi (2021) Effects of garlic extract on inflammatory cytokines in rats with type 1 and type 2 diabetes. *Gene Reports***,** 101474.

Sahin, B., M. Emirzeoglu, A. Uzun, L. Incesu, Y. Bek, S. Bilgic & S. Kaplan (2003) Unbiased estimation of the liver volume by the Cavalieri principle using magnetic resonance images. *European journal of radiology,* 47**,** 164-170.

Saisho, Y., A. E. Butler, J. J. Meier, T. Monchamp, M. Allen-Auerbach, R. A. Rizza & P. C. Butler (2007) Pancreas volumes in humans from birth to age one hundred taking into account sex, obesity, and presence of type-2 diabetes. *Clinical Anatomy,* 20**,** 933-942.

Sams, V. G., C. Blackledge, N. Wijayatunga, P. Barlow, M. Mancini, G. Mancini & N. Moustaid-Moussa (2016) Effect of bariatric surgery on systemic and adipose tissue inflammation. *Surgical endoscopy,* 30**,** 3499-3504.

Sandiford, O. A., C. A. Moore, J. Du, M. Boulad, M. Gergues, H. Eltouky & P. Rameshwar (2018) Human aging and cancer: role of miRNA in tumor microenvironment. *Exosomes, Stem Cells and MicroRNA***,** 137-152.

Sarvamangala, D. & R. V. Kulkarni (2021) Convolutional neural networks in medical image understanding: a survey. *Evolutionary intelligence***,** 1-22.

Savard, M. 2007. *Apples & Pears: The Body Shape Solution for Weight Loss and Wellne*. Simon and Schuster.

Savva, S., M. Tornaritis, M. Savva, Y. Kourides, A. Panagi, N. Silikiotou, C. Georgiou & A. Kafatos (2000) Waist circumference and waist-to-height ratio are better predictors of cardiovascular disease risk factors in children than body mass index. *International journal of obesity,* 24**,** 1453-1458.

Scheen, A. J., N. Finer, P. Hollander, M. D. Jensen, L. F. Van Gaal & R.-D. S. Group (2006) Efficacy and tolerability of rimonabant in overweight or obese patients with type 2 diabetes: a randomised controlled study. *The lancet,* 368**,** 1660-1672.

Schick, A., M. Fischer & R. Stiefelhagen (2014) An evaluation of the compactness of superpixels. *Pattern Recognition Letters,* 43**,** 71-80.

Schweiger, M., A. Lass, R. Zimmermann, T. O. Eichmann & R. Zechner (2009) Neutral lipid storage disease: genetic disorders caused by mutations in adipose triglyceride lipase/PNPLA2 or CGI-58/ABHD5. *American journal of physiology-endocrinology and metabolism,* 297**,** E289-E296.

Seide, F. & A. Agarwal. 2016. CNTK: Microsoft's open-source deep-learning toolkit. In *Proceedings of the 22nd ACM SIGKDD international conference on knowledge discovery and data mining*, 2135-2135.

Seidell, J. C., A. Oosterlee, M. Thijssen, J. Burema, P. Deurenberg, J. Hautvast & J. Ruijs (1987) Assessment of intra-abdominal and subcutaneous abdominal fat: relation between anthropometry and computed tomography. *The American journal of clinical nutrition,* 45**,** 7-13.

Sharma, P., D. R. Martin, N. Pineda, Q. Xu, M. Vos, F. Anania & X. Hu (2009) Quantitative analysis of T2-correction in single-voxel magnetic resonance spectroscopy of hepatic lipid fraction. *Journal of Magnetic Resonance Imaging: An Official Journal of the International Society for Magnetic Resonance in Medicine,* 29**,** 629-635.

Shen, W., M. Punyanitya, J. Chen, D. Gallagher, J. Albu, X. Pi-Sunyer, C. Lewis, C. Grunfeld, S. Heymsfield & S. Heshka (2007) Visceral adipose tissue: relationships between single slice areas at different locations and obesity-related health risks. *International journal of obesity,* 31**,** 763-769.

Shen, W., Z. Wang, M. Punyanita, J. Lei, A. Sinav, J. G. Kral, C. Imielinska, R. Ross & S. B. Heymsfield (2003) Adipose tissue quantification by imaging methods: a proposed classification. *Obesity research,* 11**,** 5-16.

Shuman, W. P., L. Morris, D. L. Leonetti, P. W. Wahl, V. M. Moceri, A. A. Moss & W. Y. Fujimoto (1986) Abnormal body fat distribution detected by computed tomography in diabetic men. *Investigative radiology,* 21**,** 483-487.

Sijens, P. E., M. A. Edens, J. L. S. Bakker & R. P. Stolk (2010) MRI-determined fat content of human liver,pancreas and kidney. *World Journal of Gastroenterology* 16**,** 1993-1998.

Sikaris, K. (2012) Application of the Stockholm hierarchy to defining the quality of reference intervals and clinical decision limits. *The Clinical Biochemist Reviews,* 33**,** 141.

Simonyan, K. & A. Zisserman (2014) Very deep convolutional networks for large-scale image recognition. *arXiv preprint arXiv:1409.1556*.

Sims, E. A., E. Danforth, E. S. Horton, G. A. Bray, J. Glennon & L. Salans. 1973. Endocrine and metabolic effects of experimental obesity in man. In *Proceedings of the 1972 Laurentian Hormone Conference*, 457-496. Elsevier.

Singh, R. G., A. Cervantes, J. U. Kim, N. N. Nguyen, S. V. DeSouza, D. Dokpuang, J. Lu & M. S. Petrov (2019) Intrapancreatic fat deposition and visceral fat volume are associated with the presence of diabetes after acute pancreatitis. *American Journal of Physiology-Gastrointestinal and Liver Physiology,* 316**,** G806-G815.

Singh, R. G., S. A. Pendharkar, N. A. Gillies, V. Miranda-Soberanis, L. D. Plank & M. S. Petrov (2017a) Associations between circulating levels of adipocytokines and abdominal adiposity in patients after acute pancreatitis. *Clinical and experimental medicine,* 17**,** 477-487.

Singh, R. G., H. D. Yoon, S. D. Poppitt, L. D. Plank & M. S. Petrov (2017b) Ectopic fat accumulation in the pancreas and its biomarkers: A systematic review and meta-analysis. *Diabetes/Metabolism Research and Reviews,* 33**,** e2918.

Singh, R. G., H. D. Yoon, L. M. Wu, J. Lu, L. D. Plank & M. S. Petrov (2017c) Ectopic fat accumulation in the pancreas and its clinical relevance: a systematic review, meta-analysis, and meta-regression. *Metabolism,* 69**,** 1-13.

Sjöström, L., A.-K. Lindroos, M. Peltonen, J. Torgerson, C. Bouchard, B. Carlsson, S. Dahlgren, B. Larsson, K. Narbro & C. D. Sjöström (2004) Lifestyle, diabetes, and cardiovascular risk factors 10 years after bariatric surgery. *New England Journal of Medicine,* 351**,** 2683-2693.

Smits, M. M. & E. J. Van Geenen (2011) The clinical significance of pancreatic steatosis. *Nature reviews Gastroenterology & hepatology,* 8**,** 169.

Snel, M., J. T. Jonker, J. Schoones, H. Lamb, A. de Roos, H. Pijl, J. W. Smit, A. E. Meinders & I. M. Jazet (2012) Ectopic fat and insulin resistance: pathophysiology and effect of diet and lifestyle interventions. *International journal of endocrinology,* 2012.

Sreedhar, U. L., S. V. DeSouza, B. Park & M. S. Petrov (2019) A Systematic Review of Intra-pancreatic Fat Deposition and Pancreatic Carcinogenesis. *Journal of Gastrointestinal Surgery***,** 1-10.

--- (2020) A systematic review of intra-pancreatic fat deposition and pancreatic carcinogenesis. *Journal of Gastrointestinal Surgery,* 24**,** 2560-2569.

Steven, S., K. G. Hollingsworth, A. Al-Mrabeh, L. Avery, B. Aribisala, M. Caslake & R. Taylor (2016a) Very low-calorie diet and 6 months of weight stability in type 2 diabetes: pathophysiological changes in responders and nonresponders. *Diabetes care,* 39**,** 808-815.

Steven, S., K. G. Hollingsworth, P. K. Small, S. A. Woodcock, A. Pucci, B. Aribisala, A. Al-Mrabeh, A. K. Daly, R. L. Batterham & R. Taylor (2016b) Weight loss decreases excess pancreatic triacylglycerol specifically in type 2 diabetes. *Diabetes Care,* 39**,** 158-165.

Stine, J. G., N. Munaganuru, A. Barnard, J. L. Wang, K. Kaulback, C. K. Argo, S. Singh, K. J. Fowler, C. B. Sirlin & R. Loomba (2021) Change in MRI-PDFF and histologic response in patients with nonalcoholic steatohepatitis: a systematic review and meta-analysis. *Clinical Gastroenterology and Hepatology,* 19**,** 2274-2283. e5.

Stone, M. A., L. Williams, S. Chatterjee, M. J. Davies & K. Khunti (2008) Ethnic differences in body composition in adolescents. *Primary Care Diabetes,* 2**,** 55-57.

Styner, M., G. M. Pagnotti, C. McGrath, X. Wu, B. Sen, G. Uzer, Z. Xie, X. Zong, M. A. Styner & C. T. Rubin (2017) Exercise decreases marrow adipose tissue through ß-oxidation in obese running mice. *Journal of Bone and Mineral Research,* 32**,** 1692-1702.

Styner, M., W. R. Thompson, K. Galior, G. Uzer, X. Wu, S. Kadari, N. Case, Z. Xie, B. Sen & A. Romaine (2014) Bone marrow fat accumulation accelerated by high fat diet is suppressed by exercise. *Bone,* 64**,** 39-46.

Sugii, S., Y. Kida, T. Kawamura, J. Suzuki, R. Vassena, Y.-Q. Yin, M. K. Lutz, W. T. Berggren, J. C. I. Belmonte & R. M. Evans (2010) Human and mouse adipose-derived cells support feeder-independent induction of pluripotent stem cells. *Proceedings of the National Academy of Sciences,* 107**,** 3558-3563.

Sun, Q., J. Qiao, S. Zhang, S. He, Y. Shi, Y. Yuan, X. Zhang & Y. Cai (2018) Changes in DNA methylation assessed by genomic bisulfite sequencing suggest a role for DNA methylation in cotton fruiting branch development. *PeerJ,* 6**,** e4945.

Sundborn, G., P. Metcalf, R. Scragg, D. Schaaf, L. Dyall, D. Gentles, P. Black & R. Jackson (2007) Ethnic differences in the prevalence of new and known diabetes mellitus, impaired glucose tolerance, and impaired fasting glucose. Diabetes Heart and Health Survey (DHAH) 2002-2003, Auckland New Zealand. *The New Zealand medical journal,* 120**,** 1-12.

Szczepaniak, I. Lingvay, R. G. Victor, R. Mathur, M. D. Nelson, E. W. Szczepaniak, N. Tyer, I. Chen, R. H. Unger & R. N. Bergman (2012a) Pancreatic steatosis and its relationship to beta-cell dysfunction in humans: Racial and ethnic variations. *Diabetes Care,* 35**,** 2377-2383.

Szczepaniak, K. Malliaras, M. D. Nelson & L. S. Szczepaniak (2013a) Measurement of pancreatic volume by abdominal MRI: A validation study. *PLoS One* 8**,** e55991.

Szczepaniak, E. W., K. Malliaras, M. D. Nelson & L. S. Szczepaniak (2013b) Measurement of pancreatic volume by abdominal MRI: a validation study. *PloS one,* 8**,** e55991.

Szczepaniak, L. S., P. Nurenberg, D. Leonard, J. D. Browning, J. S. Reingold, S. Grundy, H. H. Hobbs & R. L. Dobbins (2005) Magnetic resonance spectroscopy to measure hepatic triglyceride content: prevalence of hepatic steatosis in the general population. *American Journal of Physiology-Endocrinology and Metabolism,* 288**,** E462-E468.

Szczepaniak, L. S., R. G. Victor, R. Mathur, M. D. Nelson, E. W. Szczepaniak, N. Tyer, I. Chen, R. H. Unger, R. N. Bergman & I. Lingvay (2012b) Pancreatic steatosis and its relationship to β-cell dysfunction in humans: racial and ethnic variations. *Diabetes care,* 35**,** 2377-2383.

Tabák, A. G., M. Jokela, T. N. Akbaraly, E. J. Brunner, M. Kivimäki & D. R. Witte (2009) Trajectories of glycaemia, insulin sensitivity, and insulin secretion before diagnosis of type 2 diabetes: An analysis from the Whitehall II study. *The Lancet,* 373**,** 2215-2221.

Tahara, Y. & K. Shima (1995) Kinetics of HbA1c, glycated albumin, and fructosamine and analysis of their weight functions against preceding plasma glucose level. *Diabetes care,* 18**,** 440-447.

Thomas, E. L., J. Fitzpatrick, S. Malik, S. D. Taylor-Robinson & J. D. Bell (2013) Whole body fat: content and distribution. *Progress in nuclear magnetic resonance spectroscopy,* 73**,** 56-80.

Thomas, L. W. (1962) The chemical composition of adipose tissue of man and mice. *Quarterly Journal of Experimental Physiology and Cognate Medical Sciences: Translation and Integration,* 47**,** 179-188.

Thomsen, C., U. Becker, K. Winkler, P. Christoffersen, M. Jensen & O. Henriksen (1994) Quantification of liver fat using magnetic resonance spectroscopy. *Magnetic resonance imaging,* 12**,** 487-495.

Toro-Ramos, T., D. Gallagher, B. H. Goodpaster, I. Janumala, S. Lin, G. W. Strain, J. C. Thornton, P. Kang, A. P. Courcoulas & A. Pomp (2015) Continued loss in visceral and intermuscular adipose tissue in weight-stable women following bariatric surgery. *Obesity,* 23**,** 62-69.

Truesdale, K. P., J. Stevens & J. Cai (2011) Impact of body mass index levels on lipid abnormalities in Chinese Asians, American Blacks and American Whites: The People's Republic of China (PRC) and atherosclerosis risk in communities (ARIC) studies. *Atherosclerosis,* 218**,** 517-523.

Tsai, A. G. & T. A. Wadden (2006) The evolution of very-low-calorie diets: an update and meta-analysis. *Obesity,* 14**,** 1283-1293.

Turnbaugh, P. J., M. Hamady, T. Yatsunenko, B. L. Cantarel, A. Duncan, R. E. Ley, M. L. Sogin, W. J. Jones, B. A. Roe & J. P. Affourtit (2009) A core gut microbiome in obese and lean twins. *nature,* 457**,** 480.

Tushuizen, M. E., M. C. Bunck, P. J. Pouwels, S. Bontemps, J. H. T. van Waesberghe, R. K. Schindhelm, A. Mari, R. J. Heine & M. Diamant (2007) Pancreatic fat content and beta-cell function in men with and without type 2 diabetes. *Diabetes Care,* 30**,** 2916-2921.

Tushuizen, M. E., M. C. Bunck, P. J. Pouwels & M. Diamant (2008) Pancreatic fat content and beta-cell function in men with and without type 2 diabetes: Response to Saisho, Butler, and Butler. *Diabetes Care,* 31**,** e39.

Valentine, N. A., T. M. Alhawassi, G. W. Roberts, P. P. Vora, S. N. Stranks & M. P. Doogue (2011) Detecting undiagnosed diabetes using glycated haemoglobin: an automated screening test in hospitalised patients. *Medical journal of Australia,* 194**,** 160-164.

van der Zijl, N. J., G. H. Goossens, C. C. M. Moors, D. H. van Raalte, M. H. A. Muskiet, P. J. W. Pouwels, E. E. Blaak & M. Diamant (2011) Ectopic Fat Storage in the Pancreas, Liver, and Abdominal Fat Depots: Impact on β-Cell Function in Individuals with Impaired Glucose Metabolism. *The Journal of Clinical Endocrinology & Metabolism,* 96**,** 459-467.

van Geenen, E.-J. M., M. M. Smits, T. C. Schreuder, D. L. van der Peet, E. Bloemena & C. J. Mulder (2010) Nonalcoholic fatty liver disease is related to nonalcoholic fatty pancreas disease. *Pancreas,* 39**,** 1185-1190.

Vedaldi, A., Y. Jia, E. Shelhamer, J. Donahue, S. Karayev, J. Long & T. Darrell (2014) Convolutional architecture for fast feature embedding. *Cornell University*.

Verheggen, R., M. Maessen, D. J. Green, A. Hermus, M. Hopman & D. Thijssen (2016) A systematic review and meta-analysis on the effects of exercise training versus hypocaloric diet: distinct effects on body weight and visceral adipose tissue. *Obesity reviews,* 17**,** 664-690.

Virostko, J. (2020) Quantitative Magnetic Resonance Imaging of the Pancreas of Individuals With Diabetes. *Frontiers in Endocrinology,* 11**,** 920.

Wajchenberg, B. L. (2000) Subcutaneous and visceral adipose tissue: their relation to the metabolic syndrome. *Endocrine reviews,* 21**,** 697-738.

Wang, T., X. Ma, D. Peng, R. Zhang, X. Sun, M. Chen, J. Yan, S. Wang, D. Yan & Z. He (2016) Effects of obesity related genetic variations on visceral and subcutaneous fat distribution in a Chinese population. *Scientific reports,* 6**,** 1-9.

Weir, G. C., D. R. Laybutt, H. Kaneto, S. Bonner-Weir & A. Sharma (2001) Beta-cell adaptation and decompensation during the progression of diabetes. *Diabetes,* 50**,** S154.

Weiss, R., Appelbaum. L, C. Schweiger, I. Matot, N. Constantini, A. Idan, N. Shussman, J. Sosna & A. Keidar (2009) Short-term dynamics and metabolic impact of abdominal fat depots after bariatric surgery. *Diabetes Care,* 32**,** 1910-1915.

Wellen, K. E. & G. S. Hotamisligil (2005) Inflammation, stress, and diabetes. *The Journal of clinical investigation,* 115**,** 1111-1119.

WHO, O. overweight Fact sheet N 311, WHO (2015). *World Health Organization: Geneva*.

Wickremesekera, K., G. Miller, T. D. Naotunne, G. Knowles & R. S. Stubbs (2005) Loss of insulin resistance after Roux-en-Y gastric bypass surgery: A time course study. *Obesity Surgery,* 15**,** 474-481.

Wilding, J. (2014) The importance of weight management in type 2 diabetes mellitus. *International journal of clinical practice,* 68**,** 682-691.

Williams, J. M., M. A. Hilmes, B. Archer, A. Dulaney, L. Du, H. Kang, W. E. Russell, A. C. Powers, D. J. Moore & J. Virostko (2020) Repeatability and Reproducibility of pancreas Volume Measurements Using MRi. *Scientific Reports,* 10**,** 1-7.

Wisse, B. E. (2004) The inflammatory syndrome: the role of adipose tissue cytokines in metabolic disorders linked to obesity. *Journal of the American society of nephrology,* 15**,** 2792-2800.

Wolz, R., C. Chu, K. Misawa, M. Fujiwara, K. Mori & D. Rueckert (2013) Automated abdominal multi-organ segmentation with subject-specific atlas generation. *IEEE transactions on medical imaging,* 32**,** 1723-1730.

Wong, V. W.-S., G. L.-H. Wong, D. K.-W. Yeung, J. M. Abrigo, A. P.-S. Kong, R. S.-M. Chan, A. M.-L. Chim, J. Shen, C.-S. Ho & J. Woo (2014) Fatty pancreas, insulin resistance, and β-cell function: a population study using fat-water magnetic resonance imaging. *Official journal of the American College of Gastroenterology| ACG,* 109**,** 589-597.

Xiang, Q. S. (2006) Two-point water-fat imaging with partially-opposed-phase (POP) acquisition: an asymmetric Dixon method. *Magnetic Resonance in Medicine: An Official Journal of the International Society for Magnetic Resonance in Medicine,* 56**,** 572-584.

Yalçın, T., S. H. Oğuz, M. Bayraktar & N. Rakıcıoğlu (2021) Anthropometric measurements and serum TNF-α, IL-6 and adiponectin in type 2 diabetes. *Diabetology International***,** 1-11.

Yang, J. Z., D. Dokpuang, R. Nemati, K. H. He, A. B. Zheng, M. S. Petrov & J. Lu (2020) Evaluation of Ethnic Variations in Visceral, Subcutaneous, Intra-Pancreatic, and Intra-Hepatic Fat Depositions by Magnetic Resonance Imaging among New Zealanders. *Biomedicines,* 8**,** 174.

Yaribeygi, H., N. Katsiki, B. Behnam, H. Iranpanah & A. Sahebkar (2018) MicroRNAs and type 2 diabetes mellitus: molecular mechanisms and the effect of antidiabetic drug treatment. *Metabolism,* 87**,** 48-55.

Yip, S., L. D. Plank & R. Murphy (2013) Gastric bypass and sleeve gastrectomy for type 2 diabetes: A systematic review and meta-analysis of outcomes. *Obesity Surgery,* 23**,** 1994-2003.

Yokoo, T., M. Bydder, G. Hamilton, M. S. Middleton, A. C. Gamst, T. Wolfson, T. Hassanein, H. M. Patton, J. E. Lavine & J. B. Schwimmer (2009) Nonalcoholic fatty liver disease: diagnostic and fat-grading accuracy of low-flip-angle multiecho gradient-recalled-echo MR imaging at 1.5 T. *Radiology,* 251**,** 67-76.

Yokoo, T., M. Shiehmorteza, G. Hamilton, T. Wolfson, M. E. Schroeder, M. S. Middleton, M. Bydder, A. C. Gamst, Y. Kono & A. Kuo (2011) Estimation of hepatic proton-density fat fraction by using MR imaging at 3.0 T. *Radiology,* 258**,** 749-759.

Yu, H., A. Shimakawa, C. A. McKenzie, E. Brodsky, J. H. Brittain & S. B. Reeder (2008) Multiecho water-fat separation and simultaneous R estimation with multifrequency fat spectrum modeling. *Magnetic Resonance in Medicine: An Official Journal of the International Society for Magnetic Resonance in Medicine,* 60**,** 1122-1134.

Yu, Q., L. Xie, Y. Wang, Y. Zhou, E. K. Fishman & A. L. Yuille. 2018. Recurrent saliency transformation network: Incorporating multi-stage visual cues for small organ segmentation. In *Proceedings of the IEEE conference on computer vision and pattern recognition*, 8280-8289.

Zeng, G. & G. Zheng (2019) Holistic decomposition convolution for effective semantic segmentation of medical volume images. *Medical image analysis,* 57**,** 149-164.

Zhang, D., J. Zhang, Q. Zhang, J. Han, S. Zhang & J. Han (2021) Automatic pancreas segmentation based on lightweight DCNN modules and spatial prior propagation. *Pattern Recognition,* 114**,** 107762.

Zheng, W., S. Tsugane, F. Irie, A. Tamakoshi, Y. Gao, R. Wang, X. Shu, I. Tsuji, S. Kuriyama, H. Tanaka, H. Satoh, D. F. McLerran, Y. Chen, C. Chen, J. Yuan, K. Yoo, H. Ahsan, W. Pan, D. Gu, M. S. Pednekar, C. Sauvaget, S. Sasazuki, T. Sairenchi, B. Rolland, G. Yang, Y. Xiang, M. Nagai, T. Suzuki, Y. Nishino, S. You, W. Koh, S. K. Park, C. Shen, X. Zhang, M. Thornquist, Z. Feng, D. Kang, P. Boffetta, J. D. Potter, M. Inoue, K. Matsuo, J. He, P. C. Gupta & K. Ramadas (2011) Association between body-mass index and risk of death in more yhan 1 million Asians. *The New England Journal of Medicine,* 364**,** 719-729.

Zhou, B. F. (2002) Predictive values of body mass index and waist circumference for risk factors of certain related diseases in Chinese adults: Study on optimal cut-off points of body mass index and waist circumference in Chinese adults. *Biomedical and Environmental Sciences* 15**,** 83-96.

Zhou, Y., L. Xie, W. Shen, Y. Wang, E. K. Fishman & A. L. Yuille. 2017. A fixed-point model for pancreas segmentation in abdominal CT scans. In *International conference on medical image computing and computer-assisted intervention*, 693-701. Springer.

Zhu, Z., Y. Xia, W. Shen, E. Fishman & A. Yuille. 2018. A 3D coarse-to-fine framework for volumetric medical image segmentation. In *2018 International Conference on 3D Vision (3DV)*, 682-690. IEEE.

Zyromski, N. J., A. Mathur, G. A. Nagana Gowda, C. Murphy, D. A. Swartz-Basile, T. E. Wade, H. A. Pitt & D. Raftery (2009) Nuclear magnetic resonance spectroscopy-based metabolomics of the fatty pancreas: Implicating fat in pancreatic pathology. *Pancreatology,* 9**,** 410-419.

Appendices

APPENDIX A (Information Sheet)

THE UNIVERSITY OF AUCKLAND
FACULTY OF MEDICAL AND HEALTH SCIENCES

AUT UNIVERSITY
TE WĀNANGA ARONUI O TAMAKI MAKAU RAU

Participant Information Sheet

Study title:	Investigation of changes in liver and pancreatic fat after bariatric surgery in relation to diabetes remission and ethnicity		
Locality:	Auckland	Ethics committee ref.:	**16/STH/193**
Lead investigators:	Assoc Prof Jun Lu Dr Rinki Murphy	Contact phone number:	09 9219999 x 7381 09 9236313

We invite you to take part in a study looking at changes in liver and pancreatic fat that occur after bariatric surgery in relation to diabetes remission. Whether or not you take part is your choice. If you don't want to take part, you don't have to give a reason, and it won't affect the care you receive. If you do want to take part now, but change your mind later, you can pull out of the study at any time.

This Participant Information Sheet will help you decide if you'd like to take part. It sets out why we are doing the study, what your participation would involve, what the benefits and risks to you might be, and what would happen after the study ends. We will go through this information with you and answer any questions you may have. We expect this will take about 15 minutes. You may also want to talk about the study with other people, such as family, whānau, friends, or healthcare providers. Feel free to do this.

If you agree to take part in this study, you will be asked to sign the Consent Form on the last page of this document. You will be given a copy of both the Participant Information Sheet and the Consent Form to keep.

This document is 7 pages long, including the Consent Form. Please make sure you have all the pages.

Who can take part in this study?

How many and what type of people are needed for this study?
We are looking for 56 adults aged 18-65 with BMI >35 kg/m2 who are accepted to have either sleeve gastrectomy or Roux-en-Y gastric bypass type of bariatric surgery at Auckland

City hospital and have type 2 diabetes. We will ask everybody to come to the Body Composition Unit on level 3 of Auckland City Hospital for a blood sample and to have a DEXA and MRI organ scan 3 days before their surgery to assess the fat content of their liver and pancreas, then at 3 days and 1 year after surgery.

Who cannot take part in this study?
If you have any implanted metal and electronic devices e.g.: metal implants, heart pacemakers, insulin pumps, implanted hearing aids, intracranial metal clips, metallic bodies in the eyes. These devices are incompatible with MRI scanning, so you cannot take part in this study.
Other exclusion criteria for participating in this study are type 1 diabetes, prior bariatric surgery of any kind and previous antrectomy or small bowel resection. If you have any history of chronic pancreatitis or idiopathic acute pancreatitis, or if you are using oral steroids then you are not eligible to take part.

Why are we doing the study?
Bariatric surgery is currently the most effective treatment for obese patients with type 2 diabetes. However, it is unclear how bariatric surgery causes diabetes remission within a few days after surgery, before significant weight loss has taken place. We think that early loss of fat from liver and pancreas may be the driving diabetes remission status. We aim to understand whether there is an acute reduction in liver and pancreas fat after surgery; and whether these changes vary by ethnicity or surgical type: sleeve gastrectomy or Roux-en-Y gastric bypass.
Aim: This detailed MRI study will allow us to better understand the role of pancreatic and liver fat in type 2 diabetes occurring at different body mass index thresholds among people of different ethnic groups, and also to identify biomarkers in blood samples to predict who will respond best to surgery in terms of diabetes remission.

What would your participation involve?
We will ask everybody to come to the Body Composition Unit on level 3 of Auckland City Hospital on 3 occasions for a blood sample and to have a DEXA and MRI organ scan to assess the fat content of liver and pancreas.
3 days before the surgery
3 days after the surgery
1 year after the surgery
A few days before your scheduled bariatric surgery, we will ask you to come to the Body Composition Unit in Auckland where we will explain the study and ask you to consent to take part in writing. We will record your age, gender, ethnicity and ask you questions about your medical history and medications. You will be asked to provide us with your GP contact details so that should there be any unexpected findings, we will give you the information and also send it to your GP. If you are eligible to take part after the screening questionnaire, and would like to take part, we will invite you to come to the body composition unit on level 3 at Auckland City Hospital, where we will collect an early morning fasting (before breakfast) venous blood sample and a body composition DEXA scan, REE and a MRI scan at the Centre for Advanced MRI.
You will be asked to have the measurements mentioned above again a few days after and at one-year after the bariatric surgery.

What is DEXA?
DEXA is a scanning method, to measure body composition (bone, fat, muscle). The scan takes about 10 minutes. You lie quietly on an open bed and a scanning arm passes quickly over the top of you. You have to lie quietly without moving, but it is not an unpleasant measurement. As the scanning arm passes over you it emits 2 types of very low dose x-ray, similar to the radiation dose that you would receive if you took a 1 hour flight – perhaps between Auckland and Wellington. The DEXA then measures the density of the different tissues in your body. Bone is very dense so it appears bright white on the scan. Muscle is less dense and so it is less white, and fat even less dense and so it is the least white of all. At the end of the 10-minute scan we will print a picture of you showing an image of the bone, fat and lean tissue in your body for you to take home with you.

What is REE?
An REE measurement determines your resting energy expenditure, ie how many calories you are burning while resting. This will be performed at the end of the DEXA scan and will involve putting a transparent hood over your head for 10-20 minutes. During this time the air you are breathing out is collected and analyzed.

What is MRI and MRS?
MRI is a body scanning method that has been used in hospitals worldwide for many years. It uses a magnetic field and radio frequency pulse to obtain detailed images of your organs without the use of x-rays. It will identify if any fat has been stored in your liver, pancreas, or muscle. You will be asked to lie down in a relaxed state, without movement if possible, within the chamber of the machine whilst it scans your abdomen. The scan will take around 30 minutes. The MRS scan of the liver will be performed after the MRI scan has finished.

What are the possible benefits and risks to you of participating?
Having a blood sample taken may hurt a little, and some patients get a small bruise where the needle goes in. Most people have no problems.
Low levels of radiation will be used for DEXA scan which is similar to the radiation exposure on a flight from Auckland to Wellington. Research personnel will monitor you during the study for any side effects of the treatment.
There could be unexpected findings from MRI scan such as discovery of nodules, tumours of other anatomical disorders. If these abnormalities are found, we will inform you immediately and also your GP to ensure adequate follow up is in place.
It is possible that you may be diagnosed with abnormal blood results during the study. If so, you will be informed, provided with the results, and advised to contact your GP directly. Our research staff will discuss with you the significance of any abnormal result and will also make contact with your GP or specialist to ensure adequate follow-up is in place, since these disorders can have significant impact on your health. MRI scans may also pick up incidental findings that could result in a new diagnosis or require further investigation. Again, our research staff will discuss with you the significance of the results and will also make contact with your GP or specialist to ensure adequate follow-up is in place. However, follow-up investigations would not be paid for by the researchers.

What would happen if you were injured in the study?
If you were injured in this study, which is unlikely, you would be eligible for compensation from ACC just as you would be if you were injured in an accident at work or at home.

If you have private health or life insurance, you may wish to check with your insurer that taking part in this study won't affect your cover.

What are the rights of participants in the study?
You do not have to give a blood sample for this research if you do not want to. If you decide not to be in this study, you do not have to give any reason to the researcher. If the measurements or the lab find something important from the tests or measurements that might affect your health, you will be told about it as soon as possible. You also have legal rights over your blood sample and data from the scans you give for research. You keep control over any sample you donate for research. The sample can only be used for research related to this study.
If you change your mind later, just let us know, and we will either return or destroy your sample and remove your data. If you die, your family can also ask for your sample to be returned.

What will happen after the study ends, or if you pull out?
Samples will be stored for a maximum of 10 years, after which they will be destroyed by incineration.
Whether or not you take part is your choice. If you don't want to take part, you don't have to give a reason, and it won't affect the care you receive. If you do want to take part now, but change your mind later, you can pull out of the study at any time.

Confidentiality
Research files and all other information that you provide will remain strictly confidential. No material that could personally identify you will be used in any reports on this research. Upon completion of the research your records will be stored for 10 years in a secure place. All computer records will be password protected and available only to research team.

Thank you for taking the time to read about taking part in this study.

Where can you go for more information about the study, or to raise concerns or complaints?

If you have any questions, concerns or complaints about the study at any stage, you can contact:

Associate Professor Jun Lu
Faculty of Health and Environmental Sciences
Auckland University of Technology
Telephone number; 09 9219999 x 7381
Email; jun.lu@aut.ac.nz

Dr. Rinki Murphy
Diabetes Physician and Senior Lecturer in Medicine
Auckland and Counties Manukau District Health Boards and University of Auckland
Telephone number; 09 923 6313
Email; R.Murphy@auckland.ac.nz

Associate Professor Lindsay Dudley Plank
Department of Surgery
University of Auckland
Telephone number; 09 923 6949
Email; l.plank@auckland.ac.nz

Dr Nicholas James Evennett
Upper GI/Bariatric Surgeon
Auckland District Health Board
Telephone number; 09 367 0000 x 21737
Email; NicholasE@adhb.govt.nz

Dr Carl Nicholas Peters
Consultant Endocrinologist
Waitemata District Health Board
Telephone number; 09 486 8900 x 9659
Email; carl.peters@waitematadhb.govt.nz

Dr Grant Rocco Beban
Upper GI and Bariatric Surgeon
Auckland District Health Board
Telephone number; 09 367 0000
Email; GBeban@adhb.govt.nz

If you want to talk to someone who isn't involved with the study, you can contact an independent health and disability advocate on:

Phone: 0800 555 050
Fax: 0800 2 SUPPORT (0800 2787 7678)
Email: advocacy@hdc.org.nz

You can also contact the health and disability ethics committee (HDEC) that approved this study on:

Phone: 0800 4 38442 (0800 4 Ethic)
Email: hdecs@moh.govt.nz

APPENDIX B (Consent Form)

Consent Form

Declaration by participant:

I have read, or have had read to me in my first language, and I understand the Participant Information Sheet. I have had the opportunity to ask questions and I am satisfied with the answers I have received.

I have had the opportunity to use support from a family (whanau) member or a friend to help me ask questions and understand the research.
I understand that taking part in this research is voluntary (my choice), and that I may withdraw from the research at any time and this will in no way affect my future or continuing health care.
I understand that my participation in this research is confidential and that no material which could identify me will be used in any reports on this research. I understand that the sponsor of the research, others working on the sponsor's behalf, the Ethics Committee and the regulatory authorities will not need my permission to look at my health records both in respect of the current research and any further research that may be conducted in relation to it, even if I withdraw from the trial. I agree to this access. However, I understand that my identity will not be revealed in any information released to third parties or published
I understand that the treatment, or investigation, will be stopped if it should appear harmful to myself.
I understand the compensation provisions for this research.
I have had time to consider whether to take part.
I know whom to contact if I have any side effects from the research.
I know whom to contact if I have any questions about the research.
I agree not to restrict the use of any data or results that arise from this research provided such a use is only for scientific purpose(s)
I freely agree to participate in this study.

I have been given a copy of the Participant Information Sheet and Consent Form to keep.

Participant's name: _____

Signature: _____ Date: _____

Declaration by member of research team:

I have given a verbal explanation of the research project to the participant, and have answered the participant's questions about it.

I believe that the participant understands the study and has given informed consent to participate.

Researcher's name: _____

Signature: _____ Date: _____

APPENDIX C (Questionaire)

Investigation of changes in liver and pancreatic fat after bariatric surgery in relation to diabetes remission and ethnicity

Patient assessment record sheet Participant ID: …….

Date: / / Visit: baseline / 3 days / 1 year

First Name:……Last Name:……

Date of Birth:……

Participant Information

Age		Waist circumference (cm)	
Gender		Hip circumference (cm)	
Pulse (BPM)		Waist to hip ratio	
Ethnicity		Neck circumference (cm)	
New Zealand European		Height (cm)	
Asian (please specify)		Weight (kg)	
Māori		BMI (kg/m^2)	
Pacific (please specify)		BP (mmHg)	

PARTICIPANT HISTORY

If you have any of the following problems please tick the box.

- ☐ Claustrophobia
- ☐ Pancreatitis

Have you ever been diagnosed of type 1 diabetes? ☐ YES ☐ NO

LIFESTYLE

1. Are you a smoker? ☐ YES ☐ NO ☐ EX-SMOKER
   .....
2. Did you drink alcohol in the last week (if yes, How often?)
   ☐ YES ☐
   NO ……
   …
3. Are you currently using an oral steroid? ☐ YES ☐ NO

PREVIOUS SURGERY

Have you ever undergoing any kinds of these surgery?

☐ Abdominal surgery If Yes When did you have this surgery?.....

☐ Bariatric surgery

- ☐ Sleeve gastrectomy If Yes When did you have this surgery?.....
- ☐ Roux-en-Y gastric bypass If Yes When did you have this surgery……
- ☐ Other types of bariatric surgery (please specify)

  Types of surgery……
  When did you have this surgery?.....

MRI COMPATIBILITY

When did your last eat or drink?
……
……

Do you have any implanted metal or electronic device?

- ☐ Hearth pacemaker
- ☐ Insulin pumps
- ☐ Implant hearing aids
- ☐ Neurostimulators
- ☐ Intracranial metal clips
- ☐ Metabolic bodies in the eyes
- ☐ Others (please specify)……

Do you have any problem in relation to claustrophobia? ☐ YES ☐ NO

OTHER INFORMATION

Recent medicine use (past 6 months): type/indication/dose/duration (if known) Current nutritional
Supplement (s) (if any)

Would you like a Karakia during your blood disposal after the study has been finished? ☐ YES ☐ NO

Researcher Signature Date

APPENDIX D: **The operation detail of excluding pixels**

a. Use Image J to open the "fat fraction image" and the "water image" simultaneously (better to have double monitors to the PC for easy navigation through the two image stacks)
b. Identify the two candidate slices which meet the criteria for selection including: being centrally located within the pancreas in the foot-head direction and having sufficient area to place the 100mm^2 ROI distributed over head, body and tail of the pancreas.
c. Go to Image J and from the main window click Analyse and then click measure button to get the fat percentage for all highlighted ROI of fat images.
d. Save the result as spreadsheet within the renamed folder. (Click File and save as any type of image)
e. Repeat the same for the second slice then save all the ROIs (the "RoiSet" file in ImageJ terminology) under a specific name in the desired folder.

Important: The above process is ONLY required once, then you can copy the RoiSets file across to another desired folder but modify the file name, selected slices and ROI positions.

Highlight the three ROI selections on the first slice at once (ctrl+shift+ mouse click) then select from the ROI Manager main panel: More →OR (Combine) → Add (this will combine the three ROIs in one file, see illustrative below). The software will create a random name to the new file, highlight the name → Rename → label the new file that contains the three combined ROIs as "average-slice-01".

f. Repeat the same for the second slice, and label as "average-slice-02".

Highlight all the RoiSets in the ROI Manager and update the saved RoiSet file (More →Save →select the file name and overwrite it). You need first to go to ImageJ→ Analyze → Set Measurements, and then enable settings including display label, area of selection, maximum/ minimum gray value, and mean gray value.

g. From ImageJ main window click Analyze → Measure to get the percentage fat for all highlighted RoiSets within the ROI Manager (make sure that you click on the fat fraction image not anatomical map before you do this step).
h. Save the result as spreadsheet within the desired folder by selecting File→ Save As (this will generate pancreatic fat without excluding any values).
i. Highlight average-slice-01 from the ROI manager window, and select Analyze →Histogram→OK, a new window of the Histogram data of selected area will appear (see illustrative example below).

j. From the Histogram window click List →File → Save As (the software will save it as a spreadsheet under the name: Histogram of the original file name.
k. Use Excel spreadsheet to exclude values less than 1% and over 20% from final fat percentage